

RETURNING MATERIALS:
Place in book drop to remove this checkout from your record. FINES will be charged if book is returned after the date stamped below.

MAY 2 6 2005	

THE ACHIEVEMENT OF CYCLIC VOLTAMMETRY WITH A MICROCOMPUTER CONTROLLED COULOSTATIC POLARIZER

by

Robert J. Engerer

A DISSERTATION

Submitted to
Michigan State University
in partial fulfillment of the requirements
for a degree of

DOCTOR OF PHILOSOPHY

Department of Chemistry

1985

ABSTRACT

THE ACHIEVEMENT OF CYCLIC VOLTAMMETRY WITH A MICROCOMPUTER CONTROLLED COULOSTATIC POLARIZER

by

Robert J. Engerer

The fundamental experiment and characteristic data available from cyclic voltammetry (CV) are reviewed in this dissertation as well as it's areas of application and limitations. To overcome limitations of solution resistance and charging current, a coulostatic or charge injection method was suggested and applied to staircase cyclic voltammetry.

The design and performance of a charge injector were evaluated. The injection pulse was applied to a real chemical cell and to an electrical equivalent or dummy cell to investigate the cell response and circuit stability. The accuracy and precision of the charge injector were determined to be better than 6 percent for charge injection sizes ranging from greater than 50 η C to less than 2 μ C.

A microcomputer was programmed to generate a controlled potential step. Potential steps were combined to produce a staircase voltage ramp. The computer controls, entirely through software, the experiment of staircase cyclic voltammetry by program control of the step size, step

duration, initial potential, and switching potential. Investigations were made of the influence of these staircase waveform parameters on the determination of cadmium and a detection limit of the instrument was determined to be 5×10^{-7} M.

The charge injection size and the number of injections made during each potential step were stransformed by means of a FORTRAN program into 'charge voltammograms'. A computer model of sampled current staircase voltammetry was developed and modified for comparison with charge voltammograms. Experimentally determined charge voltammograms were found to be within 10 percent of the calculated charge voltammograms. Anion induced adsorption was studied in the presence of diffusion with the charge injector using staircase cyclic voltammetry.

The limitations of the instrument are investigated and errors associated with the hybrid nature of the method discussed.

For my parents

Joseph Engerer and

Marcelle Engerer and

family

ACKNOWLEDGMENT

The author wishes to express his appreciation to Dr. Chris Enke for his suggestions and criticisms throughout this investigation.

Appreciation is also extended to other faculty and members of the M.S.U. staff for their assistance and discussions. I would also like to express my deepest appreciation to other fellow students for their friendship.

Thanks for everything--you are all like family to me!

Robert J. Engerer

TABLE OF CONTENTS

List of List of List of	Figu:	res.						•	•			•						•			ix
Chapter	I. :	Intro	oduc	tic	on	•		•	•	•	•	•		•	•	•	•	•	•	•	1
	The with	a Mid	croc	omp	put													eti	· y	•	1
	A.0	Line	ear	Swe	eep	V	olt	amn	net	ry	7.	•		•	•	•	•	•	•	•	1
Chapter	Lead:	ing t	to t	he	Мо	di	fie	d (Cha	ırg	je	In	jē	ct	or	•	•	•	•	•	5
	B.0 C.0 D.0 E.0 F.0 G.0 H.0 J.0 K.0	Char Volt Theo Limi Star Pote Non- Pote Dist The Coul Summ	tammory itat irca enti -Ide enti tort Cou lost	of ion ise ost ost ion ion ati	Cy Solution Cy Solution Effication Solution	of lts sec sof tie	ic Li amm ts . th c M	Volume to the total control of	tta ry ou ol nod wi	Swint	et vee · · · · · · · ·	ry ep ed og	Vo w: ra	· iti iti m · ste	am h	· · · · · · · · · · · · · · · · · · ·	• tr	· · · · · · · · · · · · · · · · · · ·	• • • • • • • • • • • • • • • • • • •	· · · · · · · · · · · · · · · · · · ·	5 9 16 17 22 24 26 31 33 37 39
Chapter	III. to a																			•	43
	A.0 B.0 C.0 D.0 E.0	A Co Resp Cell Cell Desi	ons L Re L Re	e c spc	of ons ons	the e	e E to to	lec a E Nor	tr as	oc t de	he Id	mi lea I	ca l nj	l In ec	Ce je ti	ct on	ic is	on •	•	•	43 45 47 49 51
Chapter	IV.	Inst	rum	ent	al	•		•	•	•	•	•	•	•	•	•	•	•	•	•	55
	A.0 B.0 C.0	The Char The The	ge Com	Inj	jec et e	to: Cl	r . har	ge	In	je	ct	or		•	•	•		•	•		55 55 58

	D.0	Requirements of the Voltage Measurement
		System 60
	E.0	Requirements of Analog Switches 62
	F.0	Requirements and Calibration of the
	<i>a</i> 0	Injection Capacitors
	G. 0	Requirements of the Injecting Amplifier 66
	H.0	Circuit Characteristics 67
Chapter	v.	Instrumental Requirements to Stimulate
		rcase Cyclic Voltammetry with a Charge
		ctor
	A.0	The Instrument
	B. 0	Modes of Instrument Operation
	C.0	Generation of a Staircase Waveform
	D.0	The Potential Step
	E.0	Single Injection of Approximately
	_,,	Correct Charge
	F.0	Large Charge Injection(s) Followed by
		Small Potential Adjustment 90
	G.0	Single Injection of Precalculated Charge 90
	11.0	Single Injection of Charge Value
		Determined by Previous Experiment 93
	I.0	Method of Choice 94
	J.0	Program Control of the Charge Injector 94
	K.0	The Initial Cell Potential 96
	L.0	Step Size
	M.O	The Flow Chart
	N. 0	Trouble Shooting Instrumental Problems 97
Chapter	VI.	Results and Discussion
	A.0	A Computer Model for Staircase Voltammetry
		with Charge-Step Polarization 103
	B.0	Guidance from Theory 103
	C.0	Faradaic and Charging Current 105
	D.0	Step Charge
	E.0	The Step Time Parameters 118
	F.0	Sampling Time
	G.0	Experimental Determinations 142
	H.0	Reduction Potential Location Using
		Computer Modelling
	I.0	Step Size
	J.0	Comparisons of Computer Modelling and
		Experiments 155
Chapter	vii.	Adsorption Studies 169
	A.0	Introduction 169
	B. 0	A Chemical System for the Study of
		Adsorption 172
	C.0	A Method for the Study of Adsorption 176
	D.0	Experimental

Chapter	VIII.	Limitations and Improvements	•	•	•	•	•	186
	A.0	Effects of the Staircase Waveform		•				187
	B.0	Charge Injection Effects				•	•	189
	C.0	Variation of the Step Charge		•	•		•	192
	D.0	DAC Round-Off Error	•	•	•	•	•	192
Reference	ces .							200

LIST OF TABLES

Table	6-I. A	Calculated Current Function Values for Various Potentials $\tau/t_{m} = 11$.20
Table	6-I. B	Calculated Current Function Values for Various Potentials $\tau/t_{m} = 10 \dots 1$.21
Table	6-I. C	Calculated Current Functions Values for Various Potentials τ/t_{m} = 100 1	.22
Table	6-I. D.	Calculated Current Function Values for Various Potentials $\tau/t_{m} = 10,000 \dots 1$.23
Table	6-II. A	Calculated Charge Function Values for Various Potentials $\tau/Tl=1$, Pre-Sample Charge	.31
Table	6-II. B	Calculated Charge Function Values for Various Potentials $\tau/T1$ = 10, Pre-Sample Charge	.32
Table	6-II. C	Calculated Charge Function Values for Various Potentials $\tau/T1$ = 100, Pre-Sample Charge	.33
Table	6-II. D	Calculated Charge Function Values for Various Potentials $\tau/T1 = 10,000$, Pre-Sampe Charge	.34
Table	6-II. E	Calculated Charge Function Values for Various Potentials $\tau/Tl=1$, Sample Charge	.35
Table	6-II. F	Calculated Charge Function Values for Various Potentials $\tau/T1 = 10$, Sample Charge	.36
Table	6-II. G	Calculated Charge Function Value for Various Potentials $\tau/T1 = 100$, Sample Charge	.37
Table	6-II. H	Calculated Charge Function Value for Various Potentials $\tau/T1 = 10,000$ Sample Charge	.38

Table	6-111.	Location of the Reduction Potential on the Voltammogram
Table	6-IV.	Influence of the Step Size on the Current Function
Table		Influence of the Step Size on the Charge Function

LIST OF FIGURES

Figure 2-1.	Cyclic voltammogram and diffusion profiles for potassium ferricyanide (31)	6
Figure 2-2.	Cyclic voltammogram and Nernst line for potassium ferricyanide (31)	12
Figure 2-3.	Electrode solution interface model (31)	18
Figure 2-4.	The staircase waveform	19
Figure 2-5.	Potentiostatic control circuit (31)	23
Figure 2-6.	Distortion of voltammogram due to solution resistance (13)	27
Figure 2-7.	Electrical equivalent of the chemical cell	27
Figure 3-1.	Examples of coulostatic pulse waveforms which result in the same charge transfer to the cell	45
Figure 3-2.	Electrical equivalent of a chemical cell containing geometric capacitance	48
Figure 3-3.	Delahay's charge injection circuit	52
Figure 3-4.	Reinmuth's charge injection circuit	53
Figure 4-1.	The charge injector used in this study .	56
Figure 4-2.	The digital to analog converter	59
Figure 4-3.	The analog to digital converter	61
Figure 4-4.	Analog switch with D-MOSFET construction	63
Figure 4-5.	An example of a charge to voltage	68

Figure	4-6.	The effect of cell resistance on the injector output voltage	70
Figure	4-7.	The effect of charging voltage on the settling time	7]
Figure	4-8.	Combinations of injection capacitor and resistor to provide a rapid and stable injection pulse	72
Figure	4-9.	The effect of injector resistance on the injection amplifier output voltage .	73
Figure	4-10.	The effect of injection charge on injection amplifier output voltage	74
Figure	4-11.	The effects of the bandwidth capacitor and injector resistance on the injection amplifier's output voltage	75
Figure	4-12.	The effect of cell resistance on the injection amplifier's output voltage at a constant charge injection value	76
Figure	4-13 A.	The effect of the number of injections on the total charge injected for charging voltages: A=2.5 V, B=2.0 V, C=1.0 V, D=.498 V, C_{inj} =0.0010 μF	78
Figure	4-13 B.	See 14-A C _{inj} =0.0051 μF	79
Figure	4-13 C.	See 14-A C _{inj} =0.0103 μF	80
Figure	4-14.	The slopes of lines in Figures 4-13 A, B, and C for different charging voltages	82
Figure	5-1.	General instrumental diagram of the main components of the charge injector .	86
Figure	5-2.	A conceptual potential step trimmed to the desired level with small charge injections	91
Figure	5-3 A.	Flow chart of cyclic voltammetry	98
Figure	5-3 B.	Flow chart of cyclic voltammetry	99
Figure	5-3 C.	Flow chart of cyclic voltammetry	100

Figure	6-1.	The Faradaic and capacitive current decay curve. Step size-10 mv, step potential=0.5 V, reduction potential= -0.637 V, step time τ =500 ms, and t_m =5 ms
Figure	6-2.	Flow chart for STEPI.FTN 108
Figure	6-3.	Effect of solution resistance on the capacitive current decay curve. Resistance A=100 Ω , B=1000 Ω ; step size=10 mV and t _m =5 ms
Figure	6-4.	The effect of electrode capacitance on the charging current decay curve. Electrode capacitance A=40 μF , B=5 μF , step time τ =500 ms, and t_m =5 ms 111
Figure	6-5.	The effect of step size on the Faradaic and charging current decay curve at a constant sweep rate. Step size=6 mV, $t_m=5$ ms step time $\tau=2080$ ms and sweep rate=3.8 v/s
Figure	6-6.	The effect of step size on the Faradaic and charging current decay curve at a constant sweep rate. Step size=10 mV, $t_m=5$ ms step time $\tau=2080$ ms and sweep rate=3.8 v/s
Figure	6-7.	The effect of step size on the ratio of capacitive current to Faradaic current at constant sweep rate. Sweep rate= 3.8 mV/s and $t_m=5$ ms
Figure	6-8.	The calculated change in step charge with time for 1x10-6 M CdCl ₂ at a step potential of6 v vs. SCE 119
Figure	6-9 A.	Influence of the ratio of $\tau/t1$ on reversible current voltammograms. Step size 10 mV
Figure	6-9 B.	Influence of the ratio of $\tau/t1$ on reversible current voltammograms. Step size 10 mV
Figure	6-9 C.	Influence of the ratio of τ/tl on reversible current voltammograms. Step size 10 mV
Figure	6-9 D.	Influence of the ratio of τ/tl on reversible current voltammograms. Step size 10 mV

Figure	6-10.	Flow chart for charge voltammograms 130
Figure	6-11.	Step time periods T1 and T2 for a potential step
Figure	6-12A.	Influence of the ratio of $\tau/t1$ on reversible charge voltammograms. Step size=10 mV, A=sample charge, B=presample charge
Figure	6-12 B.	Influence of the ratio of $\tau/t1$ on reversible charge voltammograms. Step size=10 mV, A=sample charge, B=presample charge
Figure	6-12 C.	Influence of the ratio of τ/tl on reversible charge voltammograms. Step size=10 mV, A=sample charge, B=presample charge
Figure	6-12 D.	Influence of the ratio of $\tau/t1$ on reversible charge voltammograms. Step size=10 mV, A=sample charge, B=presample charge
Figure	6-13.	Charge injected during time Tl. A= large injections, B=small injections. 1 x 10 ⁻⁵ M CdCl ₂ in 0.01 M KCl 145
Figure	6-14.	Deviations of the cell potential from the desired cell potential. 1 x 10^{-5} M CdCl ₂ in 0.01 M KCl
Figure	6-15.	Non-linear potential scan resulting when no trim injections are applied. The solid line is the ideal scan from theory and circles are experimental points
Figure	6-16.	Current voltammogram increase in the step size at a constant sweep rate
Figure	6-17.	The effect of an increase in step size on charge voltammograms at a constant sweep rate. Sweep rate 3.33 v/s , $\tau/t_m=1$, $(-)=n(2)mv$, $(x)=n(10)mv$, $(*)=n(50)mv$, where n is the number of electrons

Figure	6-18.	Shift in peak potential with increasing step size. "A" step size 2 mV, $t_m=20$ ms, $\tau=520$ ms, "B" step size 10 mV, $t_m=500$ ms, $\tau=2600$ ms
Figure	6-19.	Experimental charge voltammograms at increasing sweep rate. From largest voltammogram to smallest, the sweep rate is: 15, 80, 190, 814 mV/sec 157
Figure	6-20.	Theory and experiment peak charge vs. sweep rate. Step size = 10 mV and T1-2 ms
Figure	6-21.	Theory and experiment peak charge vs. concentration. Step size 10 mV, $\tau = 105$ ms, and T1 = 5 ms 161
Figure	6-22.	Total step charge voltammogram CdCl ₂ in 0.02 KCl
Figure	6-23.	Tl charge voltammogram CdCl ₂ in 0.02 KCl
Figure	6-24.	T2 charge voltammogram CdCl ₂ in 0.02 KCl
Figure	6-25.	Peak charge vs. concentration obtained for summed multiple scans. Number of scans = $(x) = 25$, $(+) = 16$, $(0) = 9$, $(\#) = 4$, $(1) = 1$
Figure	6-26.	Total charge under voltammogram vs. peak charge. 1 x 10 ⁻⁵ M PbCl ₂ 168
Figure	7-1 A.	Adsorption study of lead chloride 182
Figure	7-1 B.	Adsorption study of lead chloride 183
Figure	7-1 C.	Adsorption study of lead chloride 184
Figure	7-2.	Determination of the adsorption of lead chloride
Figure	8-1.	Counts vs. charging voltage 196
Figure	8-2.	Relative standard deviation vs.

.

.

LIST OF SYMBOLS (ROMAN)

SYMBOL	MEANING	DIMENSIONS
A	area	cm ²
С	capacitance	F
c _{dl} c _g	differential capacitance of the	F
uı	double layer	
C_{α}	geometric cell capacitance	F
Ci	integral capacitance of the	Ī
_	double layer	
C _{inj} C*	injector capacitor	F
C*	bulk concentration	M, $mol/cm3$
[]*	concentration in bulk solution	M , $mo1/cm^3$
$C_{\mathbf{X}}$	concentration at distance x	M , mol/cm^3
	from the electrode	•
Ρj	diffusion coefficient of species j	cm ² /sec
DAC	digital to analog converter	none
ADC	analog to digital converter	none
E	potential of the working electrode	V
	vs. a reference	
ΔΕ	potential change	V
Ep	peak potential	V
$E_{\rm D}^{\rm P}/2$	half peak potential	V
Ep/2 Ei E0	initial potential	V
ΕQ	standard emf of a half reaction	V
E0'	formal potential of an electrode	V
Eeq	equilibrium potential	V
Ena	anodic peak potential	V
Epa Epc	cathodic peak potential	V
$\mathbf{E}_{\mathbf{Z}}^{\mathbf{r}}$	potential of zero charge	V
E1/2	reversible half wave potential	V
- , -	$E^{0'''}(RT/nF) ln(D_r/D_0) 1/2$	
$\mathbf{E}_{\mathbf{W}}$	working electrode potential	V
F	charge on one mole of electrons	С
i	current	Α
\mathtt{i}_{a}	anodic current	Α
ic	cathodic current	Α
id	diffusion limited current	Α
if	Faradaic current	Α
im	migration current	Α
i _C	charging current	A
ip	peak current	Α
K	conductivity of solution	a/Ω cm)
k _b	heterogeneous rate constant for	cm/sec
-	oxidation	

		: : :
		:
		:
		: :
		: :
		-
		:
		;

```
kf
          heterogeneous rate constant for
                                                         cm/sec
           reduction
in
           exchange current
                                                         Α
                                                         none
m
           step number m
          number of electrons per
                                                         none
n
                                                         M, mol/cm^3
[0]
          concentration oxidized species
          molecule
O
          charge
                                                         M, mol/cm^3
[R]
          concentration reduced species
                                                         J/(mol\ K)
R
          gas constant
           solution resistance
R_{\mathbf{S}}
R_{f}
          feedback resistor
                                                         Ω
R_{\mathbf{u}}
          uncompensated resistance
                                                         Ω
          radius of the working electrode
                                                         cm
r_w
          radius of the counter electrode
                                                         CM
r_a
          radius of the reference electrode
                                                         cm
r
Т
                                                         ٥K
          absolute temperature
TIDD
          Tl time period
                                                         sec
TIDD1
          T2 time period
                                                         sec
T1
          first time period of step
                                                         sec
Т2
          second time period of step
                                                         sec
t
          time
                                                         sec
\mathsf{t}_{\mathsf{s}}
          R<sub>s</sub>Cd1
                                                         sec
\mathsf{t}_{\mathsf{m}}
          current measurement time for step m
                                                         sec
t_{11}
                                                         sec
          RuCd1
                                                         V
          output voltage
V<sub>0</sub>
v_p
          peak output voltage
                                                        V
                                                         V
          reference voltage
\mathtt{v_r}
                                                         V
Vcel1
          cell voltage
          voltage at time t
٧+
          DAC voltage used to establish the
                                                        V
VAPDA
          initial potential
                                                        V/sec
v
          linear potential scan rate
                                                        cm
X
          distance from working electrode
          same as above
Х
                                                         Ω
Z
          impedance
          charge on species j
Ζi
                      LIST OF SYMBOLS (GREEK)
          (D_0/D_r)^{1/2}
                                                        none
Υ
                                                        V
          over potential, E-Eeq
n
          exp((nF/RT)(E_i-E^{0'}))
                                                        none
                                                        time
          total step time sec
τ
                                                        none
          current function
```

I INTRODUCTION

The Achievement of Staircase Cyclic Voltammetry with a Microcomputer-Controlled Coulostatic Polarizer

Polarography was one of the first automated intrumental analytical techniques. The dropping mercury microelectrode, invented by J. Heyrovsky in 1922, served as the transducer for converting chemical data into electrical data. The electrical data then could be converted to a number or a scale position by means of a moving coil meter or by a chart recorder. The development of automated instrumental analysis became so important that J. Heyrovsky won the Nobel Prize in the late 1950s for his work in polarography.

A.O Linear Sweep Voltammetry

Linear sweep voltammetry (LSV), first practiced by Matheson and Nichols in 1938 (1), was discovered as an off-shoot of polarography. The first experiments employed a rapidly changing voltage applied to a dropping mercury electrode. The technique was then known as oscillographic polarography. Randles and Sevcik derived theoretical expressions for oscillographic polarograms based on the diffusion of ions to a plane surface (2,3). Experiments with the use of a stationary mercury pool electrode were initially conducted to reduce the effects of current fluctuations encountered during the growth of the mercury drop

(4,5,6). The voltammograms contained peak currents which depended upon the diffusion of electroactive material to the electrode. These experiments were more sensitive than those of DC polarography and enabled the characterization of homogeneous coupled chemical reactions which could not be easily studied with the dropping mercury electrode. The technique became popular and eventually known to most workers as linear sweep voltammetry. The experiment in which the potential was reversed and returned to the initial value in a cyclic manner was first practiced by Sevcik (3) and became known as cyclic voltammetry (CV). The theory was later developed by Matsuda (7).

LSV and CV are very useful in characterizing electrochemical systems, determining the reversibility of electrochemical reactions and obtaining kinetic information about electrochemical reactions (2,3,7,8).

Despite the usefulness of LSV and CV, these techniques have not found use for routine quantitative analysis because other electroanalytical methods, such as differential pulse polarography, are more sensitive. This research project has focused on the problems encountered when conventional electrochemical methods are employed to analyze dilute solutions with low electrolyte concentrations because of large charging currents and high solution resistances. Under these conditions reversible voltammograms for normal cyclic voltammetry appear quasi-reversible. The characteristics of a charge injector enable it to be applied favorably under

these conditions and has been chosen for use in a new measurement process and instrument applied to the electroanalytical method of cyclic voltammetry. Cell potential control is achieved with a microcomputer-controlled charge pulse injector. The digital record of the charge injections takes the place of the conventional analog method of measuring the instantaneous net cell current. An algorithm is implemented in which charge injections are applied to step the cell voltage periodically to produce the staircase polarization waveform.

A coulostatic charge pulse is one which is over before the Faradaic reaction has consumed a significant fraction of the pulse charge. One advantage gained by using a coulostatic pulse is due to the discontinuous nature of the applied current. The cell potential is measured between charge pulses when no net current passes in the cell and thus IR drop error is eliminated. With the charge injector placed under microcomputer control, a step change in cell potential is achieved by the rapid application of the proper size and number of charge injections. The desired step potential is maintained by injecting small charge pulses to the electrode as needed to supply the Faradaic current. From the number and size of the charge pulses injected during the step, the total Faradaic charge consumed during the step can be calculated. The resolution in the Faradaic charge is determined by the number of injections required during the constant potential part of the step. The signal to noise ratio and the sensitivity are maximized because the Faradaic current is effectively integrated during the entire step duration. No double layer charging current occurs during this time if the electrode area is constant. In contrast to normal cyclic voltammetry, decreasing the scan rate (increasing step duration) results in larger voltammogram peaks.

Therefore with the advantages of this method, it is expected that this charge injector will find wide application in a variety of electrochemical experiments where the charging current is high and the solution resistance great.

II THEORETICAL HISTORICAL DEVELOPMENT LEADING TO THE MODIFIED CHARGE INJECTOR

A.0 Characteristics and Limitations of Voltammetry

Figure 2-1 A shows a typical cyclic voltammogram (9). The cell current is shown on the vertical axis; the horizontal axis is the range over which the potential is scanned. The analysis solution is 6 mM potassium ferricyanide in a water solution. A supporting electrolyte of 1M KCl is added to increase conductivity. The solution is kept quiet so that the principal means of mass transport to the electrode surface is by diffusion. Mass transfer by thermal convection, agitation, or stirring of the solution is minimized. Migration current, which results from the transport of electroactive ions to the electrode by electrical interaction, is avoided by adding an excess of supporting electrolyte.

In the experiment of Figure 2-1 A, three electrodes were immersed in the solution: a platinum sphere working electrode of about 0.03 cm², a saturated calomel reference electrode, and a platinum coil counter electrode which has a much larger surface area than the working electrode. The main cell current is between the working and the counter electrodes. The cell potential is measured between the working and the reference electrode. The reference



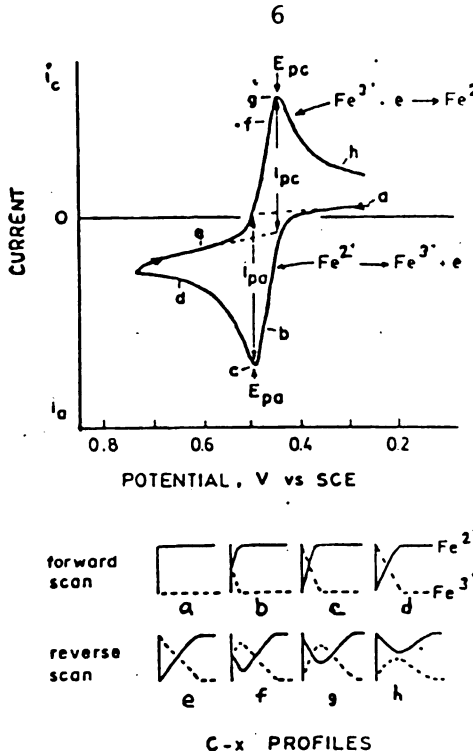


Figure 2-1. Cyclic voltammogram and diffusion profiles for potassium ferricyanide (31).

electrode current is very low because of the high impedance of the voltage measurement system.

Even though the potential scan starts well positive of E for the reduction of potassium ferricyanide, the cell current is not zero because the electrode capacitance must be charged. The charging current is equal to the sweep rate (v) in volts/sec times the double layer capacitance (C_d1). In this region there is no Faradaic current because the electrochemical reaction can not occur at this potential. As the potential becomes more negative, the electrochemical reaction begins and the Faradaic current is added to the charging current. The concentration of ferricyanide decreases and a concentration gradient is generated with the

electroactive material increasing in concentration with increasing distance from the electrode. The rate of the electrochemical reaction can be governed by the rate of diffusion of electroactive material to the electrode or by the rate of electron transfer itself, or both. In this case, the electron exchange between ferricyanide and ferrocyanide is very fast so the overall reaction is completely diffusion controlled. Under these circumstances, the relationship between the electrode potential and the surface concentration of ferricyanide and derrocyanide is given by the Nernst equation.

The behavior of the diffusion controlled current during the potential scan can be understood by carefully examining the concentration distance profiles illustrated in Figure 2-1 B (9). The current observed at any potential for the voltammogram is explained by the slope of the corresponding concentration distance profiles at the electrode surface. The current is proportional to the slope or concentration gradient as explained by Fick's first law (10):

$$i/nFA = D_0 (\partial C_0/\partial X)_{x=0}$$
 (2-1)

Where i is the Faradaic current, n is the number of electrons transferred per ion, F is Faraday's constant, A is the area of the electrode in cm², D₀ the diffusion constant for the oxidizable species in cm²/sec, C₀ is the concentration of the oxidizable species in moles/cm³, and X is the distance from the electrode surface in units of cm. The slope

is zero in profile 'a' and the current is negligible at this potential. As the potential is scanned negatively, the concentration gradient at the electrode surface increases for profiles c and d. The surface concentration changes in accordance with the Nernst equation. This establishes the concentration gradient which brings the reactant to the electrode. The cell current, corresponding to this slope, also increases. The concentration gradient of the reduced product, ferrocyanide, causes it to diffuse from the electrode surface to the bulk solution. In profiles d through e, the concentration gradients extend further into the solution as the electroactive material is depleted in the vicinity of the electrode and more product is formed. results in a decrease in the concentration gradient of ferricyanide in graphs d and e and therefore a decrease in current. Thus, the observed current behavior is for the voltammogram to increase to a peak due to the decreased surface concentration and then decrease due to the depletion of the electroactive material near the electrode. This region is known as the diffusion layer because its concentration is less than the concentration of the bulk solution. As the depletion region grows further into the solution the average distance that a reactant travels to the electrode increases and the concentration gradient decreases. Consequently, the cell current continues to decay. Beyond the peak, the current is independent of potential because the surface concentration is effectively zero. In this limiting diffusion

region the current is proportional to the inverse of the squareroot of time. At point f in Figure 2-1 A, the scan direction is then reversed and the potential proceeds back to the initial value.

In region i, the potential is in a position where both a reduction and an oxidation process can occur simultaneously. The net cell current is the sum of two opposite currents due to the reduction of ferricyanide and oxidation of the ferrocyanide. In profile k the concentration levels are approaching their initial level and the potential sweep is returned to the initial value. Not all of the ferrocyanide is converted back to the ferricyanide on the reverse scan because some material will escape by diffusion into the bulk solution. The amount of material lost into the bulk solution depends on the rate of diffusion and sweep rate. The charging current is +vC_{dl}, equal in value but opposite in sign to the initial value.

B.O Theory of Cyclic Voltammetry

Cyclic voltammetry is a relatively nondestructive technique because very little electroactive material is consumed, the bulk solution concentration, just a few millimeters from the electrode, is left unchanged. The height of the peak current, when measured from the proper baseline, is proportional to the bulk solution concentration. The baseline for the cathodic peak is easily determined by extrapolating a line drawn from two points in a region where little Faradaic reaction is occurring to the peak potential. The

peak current is then measured from this baseline to the peak. The residual or baseline current is due to electrode capacitance, impurities, and instrumental noise. The baseline for the anodic peak is more difficult to determine because the baseline must be drawn from the decay of the cathodic peak rather than a region of essentially no Faradaic current. If the cyclic voltammetry data are stored in a digital computer, points obtained from the decay of the cathodic peak can be fit to a non-linear least square line and extrapolated to the peak point under the anodic curve. The following equation is used to fit the decay curve (11):

$$i = A/(t-B)^{1/2}$$
or
$$1/i^2 = t/A^2 - B/A^2$$
(2-2)

Where A and B are arbitrarily chosen variables and t is time. If, however, the voltammogram is to be obtained on an x-y recorder the common practice is to extend the cathodic scan at least 35/n mV past the peak and extrapolate the decay current from the cathodic peak to the anodic peak potential. The anodic peak can then be measured from this baseline. When measured in this manner, the ratio of the cathodic to the anodic peak current for a reversible voltammogram is equal to one (12).

A reversible reaction is one for which there is a Nernstian ratio of the surface concentration of the reduced $([R]^0)$ to oxidized $([0]^0)$ species at each potential point

along the sweep. This relationship is defined by the Nernst equation, which pertains only to equilibrium systems (9):

$$E = E^{0} - (RT/nF) \ln ([R^{0}]/[0^{0}])$$
 (2-3)

where E is the electrode potential, E⁰ is the formal potential, [R] and [0] are the concentration of the reducible species and oxidized species at the electrode surface, x is the distance from the electrode surface and x=0 indicates a point at the electrode surface. Initially, a potential is chosen to start the potential sweep which avoids any electrolysis of the starting material. The starting solution for the experiment contains a large ratio of [R]/[0], and for the sake of this discussion the initial concentration is chosen to contain a ratio with logarithm (base 10) equal to 5. This indicates that [R]/[0] at the electrode surface is equal to a hundred thousand to one. The change in [R]/[0]is indicated by the number line in Figure 2-2 B. As the potential is scanned the ratio changes as governed by the Nernst equation and [R]/[0] decreases. At E equal to E^0 , [R]/[0] is equal to one. Past the peak the log of [R]/[0]becomes less than one. Finally, on return of the potential sweep [R]/[0] again adjusts at each corresponding potential and returns to the initial value.

To obtain the necessary theoretical equations for the diffusion controlled process at stationary electrodes it is necessary to apply Fick's laws and solve a boundary value problem. The boundary conditions are as follows (8):



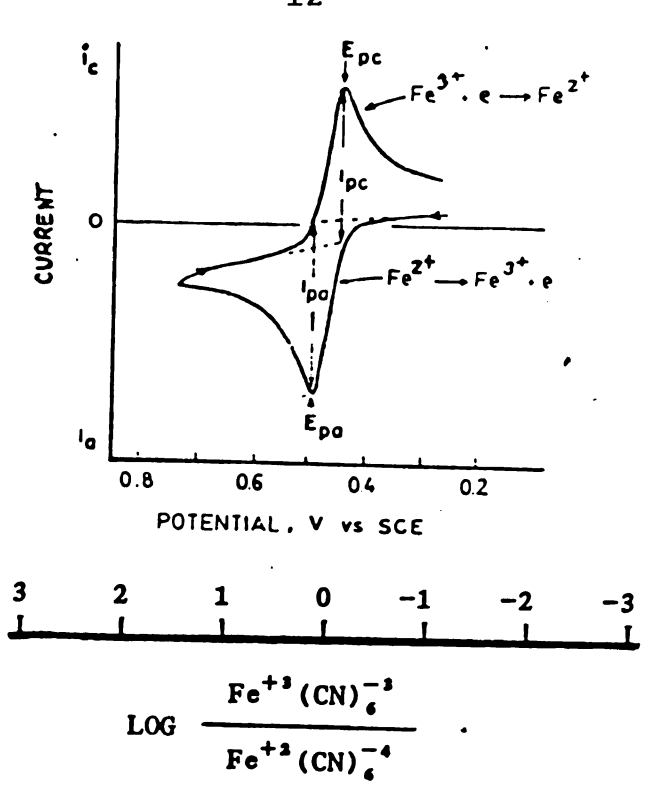


Figure 2-2. Cyclic voltammogram and Nernst line for potassium ferricyanide (31).

$$\partial [0]/\partial t = D_0 \partial^2 [0]/\partial x^2$$

$$\partial [R]/\partial t = D_D \partial^2 [R]/\partial x^2$$
(2-5)

$$t=0$$
, $X>0$, $[0]=[0]*$, $[R]=[R]*$ (2-6)

$$t>0$$
, $X\to\infty$, $[0]\to[0]*$, $[R]=0$ (2-7)

t>0, X=0,
$$D_0 = \partial[0]/\partial X = -D_R(\partial[R]/\partial X)$$

$$i/nFA=D_0 \partial [0]/\partial X)_{x=0}$$
 (2-9)

$$[0]^0/[R]^0 = \exp(nF/RT(E-E^0))$$
 (2-10)

Where []* indicates concentration in the bulk solution, equations (2-8) and (2-4) are statements of Fick's laws and the final boundary condition is given by the Nernst equation with E equal to the applied potential.

A quasi-reversible system is one in which the cell current is not always completely diffusion controlled. In

this case, the cell current is partially charge transfer controlled and the Nernstian ratio of [R] to [0] is not always maintained at the electrode surface. The cathodic and anodic peak currents are lower than the reversible case and the waves are spread out along the potential axis. The current-time relationship of a quasi-reversible system produces intermediate results (8):

$$D_0(\partial[0]^0/\partial X) = k_f[0]^0 - k_b[R]^0$$

where k_f is the forward rate constant of electron transfer and k_b is the rate constant of electron transfer for the reverse reaction. An irreversible system is the extreme case of this non-equilibrium process in which no anodic peak appears because the rates of either or both the electrochemical reactions are slow in comparison with the potential sweep rate. For a totally irreversible system the equation may be written (8):

$$D_0(\partial[0]^0/\partial X) = k_f[0]^0$$
 (2-12)

The final boundary condition is a function of the applied voltage waveform and therefore depends on the particular electrochemical technique of interest. For linear sweep voltammetry the control potential is determined by the following function (8):

$$E = E_{i} - vt \qquad (2-13)$$

Where E_{i} is the initial potential and v is the sweep rate in

volts/sec. The final boundary condition may thus be expressed as:

$$[0]^{0}/[R]^{0} = \exp(-nF/RT(E_{i}-E_{o}))\exp(-nF/RTvt)$$
 (2-14)

Where the symbols have their usual meaning. It is not possible to apply LaPlace transform procedures to these time-dependent equations. Randles (2) and Sevcik (3) were the first to consider a series solution to this problem. Later, the solution for a reversible system was presented by Nicholson and Shain by using numerical computer methods (8,12,13). Their results for a reversible system are given below (8):

$$i = nFA(aD_0C*\chi(at)^{1/2}$$
 (2-15)

Where A is the area of the electrode, $\chi(at)$ is a dimensionless flux, a=nFv/RT and v is the scan rate in volts/second. The cell current is thus predicted to be proportional to C*, $n^{3/2}$, and $v^{1/2}$. The peak width is related to the number of electrons transferred by:

$$E_p - E_{p/2} = -56.5/n \text{ mV}$$
 (2-16)

Where E_p is the potential at the peak and $E_{p/2}$ is the potential at half the peak current. The polarographic half wave potential is given by:

$$E_{1/2} = E^0 + (RT/nF) \ln (D_R/D_0)^{1/2}$$
 (2-17)

 $E_{1/2}$, is located on the rising portion of the voltammetric

peak 85.1 percent up the wave. This gives: (8).

$$E_p - E_{1/2} = -28.5/n \text{ mV}$$
 (2-18)

Because the cathodic peak is wide, it is sometimes more convenient to determine the potential at 1/2 i_p. Which is equal to:

$$E_{p/2} = E_{1/2} + 28.0/n$$
 mV at 25°_{0} C (2-19)

The location of $\rm E_{1/2}$ is about halfway between $\rm E_p$ and $\rm E_{p/2}$ and can be used as a test for a reversible wave.

ABS
$$(E_p - E_{p/2}) = 56.5/n$$
 mV at 25_0 C (2-20)

Thus for a reversible wave, the peak potential is independent of sweep rate and the peak current is proportional to $v^{1/2}$.

Cyclic voltammetry is used in many fields of study.

Organic chemists use it to study reaction pathways since after the electron transfer step many organic compounds produce unstable intermediates which then undergo chemical reactions. Electrochemically induced reactions which occur in the solution are called homogeneous coupled chemical reactions to differentiate them from the heterogeneous electrochemical reactions occurring at the electrode. Inorganic chemists often use cyclic voltammetry to evaluate the effect of ligands on a metal ion by studying the shift of the reduction potential and changes in the reversibility of redox system. Many other uses of cyclic voltammetry are found in

projects involving both research and routine quantitative analysis. It is important to understand the shortcomings of this method to avoid analysis errors and to provide insights for improving this widely used electroanalytical method.

C.O Limitations of Linear Sweep Voltammetry

In linear scan voltammetry, the charging current can limit the sensitivity. Charging current is by definition, the current which goes to change the working electrode potential. The total cell current is the sum of the charging current and Faradaic current. At fast sweep rates and in low concentration of electroactive species, the charging current can be large in comparison to the Faradaic current. The charging current increases directly as a function of the sweep rate 'v' but the Faradaic current increases only with the square root of the sweep rate 'v^{1/2}'. Thus, increasing the sweep rate does not always result in increased sensitivity because the more rapidly increasing charging current begins to interfere.

To better understand the origin of the charging current problem, a simple parallel plate model of the electrode solution interface was first proposed by Helmholtz almost a century ago. This model cannot truly represent the electrode solution interface for a number of reasons. First, the electrode is not an ideally polarized capacitor but is a 'leaky' capacitor because its charge can be consumed by electrochemical reactions. Second, it is not an ideal

capacitor but one in which the electrode capacitance is a function of potential. Third, the electrode capacitance depends on the solution chosen.

The electrode capacitance characteristics may be accounted for by considering the electrode solution interface. See Figure 2-3. The surface of the electrode is covered with a layer of dielectric solvent molecules or adsorbed species. This layer separates the charged electrode from a non-homogeneous layer made up of ions charged opposite to the electrode. This non-homogeneous layer is called the diffuse layer and ranges from a few to several hundred angstroms thick. Other workers have proposed models to account for experimentally determined electrode characteristics: P. Debye and E. Huckel (14), Gouy (15), Chapman (16), Stern (17) and D.C. Grahame (18,19,20). Theoretical corrections for, or modelling of charging current are only qualitative due to complications from specific adsorption, orientation of solvent molecules, and uncertainty of dielectric constants in the double layer. Therefore, experimental data is required for correction of charging current errors. It is necessary for modern electroanalytical methods to address this charging current problem in order to achieve useful sensitivities in many areas of application.

D.0 Staircase Voltammetry

The use of a staircase waveform to reduce the effects of charging current in linear scan voltammetry was first suggested by G. Barker and A. Gardner in 1960 (21). See

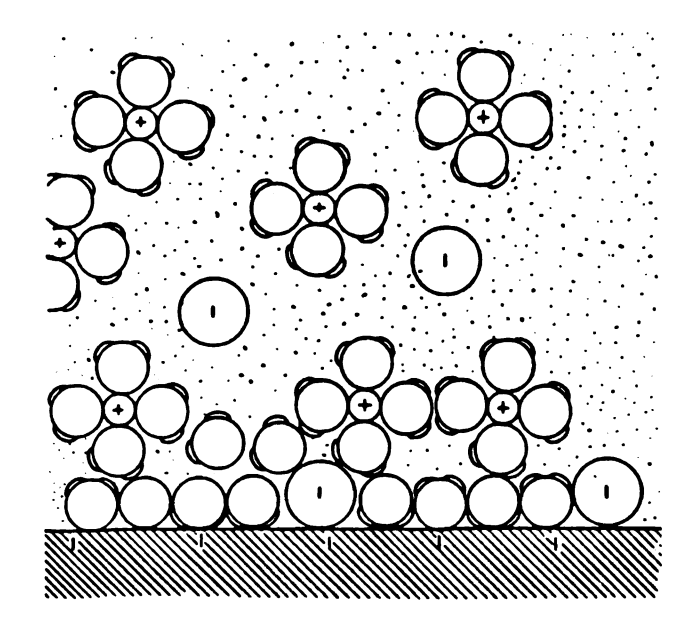


Figure 2-3. Electrode solution interface model (31).

Figure 2-4. When one attempts to step the potential of an electrode from an initial potential E_1 to E_2 , the double layer charges and the charging current decays exponentially with time:

$$i_c = (\Delta E/R_e) \exp(-t_m/R_eC_{d1})$$
 (2-21)

where i_C is the charging current, ΔE is the potential step size, R_e is the uncompensated solution resistance, C_{dl} is the double layer capacitance, and t_m is the time at which the current measurement is made. The Faradaic current resulting from the potential step increases rapidly due to the increased electrode potential and then decays as a function of the inverse squareroot of time as given by the Cottrell equation. G. Barker and A. Gardner suggested that the cell current be sampled at the end of the potential step when the charging current had decayed to a small value. The ratio of

the Faradaic current to the charging current could be made greater through this process since the decay rate of the Faradaic current is less than that of the charging current. The delay "purifies" the total cell current from the charging current interference.

POTENTIAL VS TIME

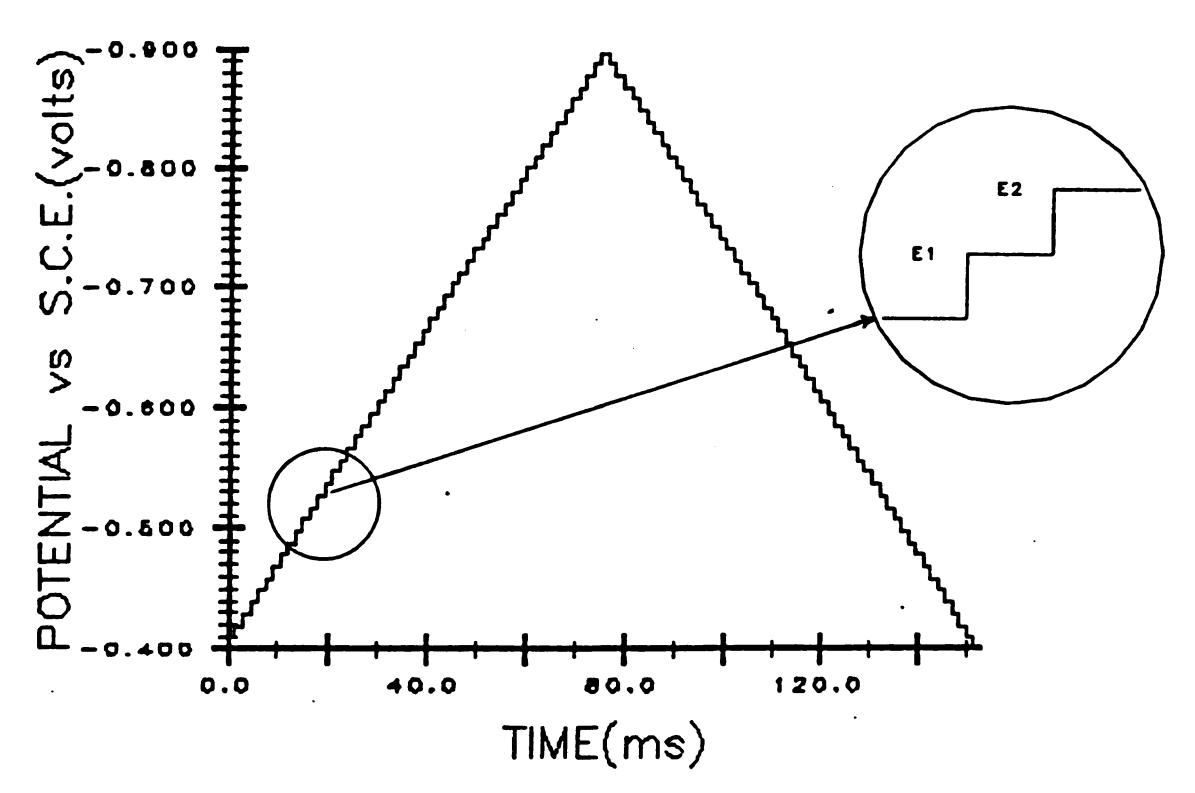


Figure 2-4. The staircase waveform.

The first experimental tests of staircase voltammetry (SV) were conducted by Mann (22,23,24) and Nigmatullin and Vyaselev (25). The staircase instrumentation they constructed enabled them to show the advantages of the staircase method and to make comparisons with linear scan voltammetry. They later developed a theory for small potential step intervals and showed how under these conditions

the results were equivalent to those of linear scan voltammetry. J. Christie and P. Lingane developed the current/potential/time relations for staircase voltammetry for any magnitude of potential step (26). They also pointed out the restrictions for the length of the step interval and the step size.

For a period of about eight years, little work was published using SV despite the distinct advantages offered by the method. The complexity of the instrumentation required for the generation of an accurate staircase waveform was the main drawback of SV when compared to the linear scan technique. When digital components increased in functionality and decreased in cost, the instrumentation requirements were more easily met. Today, because microcomputers are becoming very common in the laboratory, it could be said that staircase voltammetry is preferred to LSV and will become increasingly more popular and available on commercial In 1973, a number of workers applied computers instruments. for the control and evaluation of staircase voltammetry. Perone developed a computer compatible system for experimental and theoretical evaluation of the method (27,28). He presented the time dependence of the sampled current and showed how averaging multiple current samples could improve the signal to noise ratio. Theoretical relationships were given to show the dependence of sampling time on the voltammogram characteristics. The analytical capabilities of the method were optimized and compared with theoretical

predictions. D. Ferrier, D. Childester, and R. Schroeder developed a computer controlled instrument for evaluation of experimental and theoretical results (29,30). They developed the theory for the general reversible case, the quasi-reversible case (mixed charge transfer and diffusion control) and the irreversible case (total charge transfer control). Results were presented on the determination of heterogeneous kinetic parameters for electrode reactions. General procedures were established for the evaluation of experimental results and determination of rate constants. Errors and limitations of the staircase technique were presented. The effects of charging current and uncompensated solution resistance were also discussed. Their equations for the reversible case are presented below (30):

$$i_{m}/nFAC^* = \Sigma (2-(1+\gamma\theta_{i})/(1+\gamma\theta_{i-1}))$$

$$D_{0}-1/2(1+\gamma\theta_{i})\pi^{1/2}(t_{m}+(m-i)\tau)^{1/2}$$

$$\theta = \exp(nF/RT(E_{i}-E^{0}))$$
(2-23)

where the summation is from i=1 to step m, i_m is the current for step m, γ is the square root of the ratio of D_0/D_r , τ is the total step time, t is the instant in time that the current sample is taken and the other symbols have their usual meaning. This equation allows the calculation of the Faradaic current for any step in a staircase voltammogram. Note that the current for a given step in the voltammogram is dependent on the current from all previous steps. This

calculation is time consuming when done by hand and so computer methods are desirable. The equation does not include any charging current contributions to the cell current.

E.O Potentiostats

The first cells employed in electrochemistry contained only two electrodes, a working electrode and a combination reference and counter electrode. The accuracy of the cell potential control with the two electrode system is dependent on the solution resistance and the reaction occurring at the reference/counter electrode. By placing a third electrode, called the reference electrode, in the cell positioned as close to the working electrode as possible, these problems are reduced. The reference electrode is connected to a high impedance voltage follower to draw negligible cell current thus making the voltage measurement more independent of the cell current. The main current path is between the counter and the working electrode. The advantages of the three electrode system are especially significant with techniques which require rapid changes in electrode potential.

Figure 2-5 shows a conventional three electrode potential control circuit and cell (31). The control amplifier Al sums the input voltages so that $V_{\rm r}$ is equal to magnitude to the sum of the scaled input voltages and opposite in sign. The voltage follower output is connected to the summing point of the control amplifier Al thus providing a negative feedback loop. The potential of the working electrode relative to the reference electrode is opposite

in sign to V_r and the current at the working electrode is given a negative sign if anodic.

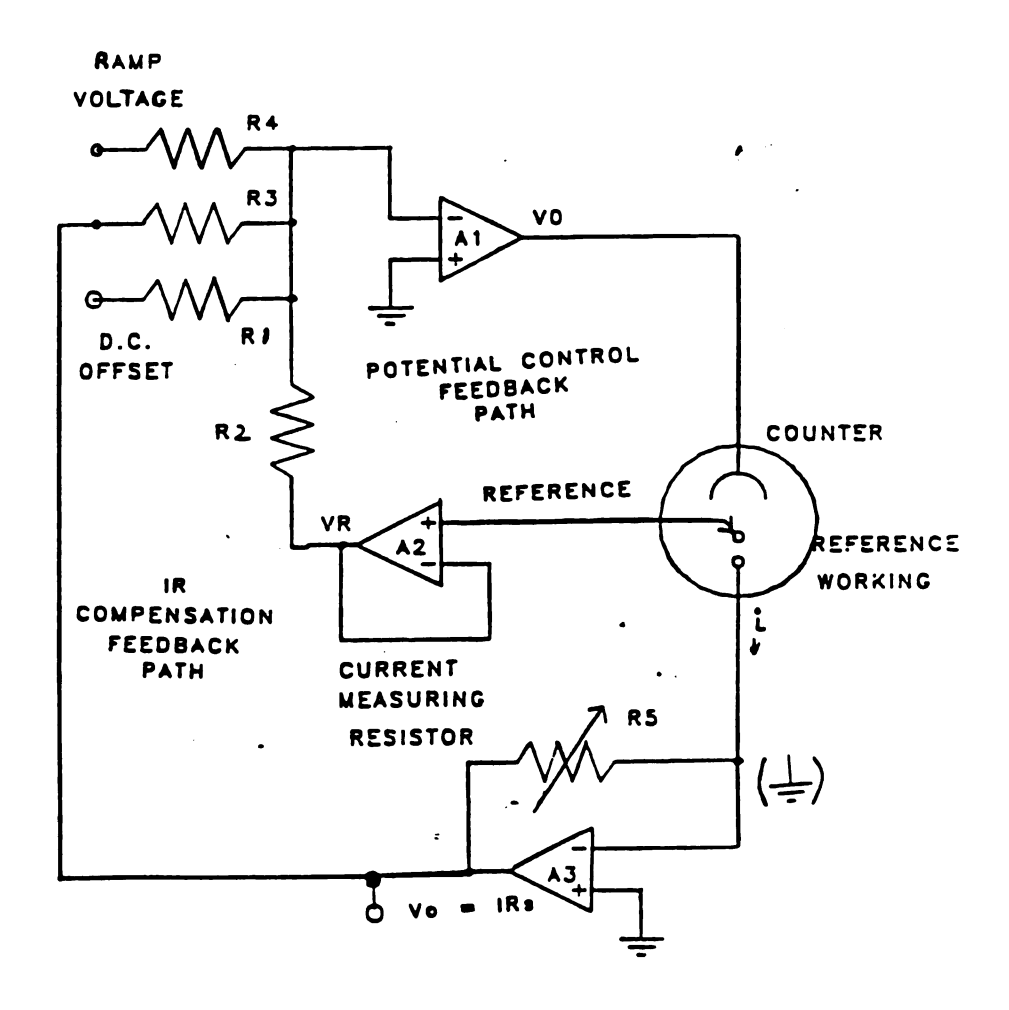


Figure 2-5. Potentiostatic control circuit (31).

The solution resistance between the working electrode and the reference electrode is not contained in the feedback loop of the amplifier Al and therefore any potential across this resistance is not compensated for. This results in an error, IR_u, in the potentiostatic control of the working electrode. As a result, accuracy of potential control is affected by solution conductivity and cell geometry. The details and consequences of this problem will be discussed next.

F.O Non-Ideal Effects Encountered with Potentiostats

The working and counter electrode in commonly used cells generate an electric field which approximates the field generated by electrodes constructed from parallel, circular planes. The resistance between the working and the auxiliary electrode can be given by:

$$R_s = 1/\pi K r_w (r_w + r_a)$$
 (2-24)

where the specific conductance of the solution is K (ohm cm) $^{-1}$, 1 is the linear distance between the working and the reference electrode, $r_{\rm w}$ is the radius of the working electrode and $r_{\rm a}$ is the radius of the auxiliary electrode. The resistance between the reference electrode and the working electrode is given by:

$$R_{11} = r/\pi K r_{w} (r_{w} + r_{a})$$
 (2-25)

where r is the radius of the reference electrode. Typical uncompensated resistance for a cell with 0.1 M KCl as an electrolyte would be 56 ohms for $r_a = 10$ cm, $r_w = 0.1$ cm and r = 1 cm. Two time constants may be defined to explain the potentiostat response to the load of the cell:

$$t_s = R_s C_{dl}$$
 (2-26)

$$t_{ij} = R_{ij}C_{dj}$$
 (2-27)

The symbols have their usual meaning. The time dependence of $\mathbf{V}_{\mathbf{r}}$ when a potential step is taken is given by:

$$V_r/V_0 = 2 - (2 - t_u/t_s) \exp(-t/t_s)$$
 (2-28)

where V_0 is the output voltage of Al, V_r is the output voltage of the reference electrode voltage follower, and t is The response of the potentiostat is exponential and there is a phase shift or time delay in V_r relative to the input voltage. The output voltage of Al may become excessively large because the corrective feedback signal is de-This will cause overshoot of the desired potential or even unstable oscillation. The benefit of decreasing R_{ij} and τ_{11} and thus IR has to be carefully considered because of problems with stability. It is often difficult to predict stability on real systems because of unknown effects of the Faradaic reaction on the electrode capacitance and re-The voltage at the working electrode is delayed sistance. behind the reference electrode and the input voltage. fast scans or potential steps where large Faradaic currents and large capacitive currents exist, errors in the potentiostat control can exist long after the perturbation force. Special care is therefore necessary to minimize R_{ij} . methods for decreasing the magnitude of the uncompensated resistance are presented below:

- High conductivity solution;
- Placement of the reference electrode close to the working electrode;
- 3. Positive feedback to correct iR, error.

The first method is impractical in organic solvents. The

second and third methods require that special attention be given to the stability of the feedback system. To avoid non-linear effects, the demand on the potentiostat must not exceed its output voltage, current, and slew rate.

G.O Distortions of the Voltammogram

Distortions of a voltammogram occur because of uncompensated solution resistance. This problem can occur even when the three electrode arrangement is used, even if the potentiostat is ideal. The distortions of the voltammogram alter the curves to such an extent that theoretical calculations which do not take this into account provide erroneous Mechanistic conclusions of the reaction rate may be misleading under these conditions. The distortion of the voltammogram is shown in Figure 2-6 (13). A reversible voltammogram is made to appear quasi-reversible because the reduction peak potential is shifted in the cathodic direction along the potential axis and the peak current is lowered. This problem is encountered in both linear scan (13,30-39) and staircase voltammetry (11,30) and can be understood by considering the electrical equivalent of a electrochemical cell as shown in Figure 2-7. The three electrodes present in the test solution are:

- 1. the counter electrode;
- 2. the working electrode (polarizable electrode);
- 3. the reference electrode (non-polarizable electrode).

Distortion of Voltammogram

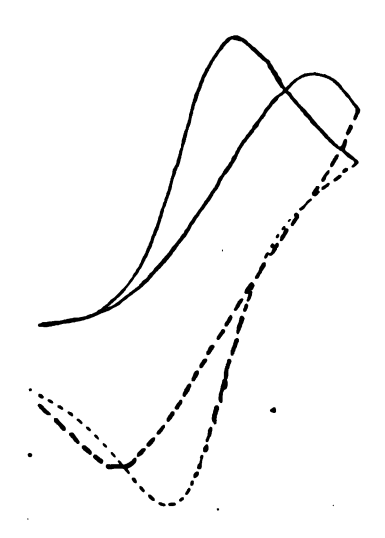


Figure 2-6. Distortion of voltammogram due to solution resistance (13).

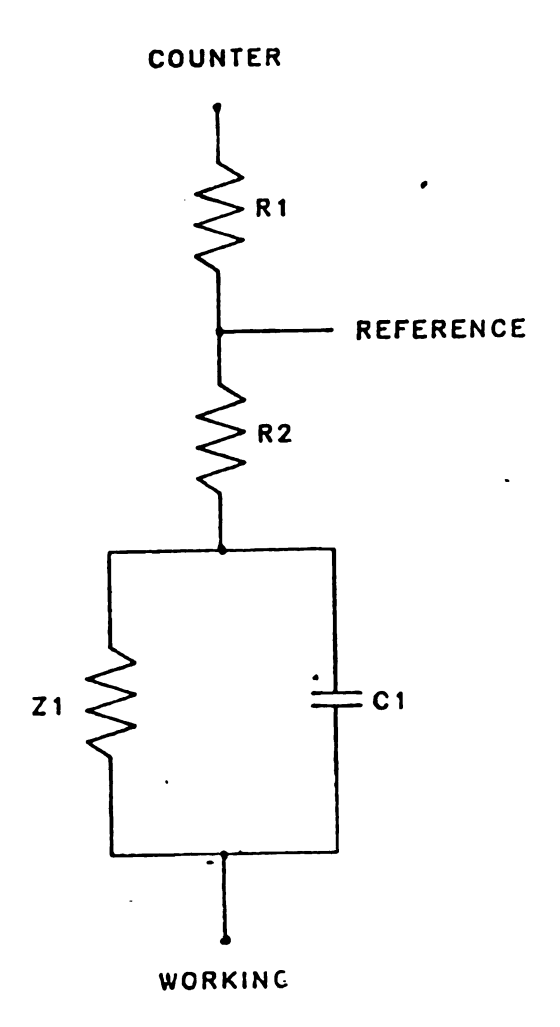


Figure 2-7. Electrical equivalent of the chemical cell.

The solution resistance which is a function of the cell geometry, and electrolyte concentration is indicated by R1+R2. This resistance can typically range from $0.1~\Omega$ to $0.5~M\Omega$. The impedance due to the rate of the electrochemical reaction is indicated by an impedance Z1. It's value depends on the reaction rate and the electrode charge density. A typical value is a hundred thousand ohms. The electrode double layer is indicated in the diagram by a capacitor.

When the potential is scanned, a continuous net current occurs between the counter and working electrode. The IR drop in the solution resistance between the reference and the working electrode causes the electrode potential to deviate from the applied potential. Thus, the potential felt at the electrode by the electroactive species is not that indicated by the potential axis on the voltammogram. This error may be several hundred millivolts. The magnitude of the error increases with the following experimental factors: current intensity at each point, electrode area, cell resistance, and sweep rate. The distortion of the voltammogram produces a cathodic displacement for a reduction peak, an anodic displacement for an oxidation peak, wider peak widths, and a non-linear potential scan.

A further problem is encountered with the staircase method because the solution resistance introduces a charging delay time for the charging of the double layer by the potential step. As a result, the measured cell current can

contain a large contribution from the charging current for an extended period of time. Another aspect of this delay time is that the step potential is not achieved instantaneously but changes in an exponential fashion. Thus, the change in C_R/C_0 at the electrode surface is slower than expected by theory. Proper mathematical analysis of solution resistance effects must take into account the Faradaic and charging current simultaneously. Mathematical analysis therefore requires complex numerical calculations and also many simplifying assumptions for the model of the electrode solution interface.

Instrumental methods directed toward reducing solution resistance affects can employ positive feedback techniques (40). The applied potential is related to the true operating potential at the working electrode by:

$$E_{w} = E_{app} - iR_{u} - \theta_{ref}$$
 (2-29)

where E_w is the potential at the working electrode, E_{app} is the applied potential, R_u represents that part of the solution resistance which is not compensated by the potential control loop and θ_{ref} is the reference electrode interfacial potential. An adjustable positive feedback is provided in the feedback loop such that the potential at the working electrode is now given by:

$$E_{w}(vs. Ref.) = E_{app} - iR_{u} + ifR_{u}$$
 (2-30)

where 'if' is the amount of positive feedback provided. In

an ideal case of 100% compensation, the entire voltage drop on the cell resistance is compensated and the voltage on the working electrode double layer is equal to the reference voltage regardless of the current in the cell. The time constant for charging the double layer in the ideal case is reduced to zero. The proper amount of positive feedback is many times difficult to determine. Too little feedback will result in the circuit being under compensated and when too much positive feedback is applied the potentiostat amplifier will oscillate.

The BAS-100 manufactured by Bioanalyical Analytical Systems is an elegant approach to these problems (41). A microcomputer controlled instrument determines the solution resistance by applying a potential pulse in a region where no Faradaic reaction can occur and then measures the resulting charging current decay curve. By extrapolating this curve back to zero time, i₀ can be determined and the solution resistance calculated from the following equation:

$$R_{11} = \Delta E/i_0 \tag{2-31}$$

where ΔE is the potential step applied and i_0 the resulting cell current at the beginning of the potential step. The positive feedback is then increased in incremental amounts and the stability of the amplifier is tested after each increase. The stability test consists of applying a 50 mV step and then measuring the resulting cell current at 20 K Hz for 50 msec. The minimum current and the maximum current

are used to determine the percent overshoot as:

% overshoot = ABS(
$$i_{min}/i_{max}$$
)100 (2-32)

The percent overshoot is compared to a preset overshoot level and when the best level is achieved, the percent compensation is decreased slightly and a stabilization capacitor is inserted between the counter electrode and reference electrode. In this way, oscillations of the amplifier are avoided and the operator is made aware of the solution resistance and the reliability of his or her data. The disadvantages of this positive feedback method are that the test of the potentiostat amplifier can disrupt the electrode surface making the study of adsorbed material impossible and the amount of compensation applied to the electrode is often less than ideal.

H.O The Coulostatic Method

The problems of solution resistance and electrode capacitance plague many electroanalytical methods. However, there is one method which offers a simple instrumental solution to this problem; it is the coulostatic or charge injection technique. The method may be explained by reviewing early experiments conducted using this method.

The earliest coulostatic experiments were performed by Delahay (42) and Reinmuth (43). The experiment consisted of charging the electrode from a potential E_i , where no Faradaic reaction is occurring, to E on the diffusion plateau of the polarographic I-E curve by the application of a

coulostatic charge pulse. An ideal coulostatic pulse is one in which all charge applied to the electrode goes to charging the electrode double layer and no charge is consumed by the Faradaic reaction during the application of the pulse. After the charge addition, the cell is placed at open circuit. Consequently, as the charge on the electrode is consumed by the Faradaic reaction, the electrode is discharged. Delahay presented the following equations for processes which were mass transfer controlled:

$$(C_i)_E(E-E_z)-(C_i)_{EC}(E_C-E_z) = \int I_d dt$$
 (2-33)

where $(C_i)_E$, and $(C_i)_{Ec}$ are the integral capacities of the double layer at E and E_c respectively, and E_z is the potential of zero charge. I_d is given by:

$$I_d = nFC* (D/\pi t)^{1/2}$$
 (2-34)

where a positive I_d designates a cathodic (+) and a negative I_d an anodic (-) process, n is the number of electrons transferred per ion, F Faraday's constant, C* the bulk concentration of electroactive material, D the diffusion coefficient and t is the time elapsed from the beginning of the experiment. C_i is assumed to be independent of potential over the interval $(E-E_C)$. From the above two equation Delahay wrote:

$$\Delta E = \pm 2 n F C_0 D^{1/2} / (\pi t)^{1/2} C \qquad (2-35)$$

The above equation suggests that the cell potential varies

linearly with $t^{1/2}$ and the bulk concentration c^0 can be determined from the slope of the ΔE vs. $t^{1/2}$ graph if the constant $P=2nFD^{1/2}/\pi^{1/2}$ C_i is determined for a known concentration. The important characteristic of this experiment is that the Faradaic current is separated from the double layer charging current by placing the cell at open circuit. No charging of the electrode can occur at open circuit, only discharging occurs as the charge is consumed by the electrochemical reaction. Therefore, the Faradaic current is exactly equal to the discharge current of the electrode double layer capacitance. Since the cell potential is measured when there is no current flowing in the cell, there is no IR drop error in the electrode potential measurement as well.

Delahay and Reinmuth used different instrumental methods to generate the potential step. Reinmuth coupled the cell to a fast rise pulse generator through a small capacitor (20-100 pF). Delahay charged a small capacitor (three orders of magnitude less than the double layer) using a high DC voltage and discharged it through the cell using a relay. Both methods required simple instrumentation and were successful in determining trace quantities of electrochemically reducible or oxidizable substances.

I.O Coulostatic Methods with Small Steps

Delahay and Reinmuth also developed a theory for coulostatic methods which employed small potential steps.

They took into account both the charge transfer rate and the

rate of diffusion of electroactive material to the electrode.

Reinmuth's equation for the change in cell potential with

time is given below:

$$\eta = \eta t = o(\beta_{+} - \beta_{-})^{-1} (\beta_{+} \exp(\beta_{-}^{2} t) \operatorname{erfc}(\beta_{-}^{2} t) + o(\beta_{-}^{2} t) + o(\beta_{-}^{2}$$

where η is the overpotential,

$$\beta_{+} = (\tau d^{1/2}/2\tau c) + 1/\tau c^{1/2}$$

$$[(\tau d/4\tau c) - 1]^{1/2}$$
(2-37)

and where the + is associated with β_+ and the - with β_- and

$$\tau c = RTC_{d}/nFI_{0}$$
 (2-38)

where τc is the charge transfer rate constant, τd is the diffusional time constant, C_R is the concentration of the reduced species, C_0 is the concentration of the oxidized species, D_0 is the diffusion constant for the oxidized species, D_R the diffusion constant for the reduced species D_R is the exchange current density.

Kinetic information about the electrochemical system can readily be obtained if the diffusion process is fast compared to the charge transfer process ($\tau c \gg \tau d$). In this case the derivation of the equation leads to:

$$\tau d = (RTC_d/n^2F^2(1/C_0D^{1/2} + 1/C_RD^{1/2}))^2$$

This charge transfer process is limiting when the solution contains a high concentration of electroactive species and

a low exchange current. The value of τc may be calculated from:

$$t_{1/2} = 0.69315 \ \tau c$$
 (2-40)

where $\tau_{1/2}$ is the time at which the overpotential is half its initial value. If C_d is known then I_0 can be calculated from Equation of τc . I_0 may also be obtained by plotting $\ln(\eta)$ vs. t.

If the diffusion process is fast compared to the charge transfer process ($\tau c \gg \tau d$) and is ignored in the derivation then the following equation is obtained:

$$\eta = \eta t = o \exp(-t/\tau c) \tag{2-41}$$

When the electrochemical system is partially charge transfer controlled and diffusion controlled obtaining, meaningful kinetic data can be difficult to obtain. The potential-time decay favors the charge transfer process at very short times. But at longer times, the diffusion control process becomes favored. This difficulty is minimized by choosing the experimental conditions to limiting the desired process. For example, high concentration and short times favor the measurement of the charge transfer process. But, problems still occur with very fast reactions. The reactant is rapidly consumed at the electrode thus creating a concentration gradient between the electrode and the bulk solution. The reaction rate can then become limited by the flux of reactant to the electrode surface, ie, diffusion once more

governs the reaction rate.

Another problem encountered is the determination of the electrode capacitance. The capacitance should be determined in the presence of the electroactive species but this presents difficulties when the concentration of the electroactive species is high because the electrode is not ideally polarizable. Adsorption may also complicate the capacitance determination.

Weir and Enke (44,45) modified the coulostatic technique by using a constant current pulse generator. The double layer capacitance could then be calculated from the slope of the charging curve during the application of the pulse by the following equation:

$$(d\eta/dt) = i_{+}/C_{d1}$$
 (2-42)

This has the advantage of avoiding the long extrapolations to zero time for capacitance determinations. It also has the advantage of rapidly determining the electrode capacitance during the injection pulse before any charge is consumed by the electrochemical reaction.

An instrumental problem is encountered in the measurement of the decay potential. The amplifier of the voltage measurement system is driven into saturation by the large voltage drop of the solution resistance. This occurs for the duration of the pulse and the voltage drop may be many times the charge transfer over potential. The amplifier recovery from saturation may be slow making the short time

response difficult to determine.

J.O Coulostatic Method with Large Potential Steps

The charge step method used by Delahay (46) moved the electrode potential from a region where no electrochemical reaction was occurring to a potential in the plateau region of the polarographic wave. This was done with a single large charge injection. If the electrode capacitance remains constant over this potential region, then the following equation applies:

$$\Delta E = 2nFC_0 (D\pi t)^{1/2}C_{d1}$$
 (2-43)

where ΔE is the change in the electrode potential with time t, n is the number of electrons transferred per ion, C_0 is the concentration of the oxidized species, and the other symbols have their usual meaning. The following typical values may be placed into the above equation: $C^*_{dl} = 20 \ \mu AF/cm^2$, $D = 10^{-5} \ cm^2/sec$, and n = 2. This yields the following formula:

$$\Delta E = 0.344 t^{1/2} C_0 \tag{2-44}$$

Therefore for a concentration of C_0 equal to 10^{-5} M the expected potential change after 1 µsec would only be 0.334 mV. For a 10^{-7} M solution the potential change is only 0.00334 mV after 1 µsec! To get potential changes which are readily measured for dilute solutions it is necessary to allow enough time between recorded data points for the potential to decay by a measurable amount.

The potential change at any given time decreases when the double layer capacitance increases. Delahay and Ide showed that sensitivity of the coulostatic method can be decreased and thus allow more concentrated solutions to be studied (47). They extended the concentration range of study from 1×10^{-3} to 1×10^{-4} M. This was accomplished by placing a capacitor in parallel with the cell. They showed that the following equation applies:

$$^{\Delta E}(cp)^{/\Delta E}(cp=0) = C_{d1}^{A/[(C_{d1}^{A})+c_{p}]}$$
 (2-45)

where ΔE_{cp} is the voltage decay with a capacitor placed in parallel to the cell, $\Delta E_{cp=0}$ is the voltage without the capacitor, C_{dl} is the double layer capacitance and A is the area of the electrode.

It is advantageous to compare the technique used in this study to that used in the original coulostatic experiment. In the original coulostatic experiment the potential decay curve was recorded as a function of time and the object of the experiment was to succeed in recording the potential decay curves at very short times after the potential step. The charge injection method used in this study seeks to prevent the potential decay by adding charge to the electrode to maintain the step potential constant. However, the new problem of adding charge quickly and accurately to the electrode is encountered. The rate of charge injections used in my research does not permit measurements on the microsecond time scale. However this is not required for

diffusion controlled electrochemical techniques which are performed on the millisecond time scale, and longer.

K.0 Summary and Relevance

The charge injection method proved to be very sensitive and applicable to a wide range of experimental systems.

Despite this fact the method hasn't gained wide acceptance.

One possible reason for it's limited use is the fact that the potential decay curve resulting from the experiment is not as easy to analyze as a peak or step function output.

Charge injection methods have been used to imitate other electroanalytical techniques and provide output data which is more characteristic of the electrochemical system and familiar to the user. By applying the charge injection technique to other methods it is hoped that the advantages of the charge injection method may be carried over and apply to these other techniques. Previous workers have applied charge injection methods to polarography (48,49), differential pulse polarography (50), chronopotentiometry (51,52), anodic stripping voltammetry (49,52,53), coulometry (54,55), and amperometry (56,57).

Delahay applied coulostatic charge injection to anodic stripping to increase sensitivity (53). A metal ion in solution is plated in a mercury crop and a coulostatic pulse is applied which brings the cell potential in a range where the metal of interest is oxidized. The cell potential is recorded at open circuit for a fixed period of time. It was shown that a plot of ΔE vs. $t^{1/2}$ for the potential decay

curve was linear if the plating time was sufficiently long.

Sensitivity was increased and difficulties resulting from double layer charge were reduced from those encountered with direct anodic stripping.

A technique which combines the coulostatic method and a scanning voltage sweep was developed by J. Kudirka, R. Abel, and C.G. Enke (48). It was called charge step polarography. In this method a dropping mercury electrode is used. Late in the drop life a potential pulse is applied to the electrode. The potential pulses are increased in size on each successive drop to step the cell potential into the diffusion limiting region. The decay curve is recorded by a small computer and the slope and intercept of the E vs. t^{1/2} plot is calculated and stored for each charge injection. A plot of the slope vs. intercept for each increasing chargestep resembles a DC polarograph. The method was shown to be useful in the analysis of dilute solutions of metals using low concentration of supporting electrolyte.

An instrument to perform scanning coulometry was developed from DC polarography by M. Katzenberger and P. Daum (50). It is called differential coulostatic polarography. A dropping mercury electrode and a linear potential ramp is used as in conventional polarography but near the end of drop life, when the area of the drop is changing the least, the ramp voltage is disconnected from the cell and a coulostatic pulse is applied to jump the cell voltage. The cell potential is then measured at open circuit for a

predetermined amount of time as in the conventional coulostatic method. A parameter related to the slope ΔE vs. $t^{1/2}$ curve is calculated and plotted vs. the cell potential. Peaks are obtained with $E^{1/2}$ at the peak and the peak height is proportional to the bulk concentration of the electroactive species.

M. Schreiber and T. Last developed a computer controlled coulostat for anodic stripping analysis (52). The instrument was programmed to perform linear sweep anodic stripping or constant current chronopotentiometry following the deposition of a metal ion onto a think film mercury/wax impregnated graphite electrode. Linear sweep voltammetry was performed by making a small potential step with each charge injection. After each injection the cell potential was permitted to decay as charge was consumed by the Faradaic reaction. The potential decay was compensated for by varying the charge injection size for the next step and thus maintaining a constant potential step size. For each potential step the differential electrode capacitance was calculated from:

$$C_{d1} = Q/\Delta E \qquad (2-46)$$

where Q is the charge size injected and ΔE is the cell potential change resulting from the charge injection. The charge consumed by the Faradaic reaction is then calculated from the electrode capacitance and dE resulting from the potential decay for each step. A plot of this step charge

vs. potential results in a peak charge which is proportional to concentration.

Chronopotentiometry was also performed by injecting constant charge sizes in equal intervals of time. This is equivalent to a constant current. Constant current chronopotentiometry was also performed by C.C. Lee using a charge injector (51). Corrections for charging current errors were made by determining the double layer capacitance from a blank and calculating the charge required for the cell potential change in the blank and then applying this extra charge in a subsequent experiment which contained the electroactive material. The dE vs. time plots were shown to become more ideal as the corrections were applied to subsequent analysis.

Charge injection methods have also been applied to liquid chromatography using flow through cells (56). Non-aqueous solutions which have high cell resistance because of their inability to dissolve a large excess of supporting electrolyte, may be analyzed by the charge injection method.

III CHARGE INJECTORS AND THE CELL'S RESPONSE TO A COULOSTATIC PULSE

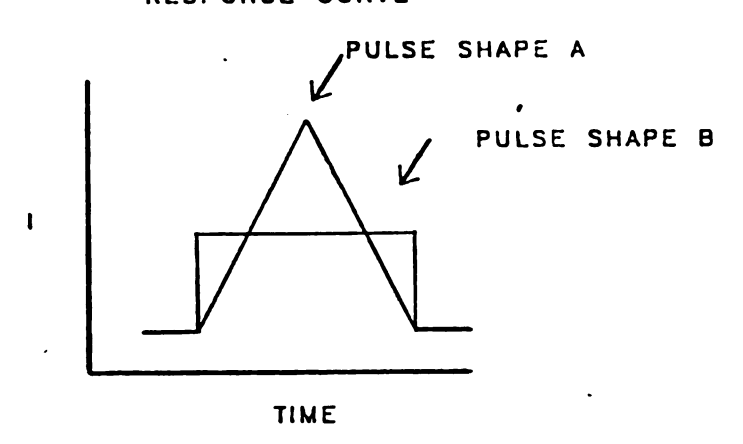
A.O A Coulostatic Pulse

The function of a charge injector is to deliver charge to the working electrode in a 'coulostatic' manner. The term 'coulostatic', as defined by Herman P. van Leeuwen (56,57), in his review of work in this area applies to charge pulse polarization in which all the charge in the pulse is used initially to charge the double layer capacitance; for the entire duration of the pulse, no charge is consumed by electrochemical reactions. The ability of the charge injector to meet this criterion depends upon the characteristics of the cell, the time scale of the electrochemical reaction, and the capabilities of the charge injector. It is the purpose of this chapter to describe the response of the electrochemical cell to charge injections and to describe the different types of charge injectors which have been used in the study of electrochemistry.

The maximum time allowed for the injection of a coulostatic pulse, as defined above, is dependent upon the characteristics of the electrochemical system being studied. The rate of electron transfer and the concentration of the electroactive species are two important characteristics of the system to consider. For example, a high concentration and very fast electrochemical reaction such as the Hg⁺²/Hg electrode system requires that the double layer be charged within a fraction of a microsecond to avoid significant Faradaic current during the charge injection. On the other hand, at low concentration or for slow irreversible system like Cr⁺³ in KCl, negligible Faradaic current would occur even if the injection pulse were to last a few milliseconds. Therefore, the term coulostatic is not absolute but is a relative term which depends upon the particular system being The term coulostatic originates from the method of application of the charge and the requirement that a known charge is applied to the electrode on each injection. Familiar names like 'coulostatic polarography' are improperly used because the chemical system must be defined before the name 'coulostatic' may be applied but these techniques have been around too long to consider ridding them from the nomenclature (56).

The charge pulse is applied to the cell in the form of a current pulse of various shapes, but brief duration. Different current-time profiles can contain the same quantity of charge and therefore they are identical in the coulostatic sense. For example, the coulostatic pulses in Figure 3-1 are considered equivalent when they contain the same charge content applied over the same duration. The resulting potential change at the electrode is the same for either wave form.

CHARGE INJECTION FORM AND RESPONSE CURVE



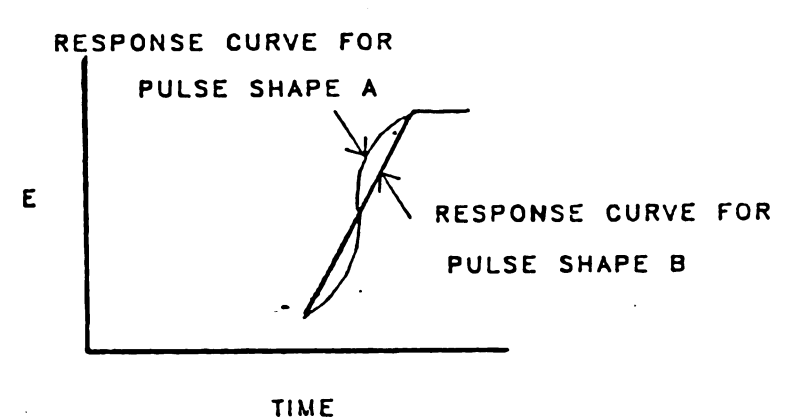


Figure 3-1. Examples of coulostatic pulse waveforms which result in the same charge transfer to the cell.

B.O Response of the Electrochemical Cell

The coulostatic method may be thought of as the limiting case of the galvanostatic or the potentiostatic method. The current vs. time pulse of the galvanostatic method in the limiting case, becomes tall and narrow. For the potentiostatic method, the limiting case is a very sharp potential step followed by the application of a current sufficient to maintain the potential. All three methods result in a sudden change in charge density at the electrode but only the coulostatic method places the cell at open circuit after the

pulse application. The cell current for the potentiostatic
method is given by:

$$i_{m} = -i_{C} - i_{f} \tag{3-1}$$

where i_m is the measured current density, i_C is the charging current density, and i_f is the Faradaic current density. In coulostatic polarization, $i_C >> i_f$ during the charge pulse, between pulses the double layer discharges through one path, the Faradaic impedance (Z_f) . Therefore:

$$-i_C = i_f \tag{3-2}$$

There is no i_m and i_c+i_f must be zero. Thus coulostatic polarization has a fundamental advantage for the determination of the cell current because the Faradaic current is exactly equal to the double layer capacitance discharge cur-In contrast, with potentiostatic polarization, it is impossible to measure independently the charging current and the Faradaic current since only their sum is measured. charging current continues after the step potential has settled because the cell is not placed at open circuit after the step. If the cell potential is stepped, the reference electrode potential includes $i_m R_{11}$. R_{11} is the term given to the uncompensated solution resistance. This error in the cell potential measurement causes the electrode to approach the desired potential exponentially, not immediately. time constant for the potential and the charging current ic, is RC_{d1}.

0.0

elect

iciti injec

of tw

subje

Under

paran

ce]]

any vo

by Fi

charge

1x10-

time.

Parall

çe{ore

nation

C.O Cell Response to a Fast Ideal Injection

It is also important to consider the response of the electrochemical cell to a very fast charge injection. The double layer can not respond instantaneously to a charge injection. Consider an electrochemical cell to be composed of two planar electrodes in a solution of a 1:1 electrolyte subjected to an ideal small-amplitude charge injection.

Under these conditions, the following frequency independent parameters apply:

- l. Geometrical capacitance C_g , which results from the formation of a capacitor from the two electrodes with the electrolyte solution in-between. C_g may have a value of about 6×10^{-11} F.
- 2. Interfacial double layer capacitance ($C_{\rm dl}$), which is created by the electrode-solution phase boundary. The $C_{\rm dl}$ of the mercury electrode in 0.01 M KCl may have a value of 2×10^{-5} F/cm².
- 3. The solution resistivity R(s), is created by the nature and concentration of the electrolyte. R_s was found to have a value of $1 \times 10^{+3}$ ohms for 0.01 M KCl for the cell used in these studies.

The electrical equivalent of a 2-electrode chemical cell containing the geometric capacitance may be represented by Figure 3-2. An ideal charge injection could charge C_g to any voltage in a very short time. For example, an ideal charge injection of 1×10^{-8} C would be able to charge the 1×10^{-11} F capacitor to 1000 V in an insignificant amount of time. If $C_g << C_{d1}$ then at times shorter than $t < R_s C_g$ the parallel combination of C_g and R_s dominates and C_g charges before any charging of C_{d1} . At long times the series combination of C_{d1} and C_g dominates. When a charge injection is

ELECTRICAL EQUIVALENT

OF CHEMICAL CELL

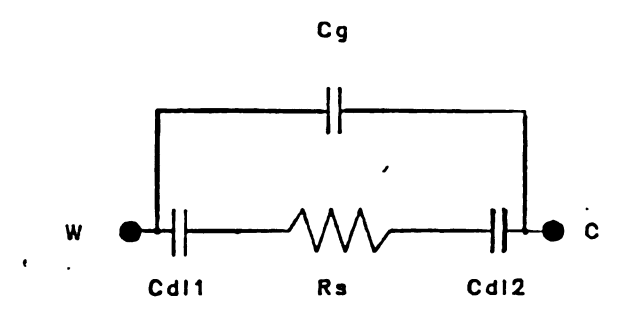


Figure 3-2. Electrical equivalent of a chemical cell containing geometric capacitance.

applied to the electrodes, C_g charges and generates an electric field across the solution between the electrodes. The electric field then causes the charge carriers in solution to move. The discharging of C_g is termed the 'relaxation process' and has the time constant of $R_s C_g$. The relaxation process is effectively the charging of the double layer capacitance which may be expressed as:

$$V_t = \Delta Q(C_q)^{-1} \exp(-t/t_e) + \Delta Q(C_{d1})^{-1} (1 - \exp(-t/t_e))$$

where V(t) is the electrode voltage at time t, ΔQ is the change in charge density of the working electrode, t_e is the time constant for the relaxation of the double layer $(R_s C_g)$, and other symbols have their usual meaning. When $C_g << C_{dl}$ the second term in the above equation is only effective at long times. A typical values of τ_e for a 1 M 1:1 electrolyte would be less than a tenth of a nanosecond but this time could increase if the cell resistance or C_g increases.

The value of τ_e increases roughly with the inverse of electrolyte concentration. The charging of electrode double layer is not restricted by the double layer relaxation process because it is much faster than the typical injection time of 1 SmAsec. The completion of this relaxation process then sets the electrode at a potential and this point marks the beginning of the electrochemical experiment for the discharge of C_{d1} by the Faradaic process.

D.O Cell Response to Non-Ideal Injections

The charge injector used in this research is not ideal because the output voltage of the charge injector is limited by the injection amplifier's maximum output voltage and because the injection time is dependent upon the input and output loads to the injection amplifier. However, the definition of 'coulostatic' does not require an ideal injection pulse but that insignificant Faradaic charge is consumed during the application of the pulse.

The ability to measure the injection time accurately may be a limitation in discerning the true coulostatic nature of a fast injection. The voltage amplitude and duration of the charge injection are influenced by the quantity of charge injected and the solution resistance. A typical charge injection may produce a voltage spike of several volts in height, when measured between the counter electrode and ground, which lasts a few microseconds in duration. The electrode potential change, measured between the working and reference electrode, resulting from this charge injection

may be only a few millivolts because of the relatively large electrode capacitance. This is indicated by the following equation:

$$V_{cell} = V_{inj} C_{inj}/C_{dl}$$
 (3-4)

where V_{cell} is the resulting cell voltage measured between the working and the reference electrode, V_{inj} is the voltage on the injecting capacitor C_{inj} , and C_{d} is the differential electrode capacitance. Therefore, the following characteristics are demanded of voltage measurement system:

- 1. high speed for recording the transient;
- insensitive to high voltage overload which can be produced in the input amplifier of the voltage measurement system during the first microseconds of injection of a large quantity of charge. A voltage overload produced in the input amplifier may allow the injection pulse time to be completed before the amplifier recovers;
- 3. sufficient sensitivity to measure a cell response which may only be a few millivolts.

To test the 'coulostatic requirement' that only a charging or discharging of the electrode capacitance can occur
during pulse application, the following tests may be applied
to the cell:

- 1. An external resistor which is of the same order of magnitude as the cell resistance is placed in series with the cell. The potential relaxation curve, which is recorded after the cell is placed at open circuit, shouldn't be effected by this added resistance for a coulostatic injection.
- 2. The charge content of the injection ΔQ is divided by the initial overvoltage ΔE to yield the differential electrode capacitance. Verification of the

- electrode capacitance confirms a coulostatic charge injection.
- 3. The duration of the pulse is varied along with the pulse amplitude such that the charge content of the pulse remains constant. The potential relaxation curve measured at open circuit shouldn't be effected by these changes for a coulostatic pulse.

Verification of any one of these tests allows the experimenter to be assured that the charge injection is indeed being applied such that the application of the perturbation force is separated in time from the electrochemical response and therefore performed in the 'coulostatic manner'.

E.O Design of Charge Injectors

An ideal charge injector is designed to meet the require-requirements of the definition of a 'coulostatic pulse' and to allow injections variable in charge content to be made rapidly. The charge injector should be able to make large or small potential steps. Large potential steps demands that the charge injector have a high current output. For example, to take a 1 V potential step in 1 μ s on an electrode with a capacitance of 1 μ F, requires a current in excess of 1 A. In spite of these difficult requirements, most charge injectors require very simple and inexpensive instrumentation.

P. Delahay applied the principles of coulostatic charge injection using a small capacitor charged to a high voltage (40). His circuit is shown in Figure 3-3. The quantity of charge which is injected to the cell with a 1 nF injection capacitor and a 100 volt power supply would be 1×10^{-7} C.

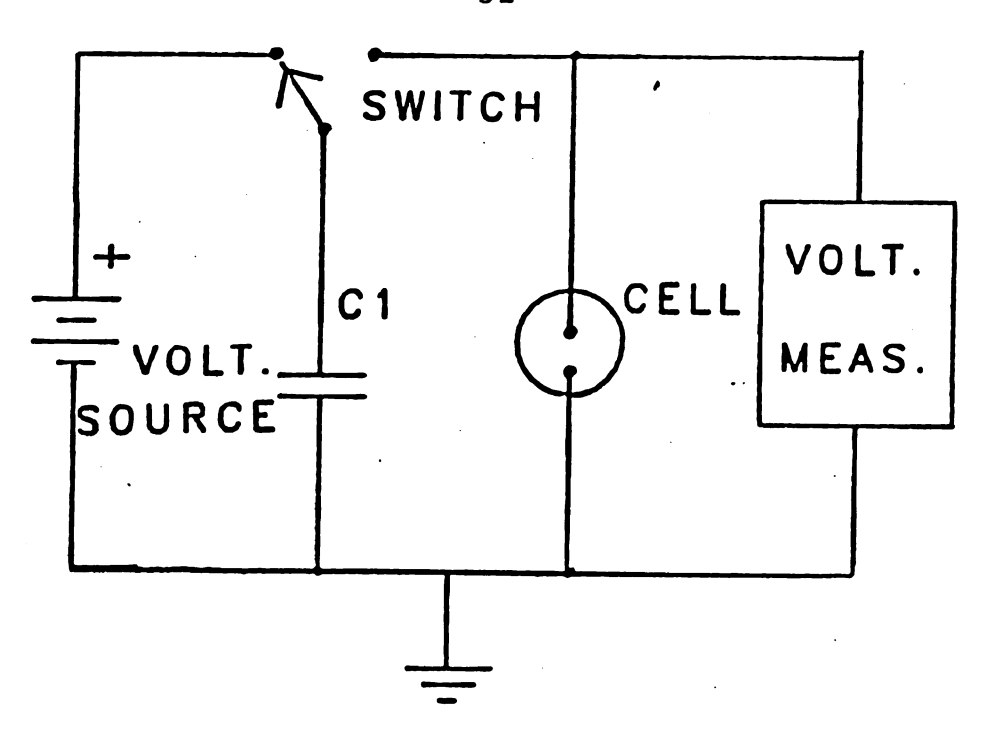


Figure 3-3. Delahay's charge injection circuit.

For an electrode capacitance of 1 μF , the resulting potential change would be 100 mV. The waveform of the charge injection is an exponential decay. The time constant of the decay is equal to $R_s C_{inj}$. To obtain fast injection times in the presence of a large solution resistance requires a small injecting capacitor. The injection of a large quantity of charge requires a high charging voltage and an amplifier for the voltage measurement capable of sustaining a high input voltage at a high impedance. For example, if a charge of 1×10^{-7} C is to be applied in 1 μsec to a cell with a solution resistance of 1 $k\Omega$, then using a 0.1 nF injection capacitor would require a power supply of as large as 1000 V. The accessable time range is thus limited as R_s increases because the rapid addition of charge to the electrode is not possible.

W. Reinmuth used a charge injector of another design (41). He coupled the cell to a fast rise pulse generator. A block diagram is shown in Figure 3-4. The load resistance is chosen to be large in comparison to the solution resistance to ensure a well defined constant current pulse. The charge content which is applied to the cell can be varied by changing the pulse amplitude and duration. The charge content of a 10 volt pulse through a 10 K Ω load resistance for a period of 1 μ sec yields 1×10^{-9} C.

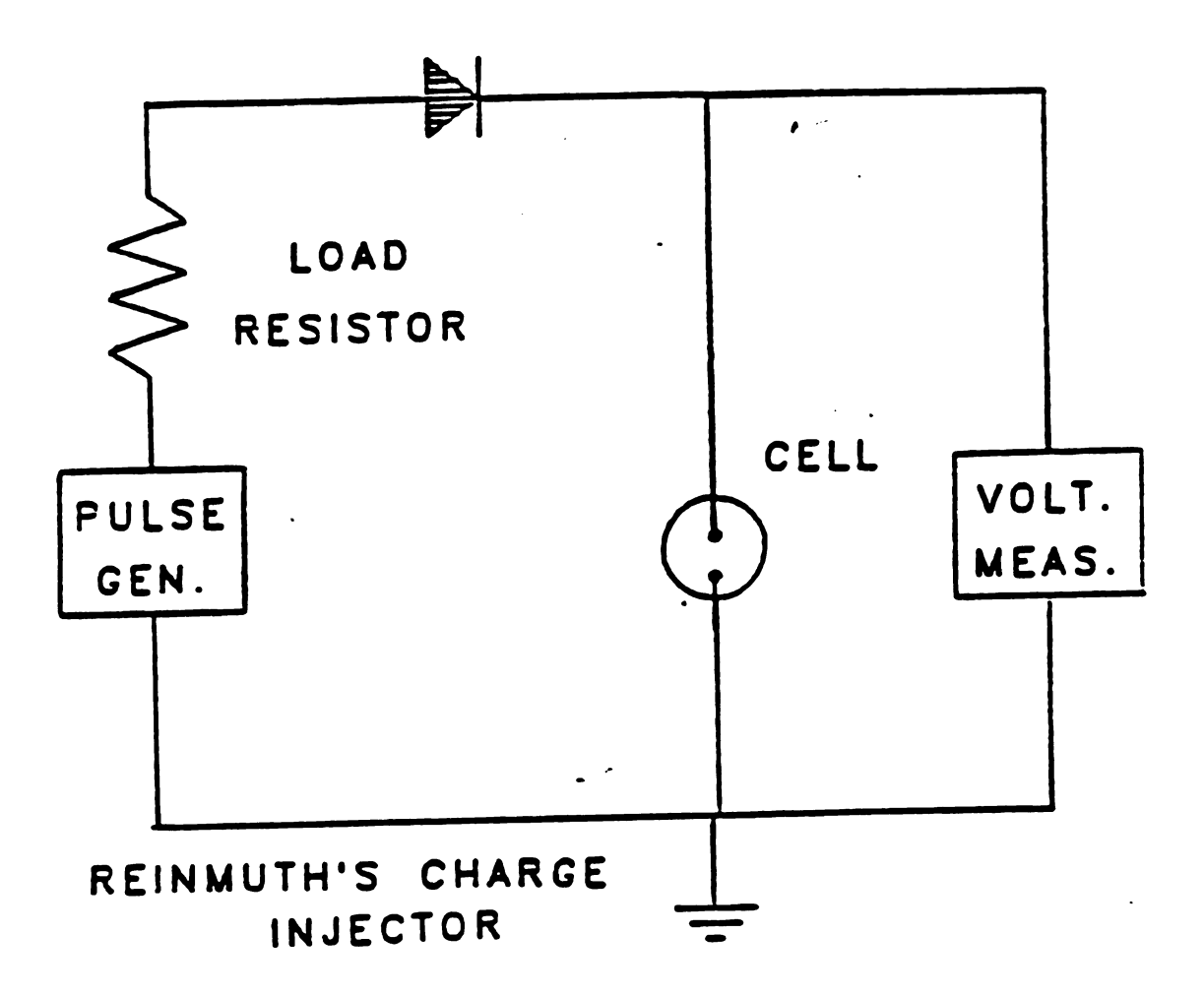


Figure 3-4. Reinmuth's charge injection circuit.

W. Goldsworthy and R. Clem developed a pulsed constant current driver which enabled the rapid addition of a variable sized injection (58). Under the load of the electrochemical cell, the charge injector was more stable to oscillation than an analog potentiostat. The current capabilities of the gated current supply and the charge injection rate, determines how rapidly the charge injector can drive a capacitive load.

Another type of charge injector was designed by S. Hourdakis and C.G. Enke (59). It employed a buffer amplifier to deliver rapidly a variable size charge injection to the cell. The buffer amplifier is able to inject charge through a large solution resistance. T. Last increased the power of the injector by adding a power state between the buffer amplifier and the cell (52).

IV INSTRUMENTAL

A.O The Requirements and Testing of the Charge Injector

The success and quality of the electrochemical experiments in this study depend on the characteristics of the charge injector. It is important to understand the requirements and limitations of each component of the charge injector to appreciate its overall capabilities and limitations. This knowledge will also permit the optimization of electrochemical experiments and maximize precision and accuracy.

In this chapter each component of the charge injector is presented and characterized. Procedures for testing, calibrating, and adjusting the components are outlined. The operation range and accuracy of the charge injector is presented.

B.O The Complete Charge Injector

Figure 4-1 shows the complete schematic of the charge injector. A general description of the charge injector will now be given to review its operation.

A ten-bit word is loaded from the microcomputer to the digital to analog converter (DAC). This voltage is used to charge the injecting capacitors Cl and C2 (when Sl and S2 are in their left positions). Because of inverter Al, capacitor Cl will be charged opposite in sign to C2.

CHARGE INJECTOR

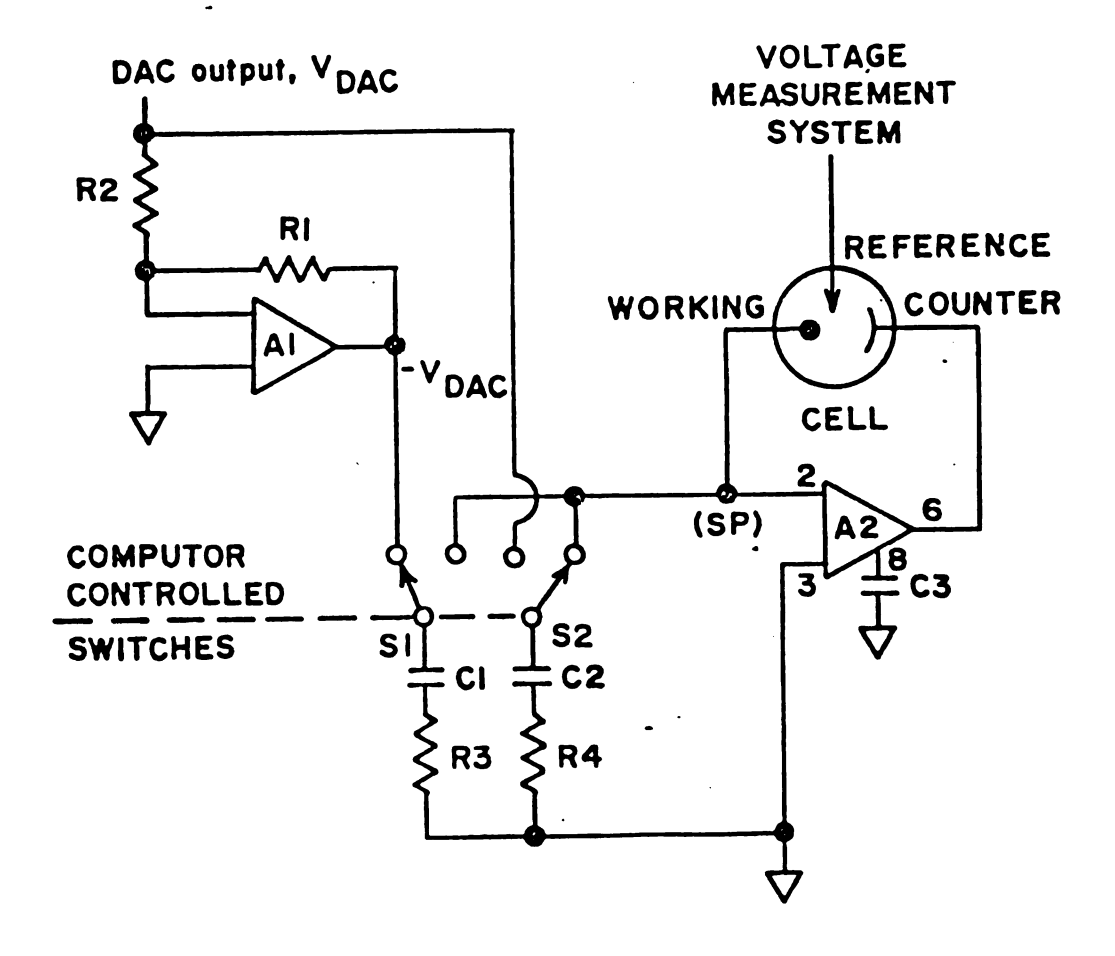


Figure 4-1. The charge injector used in this study.

Switches S1 and S2 are controlled by the computer and allow the independent charging of the injection capacitors and the dumping of charge to the injection amplifier A2. The non-inverting input of the injection amplifier is grounded so the amplifier works to maintain the summing point (SP) at virtual ground. When charge is dumped to the summing point through the switching of charge from the injecting capacitors, the summing point is quickly restored to virtual ground by the action of the injecting amplifier. This action effectively and accurately transfers all the charge on

		:
		:
		· -
		:
		:

the capacitor to the cell.

The injecting amplifier may be stabilized by one of the following means:

- 1. A feedback capacitor, not shown
- 2. An input resistor to delay the input of charge to the injecting amplifier, R3 and R4
- 3. A band-width limiting capacitor, C3.

When using the first method to stabilize the injection amplifier, it was found that capacitors between 10-1000 pF could be placed in parallel to the cell to stabilize the injecting amplifier. The injected charge is then divided between the cell and the stabilizing capacitor. The smaller the electrode capacitance and the greater the stabilizing capacitor, the greater is the error due to the diversion charge from the electrode. For example, if the electrode capacitance is 0.01 μF and the stabilizing capacitor is 1000 pF then a 10% diversion of charge will result. This calculation is not quite accurate because as the $C_{\rm dl}$ loses charge, the parallel capacitor will discharge through $R_{\rm s}$ to $C_{\rm dl}$. The time constant for the discharge of the stabilization capacitor to the double capacitance is given by the following equation:

$$\tau_s = R_s (C_s C_{d1} / C_s + C_{d1})$$
 (4-1)

where C_s is the stabilization capacitor. Besides charge inaccuracy, there is a possible IR drop error involved as well since the cell is no longer strictly at open circuit. For these reasons, the feed back capacitor was removed from the amplifier.

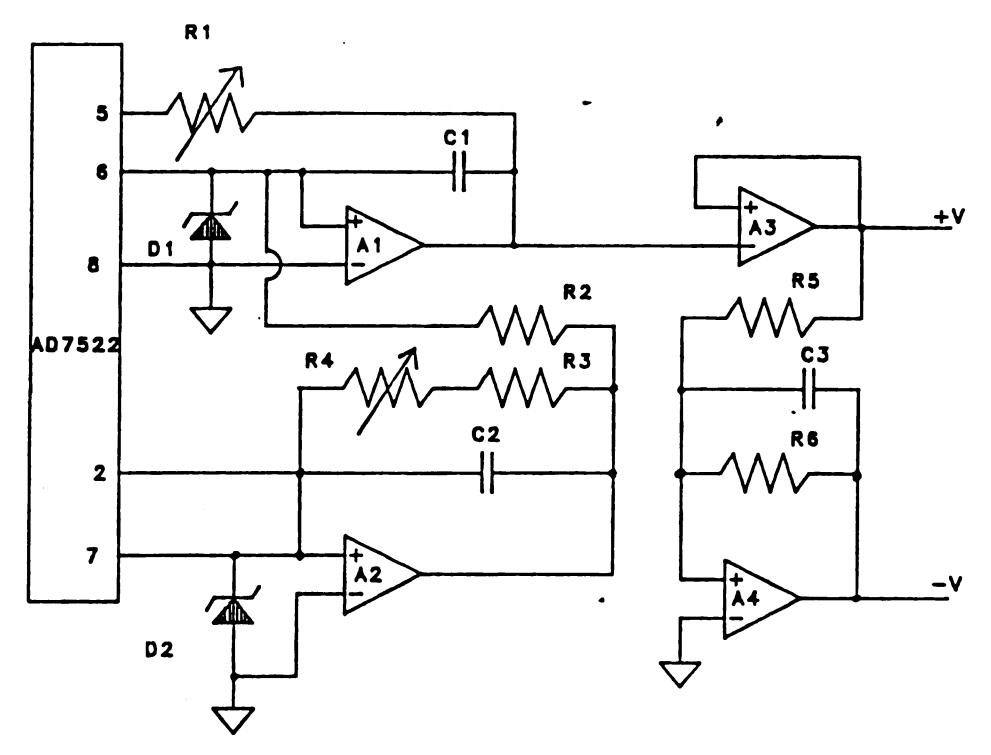
The second two methods to stabilize the injecting amplifier were therefore preferred. With the proper choice of the bandwidth capacitor (C3) and the input resistors (R3 and R4), a wide range of solution resistance can be studied. The input RC time constant for the discharge completely of the injection capacitor is calculated from the value of the input resistor and the injection capacitor used. Five or six time constants are given to allow the injection capacitors to discharge before the analog switches are thrown to recharge the injection capacitors.

C.O The Digital to Analog Converter

The digital to analog converter (DAC) is a ten-bit multiplying DAC (Analog Devices AD7522) it has a resolution of one part in 1024. The DAC may be configured for bipolar operation with a range of -2.5 to +2.5 V or for unipolar operation with a range of 0.0 to +2.5V. The unipolar DAC is therefore the preferred configuration since it provides the best voltage resolution (2 mV unipolar and 5 mV bipolar). However, the unipolar DAC can not always be used because in many cases a charging voltage of both polarities is required on both injection capacitors. This problem can be solved by using another analog switch which can be used to connect either polarity input to either injecting capacitor.

In the bipolar configuration either capacitor may be charged negative or positive. The DAC offset is adjusted by

loading the binary zero code into the DAC and then adjusting the current summed into the DAC amplifier so that the amplifier's output voltage is zero. This is done by adjusting the offset potentiometers (Rl and R4) shown in Figure 4-2.



THE BIPOLAR DIGITAL-TO-ANALOG CONVERTER

Figure 4-2. The digital to analog converter.

A convenient test of the DAC is made by running the program ADC.OBJ which can be downloaded into the microcomputer from the DEC 11/40 by running the program DOWNLOAD.TSK. Option one of this program allows the user to check fully the DAC. The following tests may be chosen:

- 1. Input a binary number directly into the DAC;
- 2. Specify the desired output voltage in millivolts;

- 3. Increment or decrement the DAC at a specified rate;
- 4. Alternate between two DAC values.

The output of the DAC has a range of ± 2.5 volts. The ten bit DAC thus has a resolution of 5.0 V/2¹⁰ which equals 5 millivolts (Monotonic DAC require accuracy to less than $\pm 1/2$ LSB). To avoid a large quantization error, it is therefore imperative that the DAC charging voltage not be too low. For example, a charging voltage of 1000 mV results in a quantization error of up to 0.5 percent. The non-linearity of the DAC is rated at 0.05 percent FSR. This factor is important when a large range of DAC values are used.

D.O Requirements of the Voltage Measurement System

The voltage measurement system is shown in Figure 4-3. The cell potential is measured between the working and the reference electrode. Very little current is drawn from the reference electrode because of the high impedance of the voltage follower amplifier A3. Amplifier A4 has a gain of two to allow the full ±5 V range of the ADC to be used to measure electrochemical cell potentials which rarely exceed +2.5 V.

Injection pulses may be as short as 1 μ sec and repeated every 0.2 msec. The voltage measurement system measures the voltage between charge injections pulses when the current between the counter and the working electrodes is zero, this avoids any IR drop error in the cell potential measurement. A sample and hold circuit is used to track the voltage

continuously and then to hold it constant during the digitization. The ADC (Datel ADC HY12BC) is a 12-bit successive approximation converter with a conversion time of eight microseconds.

VOLTAGE MEASUREMENT SYSTEM

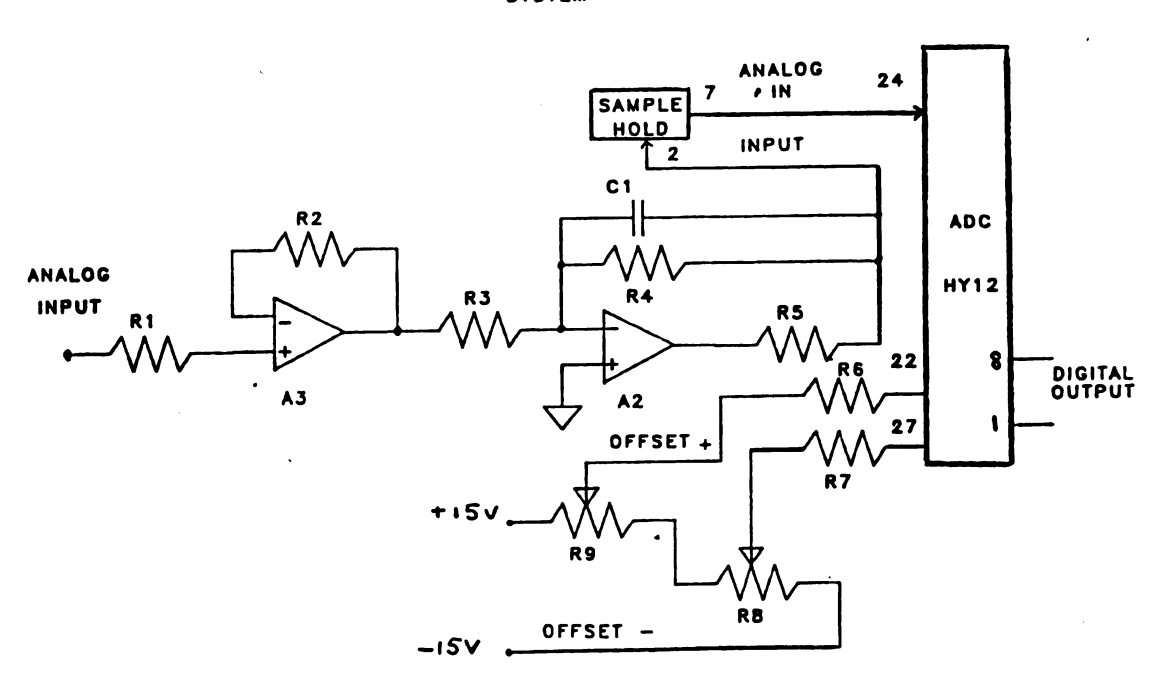


Figure 4-3. The analog to digital converter.

The ADC may be calibrated by downloading the program ADC2.OBJ. This program allows the user to make voltage measurements and to display them on the monitor one at a time or to cycle through and make repetitive measurements. A reference voltage source may be connected between the reference electrode and the instrument ground to provide the calibration source. Adjusting potentiometers R8 and R9 will allow the ADC to be set to the calibration source. A control-z breaks the program execution.

E.O Requirements of Analog Switches

The characteristics of analog switches are important for determining accurate signal transfer. The Signetics SD5000 D-MOSFET switches are used in the charge injector. The switches have an on resistance of 30 Ω and an off resistance of 10^{10} Ω . Isolation from output to input for a 3 KHz signal is -107dB. The switches have a very low input and output capacitance. Typical values are less than 3 pF. This allows charge to be quantitatively transferred through the switches to the cell. The SD5000 can be turned on at sub-nanosecond speeds and can more than meet our present charge injection rates. Mechanical or reed relays are limited to speeds of less than 5 KHz and have large input capacitance values and therefore are not suitable for this application.

The leakage current from the charge injector was measured to be in the nanoampere range. Since the switches are connected to the summing point of the injecting amplifier, the leakage currents from all switches are summed together. The leakage current was found to be independent of the DAC charging voltage (ie, the voltage across the open switch elements).

The leakage current for the charge injector was measured by putting a small capacitor in place of the cell and monitoring the voltage across the capacitor as a function of time. To avoid a measurement error, a balanced voltage follower was used for the measurement of the capacitor's

voltage. The leakage current of the analog switch connected to the SP of the injection amplifier was measured to be 1.0 nA with the switch open and 1.6 nA with the switch closed.

The switches are of D-MOSFET design, Figure 4-4. This design is different than the J-FET design in an important way. The D-MOSFET design reduced the source-gate and draingate leakage current in the off state to a value of less than one picoampere (63). However, leakage charge will flow from the p-type source and drain into the n-type substrate.

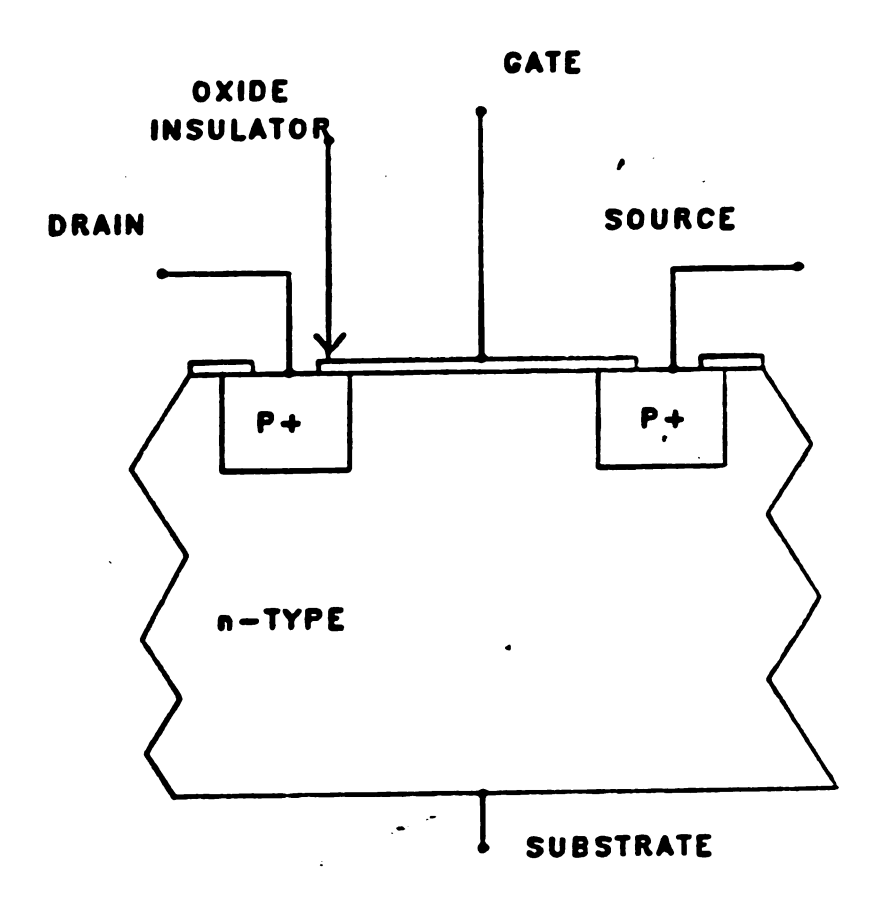


Figure 4-4. Analog switch with D-MOSFET construction.

Another factor necessary for low leakage is to ensure that the board material used for mounting the switch has high insulating characteristics and is clean. A fiberglass

board is used in mounting the charge injector switches.

When an analog switch is turned on and off a voltage spike is created at its output. The magnitude of the spike is a complex function of the circuit capacitances, resistances, input voltage and the applied gate voltages (59). These spikes are found to be only a few tenths of a microsecond in duration and do not present a problem because the charge content of a spike is small compared to the total injected charge (less than 0.1%).

F.0 Requirements and Calibration of the Injecting Capacitors

Capacitors with polystyrene and mica dielectrics were

chosen for use. These capacitors were chosen because they

have a low temperature coefficient, are unaffected by humid
ity, have low leakage so that charge can be held for

extended periods, possess a low dielectric absorption factor

so that charge can be removed quickly and have a wide fre
quency response. All capacitors were calibrated before use.

Two different methods were used for calibration:

- 1. The capacitors were placed in the charge injector and the test program CAPCLB.OBJ was run with a dummy cell in place.
- An external test circuit was used to calibrate the injecting capacitors.

In the first method the capacitors to be calibrated are placed in the charge injector and the program CAPCLB.OBJ is downloaded into the microcomputer. A dummy cell similar to Figure 2-2 is positioned after the charge injector. Typical

values are R_1 =1 k Ω , C_1 =1 μF , and Z_f =500 k Ω . The parameter command, PRAM, is given and the parameters TIDD and DAO are entered. DAO is the charging voltage of the injecting capacitors. The value is entered in millivolts. TIDD is half the period of the injecting rate, entered in microseconds. Typical values of TIDD range from 100 to 1500 μ sec. A 'control z' is entered to return to the main operating system and the program CAPCLB run. Typing a 'g' begins execution. The voltage which appears on the monitor screen is given by:

$$V_{\text{(out)}} = C_{\text{inj}} DAO R_{\text{f}}/2TIDD$$
 (4-2)

This equation can be used to calculate C_{inj}. To increase the accuracy of the method, DAO should be made large to avoid quantization error. When DAO is set to the maximum value of 2.5 V, a change in 1 LSB causes a 0.1 percent error. TIDD is adjusted to provide a high injection rate and a large output voltage to avoid quantization error of the analog to digital converter. The ADC is a 12 bit converter with a 5 volt range and a resolution of 1.2 mV. Small injection capacitors will require faster injecting rates and smaller values of TIDD. Time TIDD is accurately determined by a 16 bit counter on the timer controller chip (AM 9513). The largest error for calibrating capacitors by this first method is due to the resolution of the DAC. This error is reduced by keeping the DAC charging voltage above 1000 mV.

The second method used to standardize the injecting capacitors was with an integrator circuit constructed from a The LF 351 was chosen because its offset can LF 351 op amp. be balanced. The standarization procedure is to connect first the injection capacitor to a known voltage. A chargeto-voltage converter is constructed from a known standard capacitor and the LF 351 operational amplifier (OA) (64). The integration capacitor in the feedback loop of the OA is shorted across its terminals with a 100 ohm resistor and the OA balanced with the offset potentiometer. This initializes the integration capacitor. The charged capacitor to be tested is then removed from the voltage source and connected to the input of the charge-to-voltage-converter. The unknown injection capacitor may then be calculated from the following:

$$C_{ijnk} = C_f V_0 / V_C \tag{4-3}$$

where C_f is the integration capacitor of the charge to voltage converter, V_0 is the output voltage of the charge to voltage converter, and V_c is the charging voltage of the unknown injection capacitor. The accuracy of this method is dependent upon how accurately the feedback capacitor is known.

G.O Requirements of the Injecting Amplifier

The performance characteristics of the injecting amplifier are important for all electrochemical experiments. The AM405-2 by Datel was chosen because of its high input

migh Migh

The :

allo tion

the

reni fast

E.J

vert tran

rep

Wher

capa

Wher

char

Wher

impedance $(10^{10}~\Omega)$, fast slew rate (120~volts/µsec), and high power bandwidth. The output voltage range is $\pm 10~\text{V}$. The peak current output is 50 mA. A high output voltage allows the amplifier to drive current through a large solution resistance. The amplifier bandwidth capacitor allows the response characteristics of the amplifier to be conveniently adjusted. A small bandwidth capacitor allows a fast response but makes the OA more prone to oscillation.

H.0 Circuit Characteristics

The charge injector circuit is a transducer which converts a transfer of charge into a change in voltage. Such transducers have been used in capacitive microphones and proportional counters. See Figure 4-5. The midband gain may be expressed as:

$$\Delta V_0 / \Delta V_{in} = -(C_{inj}/C_f) \qquad (4-4)$$

where ΔV_0 is the output voltage, $\Delta V_{\rm in}$ is the input voltage, $C_{\rm inj}$ is the injection capacitor, and $C_{\rm f}$ is the feedback capacitor. The lower cut off frequency (-3db) is:

$$f(1) = 1/(2\pi R_f C_f)$$
 (4-5)

where R_f is a feedback resistor which is used only to discharge C_f . The upper cut off frequency (-3db) is:

$$f(2) = 1/(2\pi R_i C_{ini})$$
 (4-6)

where R_{i} is the input resistance of the injecting amplifier.

CHARGE TO VOLTAGE CONVERTER

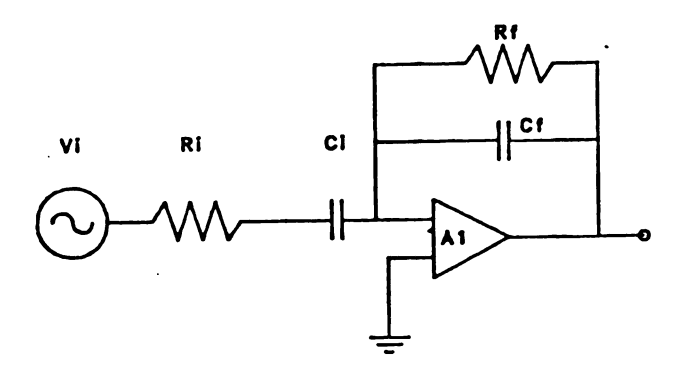


Figure 4-5. An example of a charge to voltage converter with an AC input.

It is important that the injecting amplifier remain stable over the operating range of the experiment. If the injecting amplifier operates out of its stability range, errors can result due to:

- 1. Inaccurate charge transfer from the injecting capacitor to the cell;
- 2. excessive noise;
- 3. slow injection times;
- 4. oscillation or ringing of the injecting amplifier;
- 5. damage to the injecting amplifier.

The time of injection for a given pulse is limited by the input RC time constant. RC is the product of the input resistance and the injection capacitor. The injection rate must be slower than 5 RC time constants to ensure that the injecting capacitor has fully discharged before the DAC voltage is applied for the next injection.

When the analog switch is thrown connecting C_{inj} to the cell, the output of the injecting amplifier jumps to a peak voltage and then decays exponentially. The following equation may be used:

$$V_{out} = V_{p} (1-exp(-t/RC))$$
 (4-7)

where V_{out} is the amplifier output voltage, V_{p} is the peak amplifier voltage, and t is time. Figure 4-6 shows the natural logarithm of the amplifier output voltage vs. time for an injection using a 0.001 µF injection capacitor, DAC voltage of 1.000 V, and an input injection resistance of **456** Ω . Output voltage plots were made to test the injector's response using various values of injecting capacitor, input resistance, charging voltage, electrode capacitance and cell The average slopes from the plots were used to calculate the time constant for the output voltage decay. The time constants were all within 6.4 percent of the injector input RC time constant as calculated from the injection capacitor and injection resistor. This proves that the injection amplifier is responding in a well behaved manner to the input charge. The settling time for an injection pulse is defined to be the time it takes the output voltage of the amplifier to reach 1 percent of its final output voltage. After 4.6 RC time constants the amplifier output voltage will have reached this level. The injection time as defined above will not depend on the quantity of charge being injected. Figure 4-7 shows the settling time plotted vs.

charging voltage as measured with a cell containing 0.01 M KC 1 using an injection capacitor of 0.001 μF and an injection resistance of 220 Ω_{\star}

O.A. OUTPUT VS CELL RESISTANCE INJ. RESISTANCE=730 Ohmo, CELL CAP.=1. #F

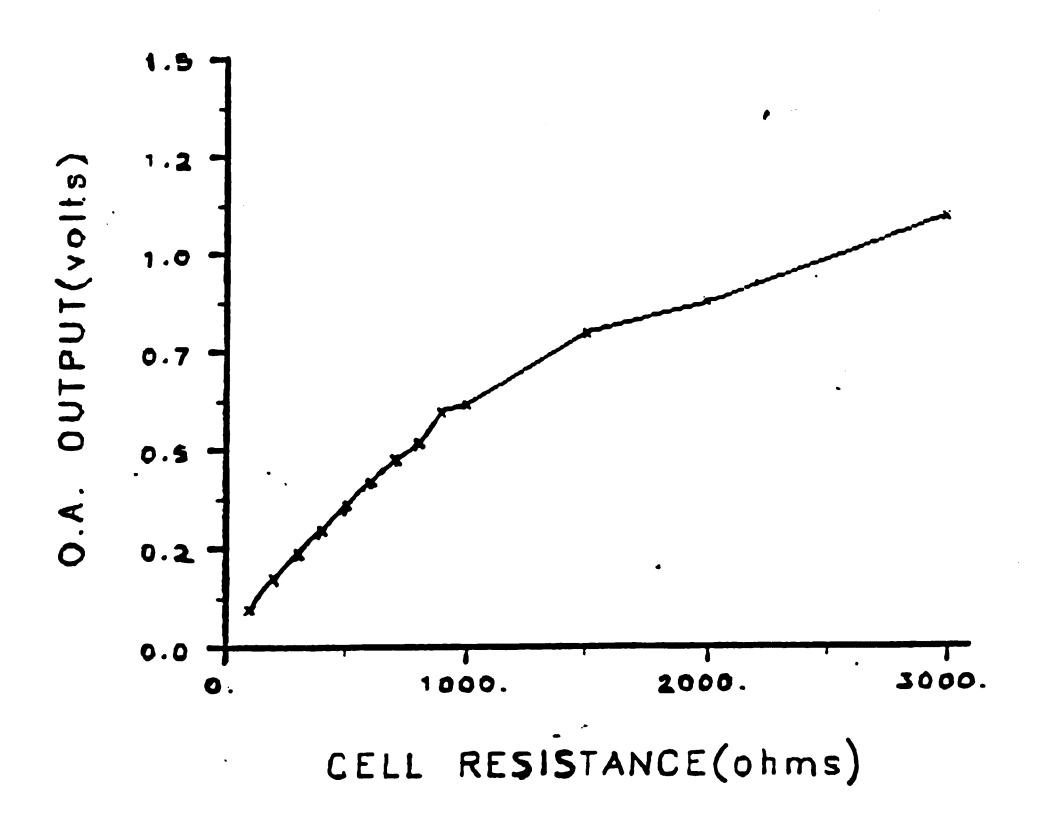


Figure 4-6. The effect of cell resistance on the injector output voltage.

SETTLING TIME VS CHARGING VOLTAGE
GELL=.01KG, INJ. CAP.=.001µF, INJ. RES.=220 Dhm.

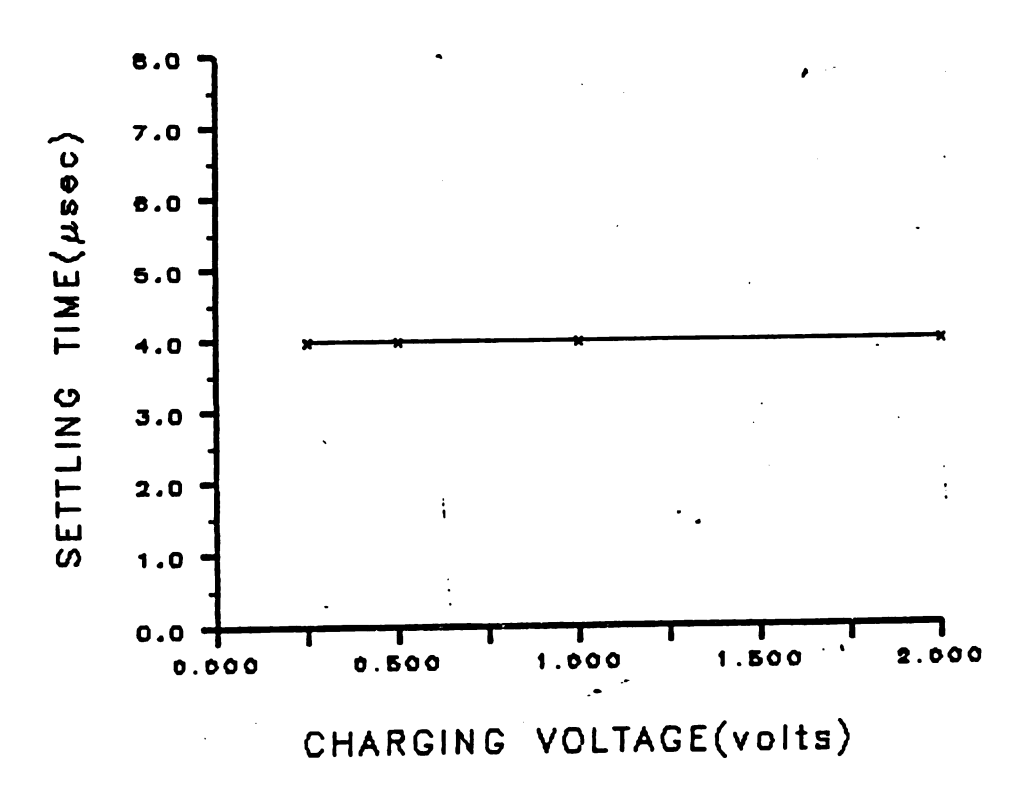


Figure 4-7. The effect of charging voltage on the settling time.

If charge is dumped on the injection amplifier too quickly, the amplifier may become unstable and oscillate between limits. For an increase in injecting capacitor size, the injection resistor may be decreased in value and still provide a rapid and stable injection pulse. This is shown in Figure 4-8.

If the injector resistor is decreased with the injection capacitor size held constant, the peak amplifier output voltage will increase as shown in Figure 4-9. The more

MIN. INJ. RES. VS INJ. CAP. SIZE CHARGING VOLTAGE=500 MV

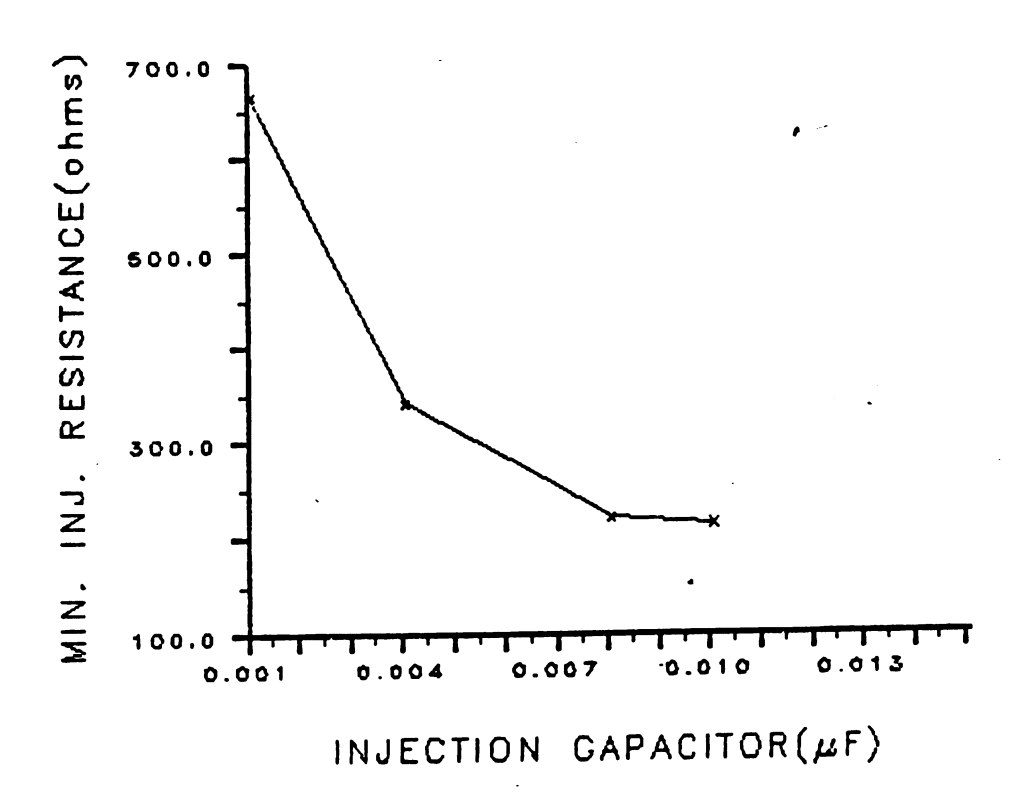


Figure 4-8. Combinations of injection capacitor and resistor to provide a rapid and stable injection pulse.

O.A. OUTPUT VOLTAGE VS INJ. RESISTANCE
INJ. GAP.=.001#F, V=1.0 v , GELL RES.=1K Ohms

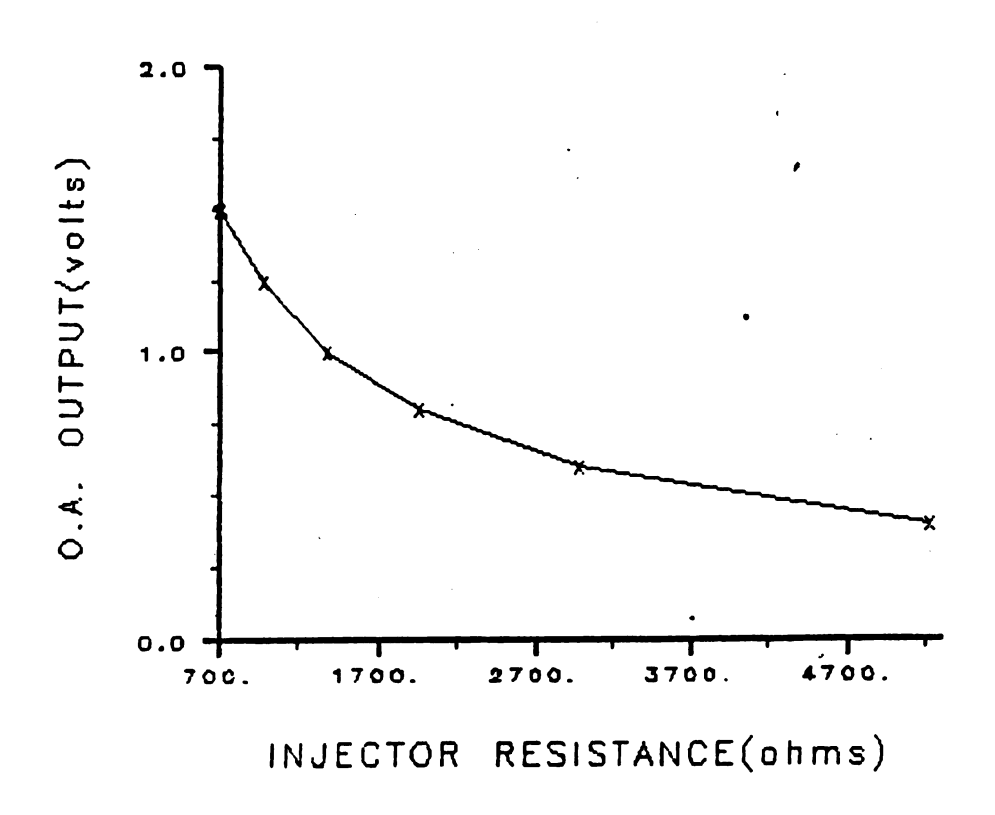


Figure 4-9. The effect of injector resistance on the injection amplifier output voltage.

charge injected the higher will be the peak amplifier output voltage. This is shown in Figure 4-10. If the input resistor and the injecting capacitor are held constant and the charging voltage increased, the amplifier peak output voltage increased, the amplifier peak output voltage is shown to increase linearly with the charging voltage. These tests were performed on both a real and dummy cells to check fully the charge injector.

O.A. OUTPUT VS CHARGING VOLTAGE CELL=.01M KCI, INJ. RES.=220 @hms, INJ. CAP.=.0014F

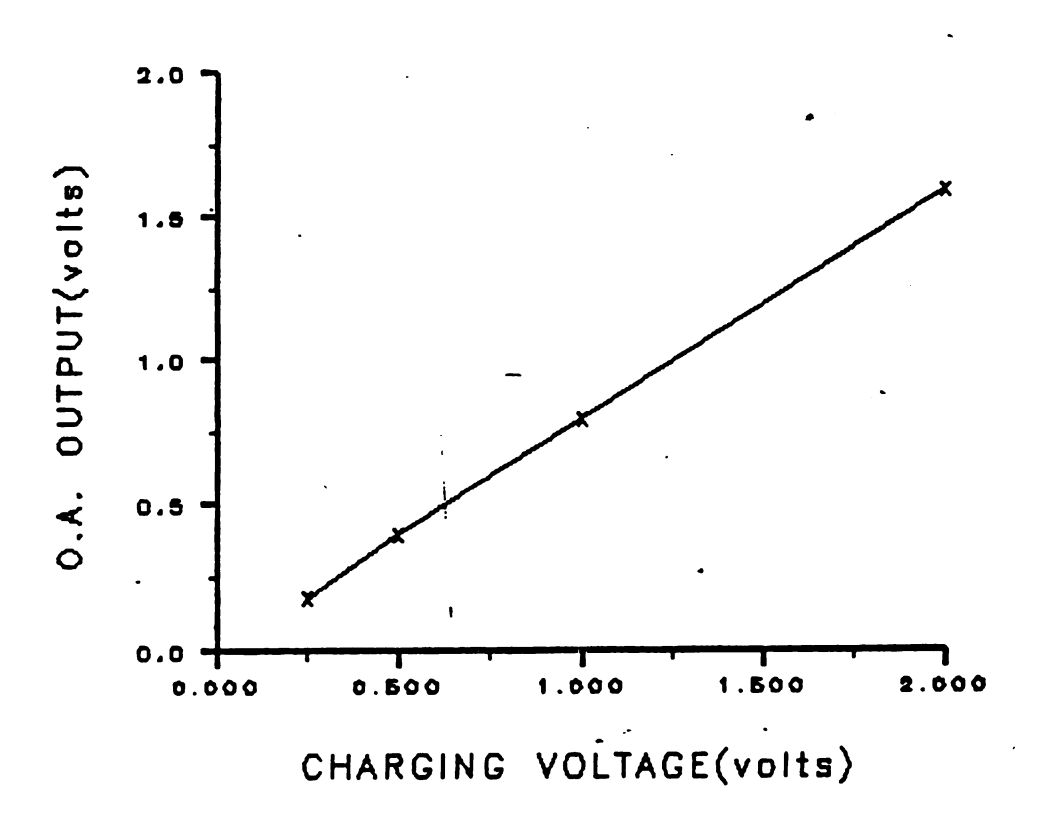


Figure 4-10. The effect of injection charge on injection amplifier output voltage.

The speed with which the amplifier responds to any input signal can be controlled with the bandwidth capacitor of the amplifier. Decreasing the bandwidth capacitor value causes the amplifier output voltage to respond more quickly to an input signal. As the injection resistor is decreased charge is more quickly dumped on the summing point of the amplifier because the input RC time constant is smaller. With a smaller bandwidth capacitor the amplifier is shown

to send its output voltage to a higher voltage level.

Figure 4-11 shows the effect of the injector resistance on the amplifier output voltage.

O.A. OUTPUT VS INJECTOR RESISTANCE
INJ. CAP.=.001 #F, CELL=1K ohms, A=10pF, B=47pF, C=100pF

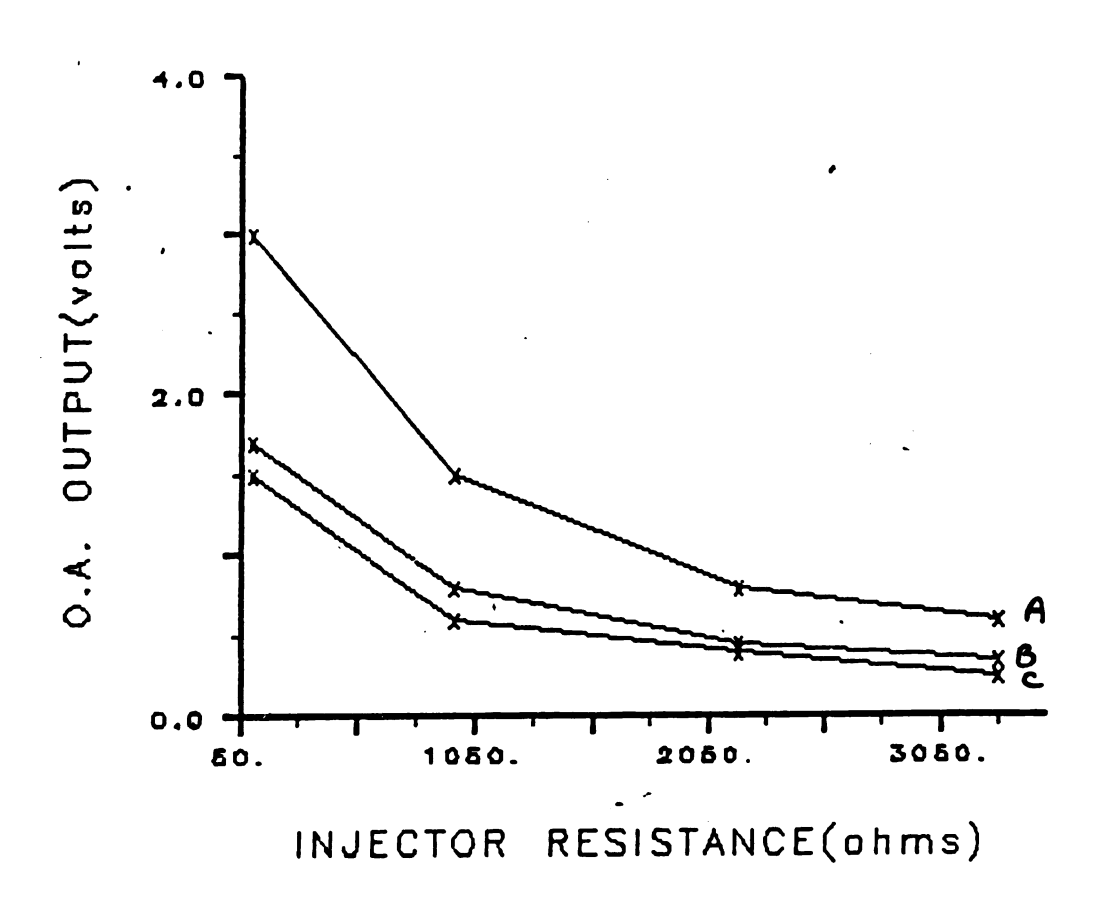


Figure 4-11. The effects of the bandwidth capacitor and injector resistance on the injection amplifier's output voltage.

Responding quickly is an advantageous quality of a charge injector but the input and output loads of the charge injector will determine how quickly it can respond in a stable manner. The injection amplifier may become unstable when the input charge causes the output to approach the

upper or lower voltage limit. With a constant charge injection size, the peak output voltage of the amplifier increases with increasing cell resistance. This is shown in Figure 4-12. When the solution resistance becomes too large, the output voltage of the amplifier is found to ring as the amplifier slowly responds to the changing input.

O.A. OUTPUT VS CELL RESISTANCE INJ. RESISTANCE = 750 Ohms. CELL CAP. = 1, 4F

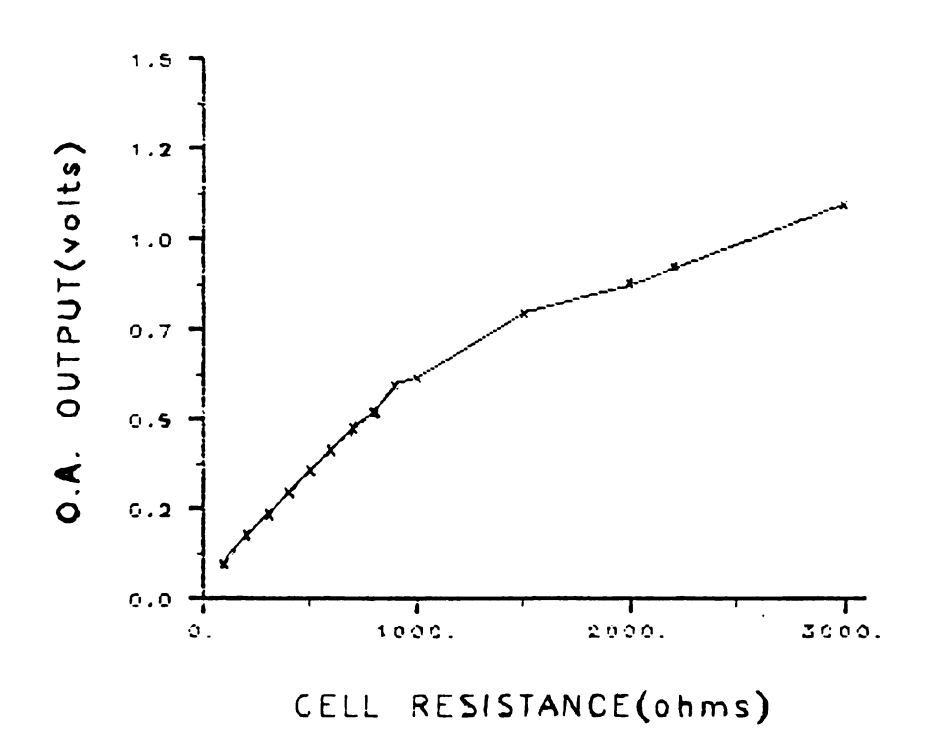


Figure 4-12. The effect of cell resistance on the injection amplifier's output voltage at a constant charge injection value.

Charge injectors which employ a gated constant current source have the disadvantage of requiring accurate control of time for precise injection of charge. The charge

injector used in this research does not require accurate control of time because the OA works until its summing point returns to virtual ground. It does this by driving charge through the cell. Since the cell is the only element in the feedback loop of the OA, the charge must go quantitatively to the cell. The accuracy of this charge injector has been tested by the following methods:

- A small known capacitor was put in place of the cell and the resulting output voltage was measured after a number of charge injections.
- 2. A dummy cell was put in place of the cell and a constant rate of charge was injected. The resulting cell current is determined by measuring voltage across $R_{\rm S}$.

The first method was tested by downloading the program DPR.OBJ into the microcomputer and putting a standard capacitor in place of the cell. Parameter DAO is used to set the DAC charging voltage and parameter N4 sets the number of repetitive injections. The cell voltage is measured after the last charge injection by the voltage measurement system and displayed on the monitor screen. Three different injecting capacitors were tested: $0.001 \mu F$, $0.005 \mu F$, and 0.01 µF. The number of charge injections tested ranged from 255 to 10. Four different charging voltages were tested for each capacitor, 2.500 V, 2.002 V, 1.001 V, and 0.498 V. Figures 4-13 A, B, and C show results for the testing of the charge injector. The solid lines on the graphs are the least squares lines through the data points. The standard error estimate is a measure of the extent of spread or

CALIBRATION OF THE CHARGE INJECTOR C=.0010 #F, A=2.5Y, B=2.0Y, C=1.0Y, D=.498Y, L.SQ.L.=(-)

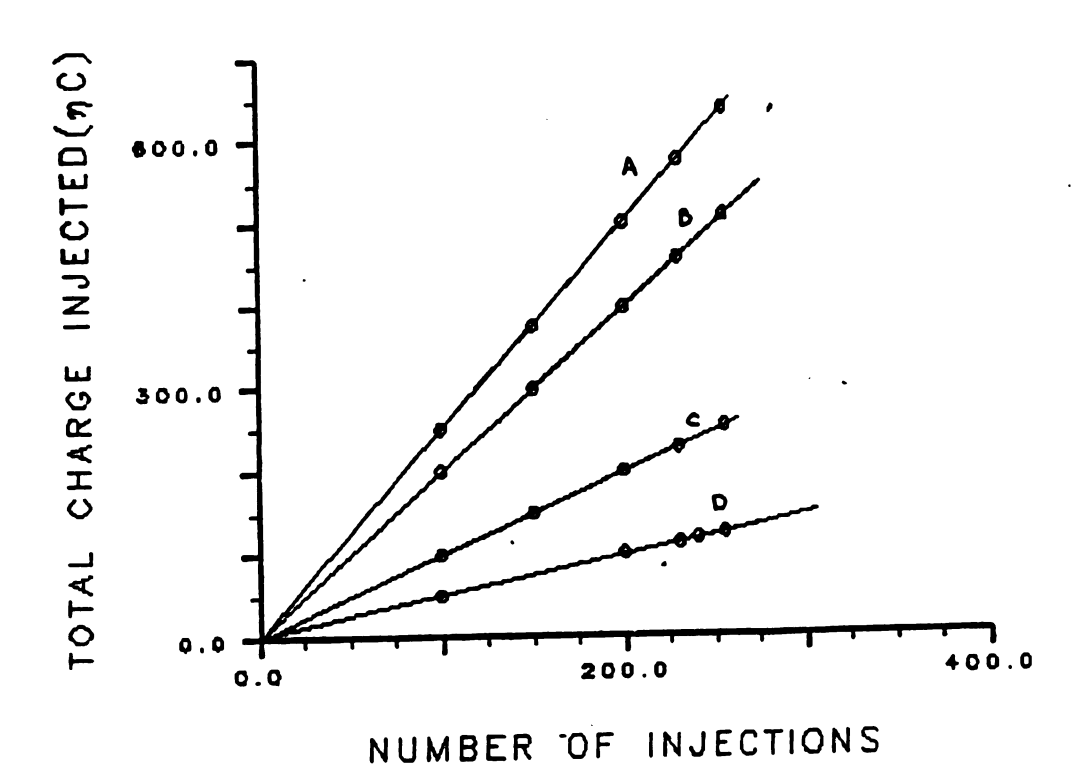


Figure 4-13 A. The effect of the number of injections on the total charge injected for charging voltages: A=2.5 V, B=2.0 V, C=1.0 V, D=.498 V, C_{inj} =0.0010 μF .

CALIBRATION OF THE CHARGE INJECTOR C=.0051 \(\mu \)F, A=2.5V, B=2.0V, C=1.0V, D=.498V, L.Sq.L(-)

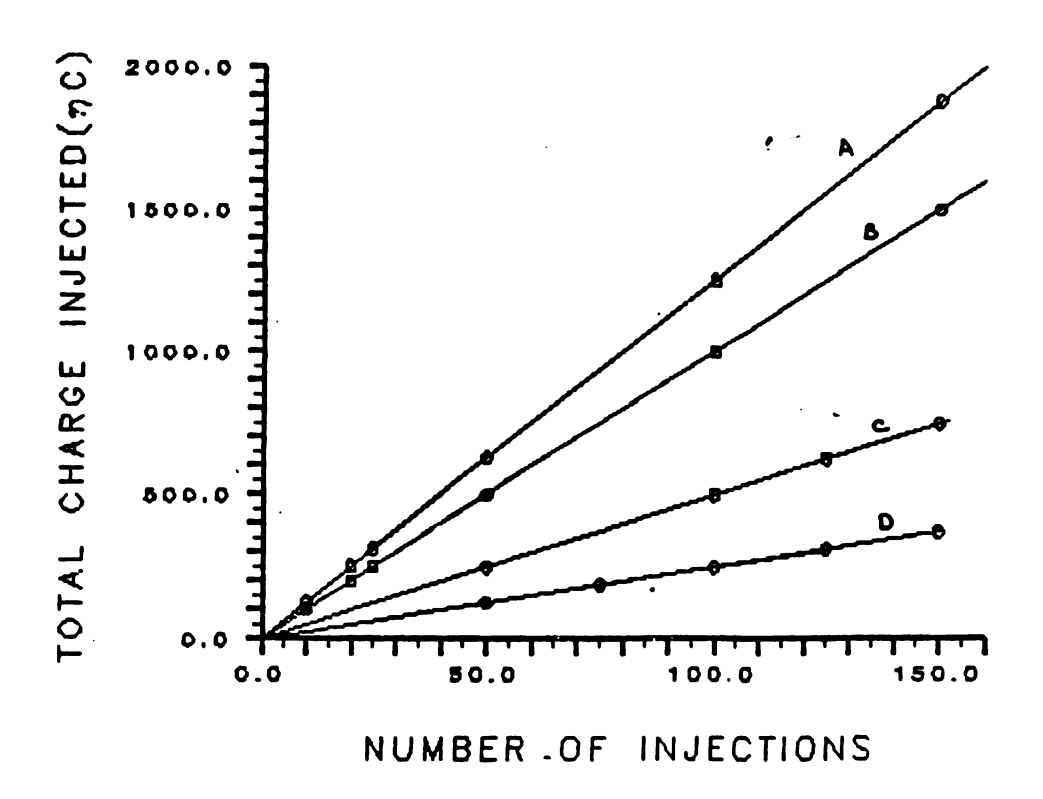


Figure 4-13 B. See 14-A C_{inj} =0.0051 μF .

CALIBRATION OF THE CHARGE INJECTOR C=.0103µF, A=2.5V, B=2.0V, C=1.0V, D=.498V, L.SQ.L.=(-)

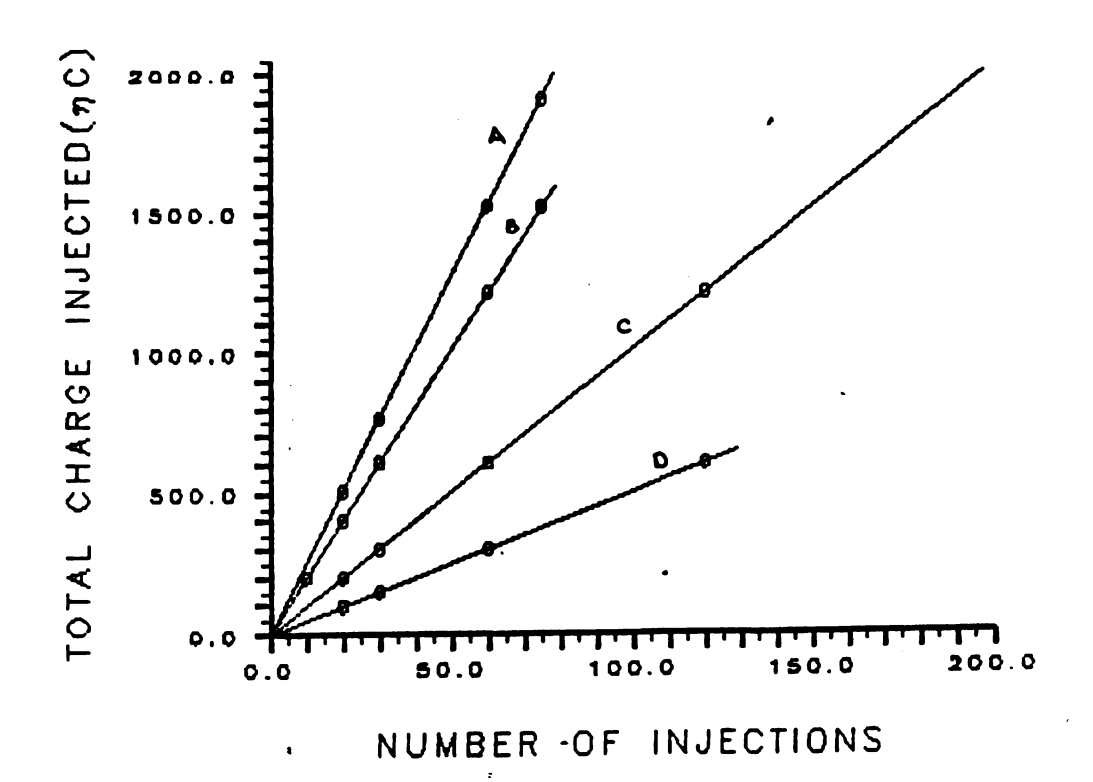


Figure 4-13 C. See 14-A C_{inj} =0.0103 μF .

scatter of the dependent variable (charge) from regression.

The standard error estimate is given by the following formula:

$$S_E = (\Sigma(Y_i - Y)^2 / (N-2))^{1/2}$$
 (4-8)

The summation is from i=1 to the last point. Y_i is the dependent variable data point. Y is the value given by the equation of the least square line Y=mX+B, where m=slope and

B=intercept and Y is obtained from the trend line analysis.

N is the number of data pairs. The results of the standard error analysis was less than 1 nanocoulomb for all plots.

The charge which is predicted from the injections can be calculated from the following equation:

$$Q_{thy} = (DAC)C_{inj}$$
 (4-9)

where (DAC) is the charging voltage, and C_{inj} the injecting capacitor. The injected charge Q_{exp} , is determined from the experimental slopes of the least square lines. From Q_{thy} and Q_{exp} the absolute experimental error in the charge injector can be calculated. Errors in the charging voltage, due to the limited resolution of the DAC lead to largest errors when the number of injections is greatest and the charging voltage the smallest. The value of Q_{thy} was not corrected for leakage current or a charge offset. The maximum absolute error was found to be less than 5.7 percent.

The slopes of Figures 4-13 A, B, and C were plotted vs. the charging voltage in Figure 4-14. The standard error estimate was less than 1 nanocolumb for all three injecting capacitors tested.

The second method used to test the performance of the charge injector was to measure the voltage drop across an accurately known resistor while the charge injector was supplying a constant current. A dummy cell similar to Figure 2-2 was put in place of the cell and a known resistor was put in place of Z_1 . The resistor was measured on an AC

CALIBRATION OF THE CHARGE INJECTOR

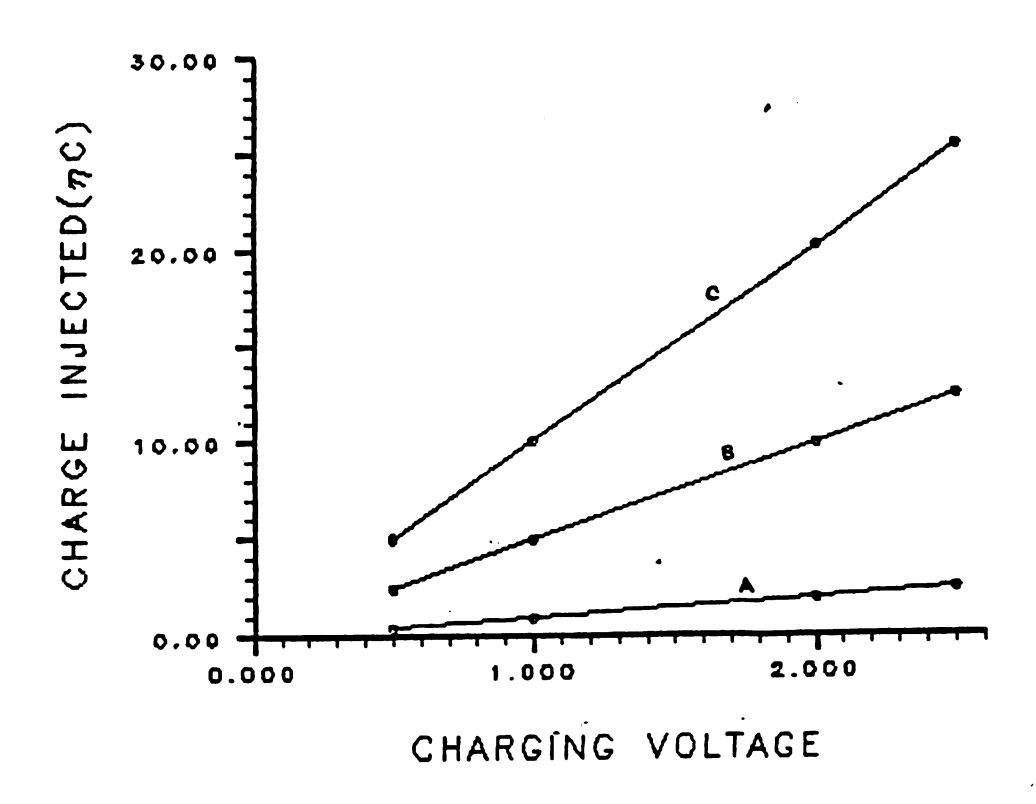


Figure 4-14. The slopes of lines in Figures 4-13 A, B, and C for different charging voltages.

bridge to be 100,320.0 Ω . The program CAPCLB.OBJ was downloaded into the microcomputer. Important experimental parameters are DAO and TIDD. DAO is the charging voltage and TIDD is half the injection period. Eight different DAC values were tested from 2.5 V to 500 mV. TIDD values ranged from 1500 μ sec to 100 μ sec which yielded periods of 3 msec to 0.1 msec. Two injecting capacitor sizes were tested: 0.001 μ F and 0.01 μ F. The equation for calculating the injected charge is given by:

where $\mathbf{V}_{\mathbf{R}}$ is the voltage across standard resistor $\mathbf{Z}_{\mathbf{1}}$ and TIDD is half the injection period given in microseconds.

The greatest accuracy with this method was obtained with the highest injection rate, the largest injecting capacitor, and the highest DAC charging voltage. The absolute charge error for this method ranged from 1.6 percent to 9.4 percent for DAC values which ranged from 2.50 V down to 500 mV with the 0.001 μF injecting capacitor.

Method number 1 is the method of choice for testing the charge injector at slow injection rates because large measurement errors can occur with method 2 under these conditions unless a very large standard resistor is used. On the other hand, if a large standard capacitor is not available, method 2 might be the method of choice because a cell resistor can easily be measured with an ohmmeter. The two methods are complementary and enable different experimental conditions to be tested favorably. For example, the injector can be tested at high injection rates for extended periods under a large resistive load with method 2 but can not be tested favorably with method 1 under these conditions because of the high voltage which results on the cell capacitor. Method 1 is used favorably to test the injector when a limited number of injections are made with a large capacitive load.

These tests show that the charge injector can operate in a linear manner and inject charge in incremental amounts

using various injecting capacitors and a wide range of DAC charging voltages. These tests also suggested how the charge injector can be improved. The following are a number of ways in which improvements might be made:

- 1. The noise level in the injection pulse can be reduced by decreasing the length of wire leads which run to the cell.
- 2. The leakage current can be reduced by:
 - a. Using a low leakage analog switch;
 - b. biasing techniques which are given in the analog switch application book;
 - c. switching the leakage current from several switches to ground with a single switch.
- Using an injection amplifier which has a higher output voltage to enable greater solution resistances to be studied.
- 4. Designing an injector to operate at faster injection rates.
- 5. Designing two injectors, one injector which can inject very small charge pulses and another for large charge pulses.
- 6. Using a high resolution DAC.

It is hoped that future charge injectors will enable greater accuracry, precision and sensitivity. It is expected that the charge injector will enable the analysis of very dilute solutions because with improvements it will be able to add accurately and quickly increasingly smaller and smaller amounts of charge to the chemical cell.

a a: e:

> t) t)

in th

V INSTRUMENTAL REQUIREMENTS TO SIMULATE STAIRCASE CYCLIC VOLTAMMETRY WITH A CHARGE INJECTOR

A.0 The Instrument

Microcomputers can aid automated control of instrumental functions or measurement processes. Computer-based automation can result in an increase in precision and speed of analysis. With 'friendly' software, the instrument operation can be made simpler to the user and greater overall throughput can result. The future of analytical chemistry rests heavily with the incorporation of microcomputers into a new breed of instruments which will enable a sophisticated array of experiments controlled from a single keyboard. this way the analysis of a chemical system may be studied by a variety of techniques which are all under computer control and thus allow the chemical system to be viewed from different angles. Constructing an instrument with these capabilities were the design goals of a microcomputer controlled charge injector. Analysis performed with a microcomputer would enable programmable control of charge injections and thus enable a greater variety of experiments and a greater throughput of results.

The overall block diagram of our microcomputer controlled charge injector is shown in Figure 5-1. Details of the charge injector and the voltage measurement system are

GENERAL BLOCK DIAGRAM

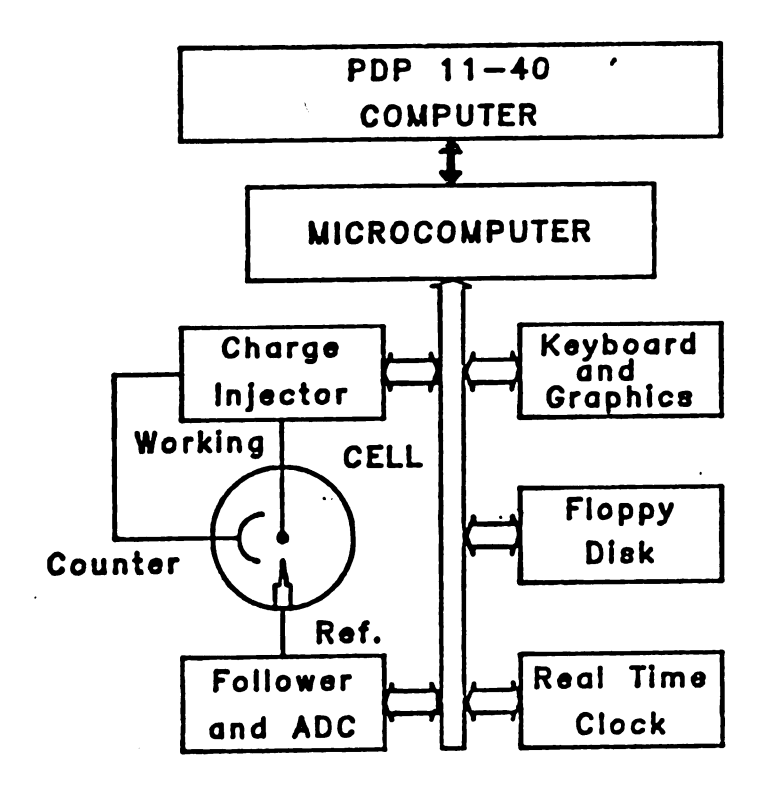


Figure 5-1. General instrumental diagram of the main components of the charge injector.

found in S. Hourdakis's dissertation (58). The design of the computer interface is found in C.C. Lee's dissertation (49) and in Bruce Newcome's (60) dissertation is found the design and construction of the 8085A microcomputer and data bus.

The elementary operations of the instrument are to charge the electrode, measure the electrode potential, and "keep track" of time. These basic operations are fundamental to many electrochemical techniques. The sequencing and

instrumental means of performing these basic operations is what usually differentiates one technique from another. The microcomputer provides control over these operations through flexible software. This allows the operator to perform complex electrochemical experiments which can be implemented as combinations and sequences of these three simple operations. Because the microcomputer controls these basic operations, the instrument can operate in various modes to perform a variety of electrochemical techniques.

B.O Modes of Instrument Operation

There are four basic categories of electrochemical experiments; they are galvanostatic, potentiostatic, coulostatic, and potentiometric. Although quite different in their analog instrumentation, each of these types of experiments can be performed by fast computer control of the basic operations of charge injection, potential measurement, and timing. In a galvanostatic experiment, charge injections are made at a constant rate thus generating a constant current. Potential measurements, free of IR error, are made between each injection. In potentiostatic control, the cell potential is measured and charge injections made as needed to reach and maintain a desired cell potential. The dependent variable, current or charge, is measured as the computer record of charge injections. Coulostatic experiments require the controlled addition of charge and may be performed by changing the charge injection size. The potential time profile is measured after each injection.

Potentiometric experiments are performed by measuring the cell potential at a specified rate without charge injection. Since the difference in instrumentation from one technique to the other is in the program of the computer and not in the hardware, all the basic electrochemical techniques are easily performed by a single instrument. It would even be possible to switch rapidly from one technique to another to provide experiments that couldn't be achieved by any combination of analog instruments. Some examples of techniques which can be implemented are: chronopotentiometry (galvanostatic mode), capacitance measurements (coulostatic mode), cyclic voltammetry (potentiostatic mode), and pH measurements (potentiometric mode). This dissertation focuses on the potentiostatic mode, and in particular, on the technique of staircase cyclic voltammetry.

C.O Generation of a Staircase Waveform

The control of the charge injector to perform staircase cyclic voltammetry is a challenging test for this instrument because all functions of the instrument are required to perform rapidly to achieve the staircase waveform at reasonable sweep rates. The voltage measurement system is required to make quick measurements between each charge injection. The charge injector is required to make both large and small injections. And all these functions are tested at scan rates which can change over several orders of magnitude.

Computer programs often require decisions which must be made by the operator as to the function and organization of

program options and parameters. The program can become progressively more complex as the program length increases and thus it is important to structure the program in a flow chart so that the outcome of each decision on important program attributes are considered. It is the purpose of the remainder of this chapter to discuss how important program decisions were made and to suggest the outcome of these decisions on electrochemical experiments.

D.O The Potential Step

A fundamental question concerning the entire program algorithm for staircase voltammetry is how the potential step is brought to a desired step voltage. Four basic control methods or algorithms have been identified. They are:

- single injection of an approximately correct charge;
- 2. large charge injection(s) followed by small potential adjustment injections;
- single injection of precalculated charge;
- 4. single injection of charge value determined by previous experiment.

E.O Single Injection of Approximately Correct Charge

A non-uniform step results from the use of a single constant charge injection size to step the cell potential to a new value. The resulting cell potential reached after this single injection is maintained constant for the remainder of the step by a succession of smaller charge injections as needed. The potential step is non-uniform in magnitude

be

it

ti.

ti

p: d:

F.

li pi

ď

Ti f(

C(

a:

S

ť

G,

Sį

because the step size will depend on the double layer capacitance. The step voltage is reached in the fastest possible time with this method because only one injection is made for the potential step. The disadvantage of this method is that the voltammogram has a non-uniform scan rate. This distortion is along the potential axis makes quantitative interpretation and comparison with theory and linear scan methods difficult.

F.O Large Charge Injection(s) Followed by Small Potential Adjustment

The trimmed step potential method can be performed by applying a rapid series of small charge injections after the large charge injection to adjust each potential step to the proper value. See Figure 5-2. This method results in a constant potential step size for the entire voltage scan. The disadvantage of this method is the time required to perform the multiple injections with the computer checking the attained potential between each injection. Since the step duration time (T2) should be long compared to the time required to reach the step potential (T1), a long T1 will seriously limit the scan rate. The injection generator must be able to apply either positive or negative charge in order to move the cell potential in the direction of the desired step voltage.

G.0 Single Injection of Precalculated Charge

A uniform step size can also be achieved by using a single injection of variable size which is automatically

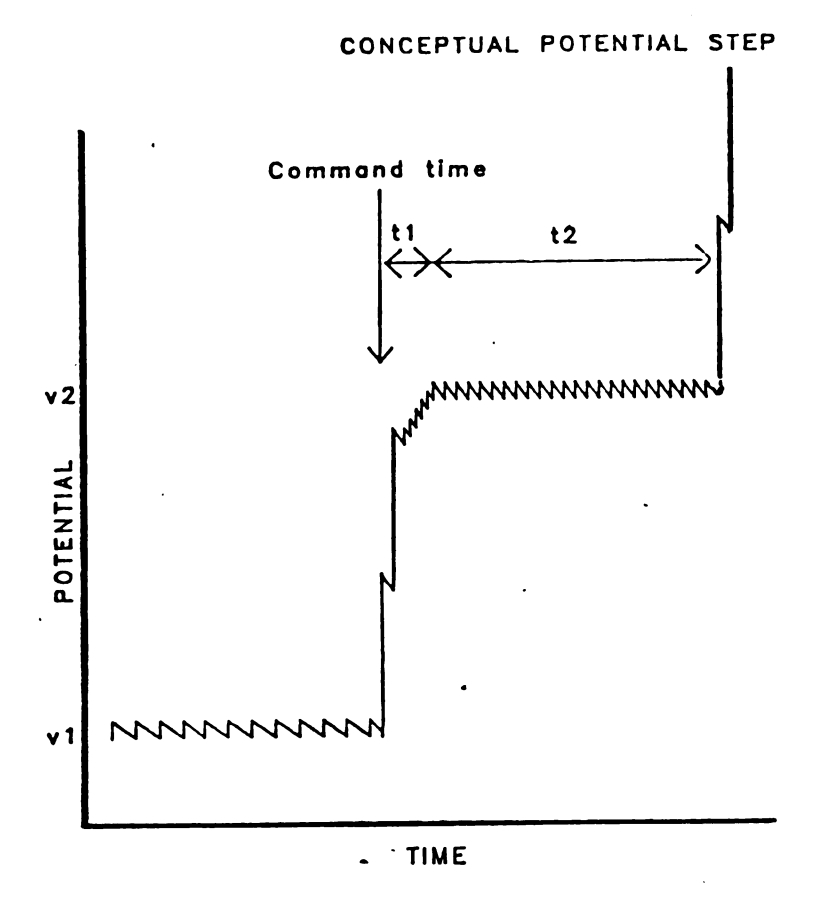


Figure 5-2. A conceptual potential step trimmed to the desired level with small charge injections.

adjusted to compensate for changes in the double layer capacitance. Consider a charge injection of \mathbf{Q}_1 which results in a change in cell potential from \mathbf{V}_0 to \mathbf{V}_1 . The double layer capacitance may be calculated from:

$$C_{d1} = Q_1/(V_1-V_0)$$
 (5-1)

The injected charge needed to reach the second step potential V_2 can then be calculated from the equation:

$$Q_2 = C_{d1}(V_2 - V_1)$$
 (5-2)

Assuming that the double layer capacitance does not change

over the potential region from V_0 to V_2 , (5-1) and (5-2) may be combined by substituting the double layer capacitance from the former equation into the latter to yield:

$$Q_2 = Q_1 (V_2 - V_1) / (V_1 - V_0)$$
 (5-3)

Deviations from the desired size for each step can be made up through variation of the next charge injection size.

This method would tend to be self correcting when the step size is small and there are many steps in the potential scan.

The advantage of this method is that the desired step potential can be reached with a single injection. The disadvantage of the method is that to be effective, the charging voltage calculation must be accurate and fast. Accuracy of calculation is a problem because quantization noise and electrical noise in the voltage measurement is a significant fraction of the step size. A problem may also exist when the charge to be injected is small because this requires a small charging voltage which yields a large relative error in the DAC voltage. The result is inaccurate charge addi-Another ever-present problem is electrical noise. Electrical noise in the voltage measurement is difficult to bring below one millivolt and therefore when the step size is small a large error can result from this source. changes in the double layer capacitance can be small from one step to the next, a smoothing operation on the capacitance value is possible and probably necessary.

When fast potential sweeps are required, the time needed for a microcomputer, which has only software integer arithmetic, to make the charge calculation becomes long in comparison to the desired step times. High speed calculation hardware (math coprocessor) is thus required to avoid the time for the charge calculation being the limiting factor in the sweep rate of the instrument, will thus limit the sweep rate of the instrument.

H.0 Single Injection of Charge Value Determined by Previous Experiment

The last suggested method for potential step control is the lookup table. In this method the program utilizes a table of preprogrammed charge amplitudes which results in a uniform potential step throughout the scan. This method can be fast but presents a practical problem of determining the correct values for the lookup table. Possible methods which can be used for determining the values in the lookup table are:

- calculation from the known or measured electrode capacitance at each potential;
- determination of the charge required for each potential step from a previous experiment and calculation of the values for the lookup table for the experiment at hand.

The first method is often not possible because the double layer capacitance is not predictable at each potential beforehand. The second method is undesirable because it requires that the electrode area and the electrode surface

characteristics remain unchanged from the previous experiment. This may not be true for solutions in which adsorption is occurring or when the electrode surface is changing as through plating or oxidation.

I.O Method of Choice

Of the four methods for attaining the potential step listed previously, method two in which the step potential is trimmed to the desired step value was chosen for programming because useful sweep rates are possible and results can be compared with the theory of staircase voltammetry. Method one, the single uniform charge injection, was also programmed because it employed a single charge injection to step the potential and therefore offered the greatest speed and sensitivity.

J.O Program Control of the Charge Injector

The program controlling the analog switches determines how the injecting capacitors are charged and discharged. There are two injecting capacitors present in the instrument. The number of injecting capacitors was limited at two so the number of analog switches would not exceed two. The total leakage current into the electrochemical cell increases with the number of switches present. The basic requirement for a controlled potential scan is that the injector be able to inject both positive and negative pulses and that the injector be able to inject both large and small charge pulses. It is advantageous to use a unipolar

DAC with an inverting amplifier to obtain a simultaneous negative voltage because of the increased charge injection resolution. For example, a bipolar 10 bit DAC with a 5 V range has a resolution of 4.8 mV. When the same DAC is placed in a unipolar configuration and used in conjunction with an inverter to obtain negative charge injections, the resolution of the DAC is 2.4 mV. It is also advantageous to have two different sizes of injecting capacitors. A large capacitor is needed to enable large potential steps and a small capacitor is needed to maintain the step voltage with small charge injections. There are two schemes which can be used to add charge to the cell. They are as follows:

- 1. Both injecting capacitors are made to be of the same size. One injecting capacitor is used exclusively for injecting negative charge and the other for injecting positive charge. The inverting ampliflier is used as a source of negative charging voltages. This allows a DAC to be used in a unipolar configuration and thereby increase the charging voltage resolution.
- One injecting capacitor is made large and the other small. A bipolar DAC is used to change the polarity of the charging voltage on either injecting capacitor.

The problem that presents itself is that there isn't a convenient method with the present switching circuit to have both different sizes of injecting capacitors and a unipolar DAC. To accomplish this would either require programming equal charge injections sizes from different capacitor sizes or a circuit design change.

Two time controls are needed for the generation of the

staircase waveform. The first time control identifies the beginning of the potential step and the second identifies the establishment of the desired step potential. The computer may receive these time controls by reading the real time clock or by receiving an interrupt signal.

K.0 The Initial Cell Potential

To set the cell potential to an initial voltage the microcomputer is programmed to make rapid charge injections to reach and maintain the desired initial cell voltage. Positive or negative charge injections may be required depending upon which side of the desired voltage the open circuit cell potential lies. The time required to reach the initial desired potential depends upon the voltage change from the open circuit potential, the rate of injection, the size of each charge injection, the Faradaic current at the initial potential desired and the electrode capacitance. The charge injection size used to maintain the initial potential is made small to ensure that the cell potential is held within a few millivolts of the desired initial value. The final, or switching potential, as it is often called in cyclic voltammetry, determines the direction of the voltage scan from the initial potential.

L.0 Step Size

The step size selected determines the number of data points which will result from each voltage scan. For example, if the total voltage scan range is 1000 mV and the

selected step size is 10 mV there will be 100 data points for each scan. The desired potential at each step is calculated and stored in the microcomputer before each voltage scan. The scan rate is determined by dividing the step voltage change by the total step time.

M.O The Flow Chart

The computer program for performing staircase cyclic voltammetry was constructed in a flow chart so the proper sequence of events for the program could be easily deter-See Figure 5-3 A, B, and C. A final, but very immined. portant decision which needs to be made before programming can begin, is the manner in which the program is to be executed. Programs which require a small amount of input are easily executed by entering the required program variables in a structured dialog format. For programs which require a longer amount of input, it becomes very undesirable to use a structured dialog because of the long list of variables which need to be entered for each execution of the program. A command point format is more desirable since the operator may enter only the program variables which change from one experiment to the next.

N.O Trouble Shooting Instrumental Problems

A great deal of time can be spent in maintaining the electronics of the charge injection instrument. It is important to recognize when the instrument is malfunctioning and to identify the causes quickly. In the following

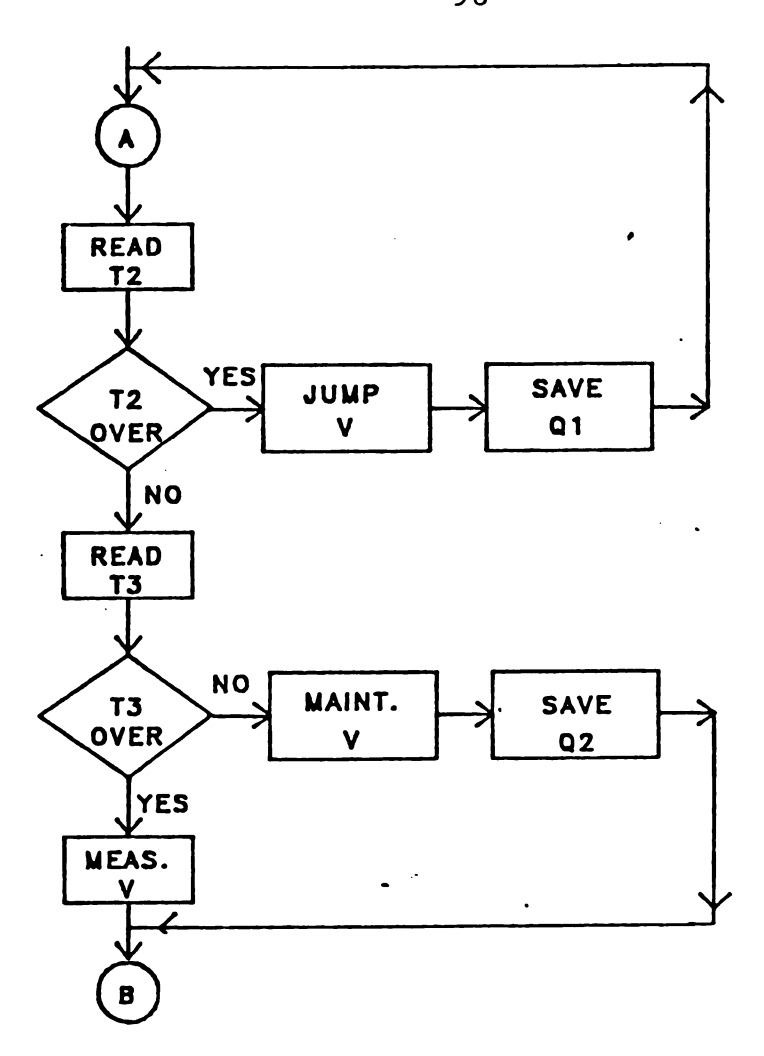


Figure 5-3 A. Flow chart of cyclic voltammetry.

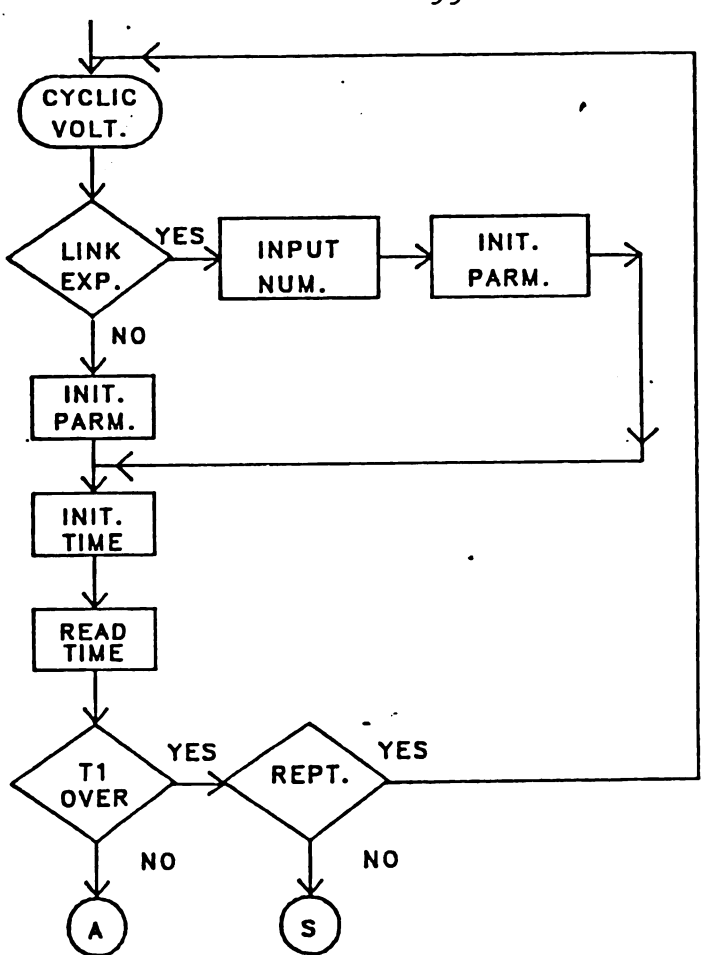
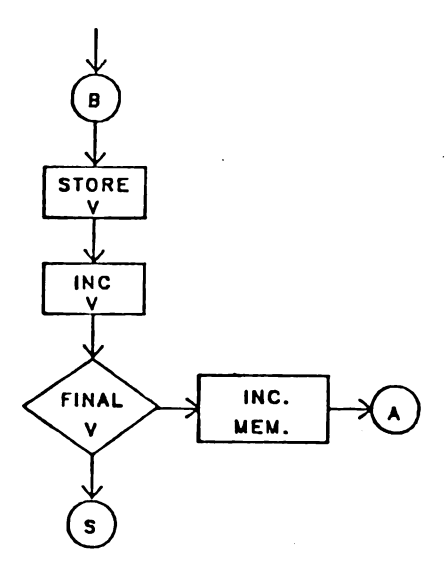


Figure 5-3 B. Flow chart of cyclic voltammetry.



CONT FLOW CHART

CYCLIC VOLTAMMETRY

Figure 5-3 C. Flow chart of cyclic voltammetry.

section I would like to point out how to attack these problems with the hardware and software tools available.

A basic test of the electrochemical system is "to jump" the cell potential and maintain it constant. The program CKCV.OBJ can be used for this test. The initial potential is set with parameter INIT and the charging voltage is set with parameters VAPDA (+ voltage) and VAPDAl (- voltage). When the program is run, if the initial potential is reached, the word READY will be sent to the monitor screen. It is usually best to do the test on a dummy cell similar to Figure 2-2. Initial potentials greater than and less than zero should be used to test if both positive and negative charge is being injected. The $R_{\rm f}$ resistor in the dummy cell should be large (500 k Ω) to reduce the current demand on the

charge injector. A wire can be used to discharge the capacitor between tests.

If the initial potential cannot be reached, it is first important to make doubly sure that the dummy cell is correctly constructed.

Next, check the output voltage of all power supplies to be certain that they are working correctly. The program CKCV.OBJ tests the charge injector and the voltage measurement system but not the real time clock. We therefore need to turn our attention to these two systems if this initial test fails.

The charge injector system is easily tested at this time with the aid of an oscilloscope. The scope probe can be placed at the counter electrode and its ground connected to the power supply ground. To observe the charge injection pulses easily, the charging voltage (VAPDA and VAPDA1) should be made large. The program CKCV.OBJ is then run and the counter electrode voltage monitored on the scope. frequency of the oscilloscope time base can be set "HIGH" to observe a single charge injection or set "LOW" to observe multiple pulses from the charge injector. If the counter electrode is held at a constant DC voltage of + 12 volts then the charge injector is at limit and there is a problem with the charge injection system. The injecting amplifier, analog switches or switch drivers are suspect. Only switch A and capacitor A of the charge injector are active in this initial test with CKCV.OBJ therefore it is best to test the switches by another method.

The switches can be tested manually from the keyboard. This is done by first activating the break switch. A capital 'O' is typed to obtain octal numbers and /173600 is typed to address the switches. The number '1' and a line feed are then typed to connect the switches to the DAC. A '4' line feed is typed to discharge the capacitors. The charging and discharging process can be observed by connecting a digital voltmeter to the injecting capacitors nongrounded side or pin 8 of the analog switch (SD5000).

The DAC converter may be tested at this time by running the program CKDAC.OBJ. Option 2 of this program allows the DAC to be set to any value. The output voltage can be observed at the voltage follower output of the DAC or the injecting capacitors by throwing the switches from the keyboard in the above manner.

The instrument may not be able to reach the initial voltage if the voltage measurement system is working improperly. To test the ADC, the reference electrode is connected to a voltage reference source and the program CKADC.OBJ is run. This program reads the ADC and displays the result on the monitor after typing the enter key. The ADC may be calibrated by adjusting the offset potentiometer at this point if needed.

These simple tests allow the user to quickly isolate possible system problems. The testing of each system circuit must then follow using a circuit diagram and one's electrical knowledge and intuition.

VI RESULTS AND DISCUSSION

A.0 A Computer Model for Staircase Voltammetry with Charge-Step Polarization

When a chemist is faced with the challenge of exploring a new analytical technique, decisions must be made as to what experiments are going to be investigated and how the experiments are to be conducted. Analytical chemists by their training have a good idea of how to optimize the measurement process but it is often more difficult to decide which experimental variables to maintain constant and which to vary. To aid in these decisions theory must be consulted.

B.O Guidance from Theory

The theory of staircase voltammetry was chosen to aid in the development of experiments. This theory was chosen because the diffusion process occurring at the stationary electrode remains fundamentally unchanged in the coulostatic experiment. This is because, in the over all result, it doesn't matter how the potential is controlled, whether by an analog potentiostat or a charge injection potentiostat. The end result is still the same, the electrode is charged and a potential step is taken. The experiments performed in this research are the digital equivalent to the conventional analog experiment. It must therefore be expected that the

total charge delivered during the step, which is measured, is numerically related to the instantaneous current measured in analog experiments.

The equation for the theory of staircase voltammetry (29) was integrated to provide an equation expressed in charge. The result is presented below:

$$m \qquad (1-1+\gamma\theta_{i})/(1+\gamma\theta_{(i-1)})D_{0}1/2$$

$$Q_{m} = 2nFAC* \Sigma$$

$$i=1 \qquad (1+\gamma\theta_{i})\pi^{1/2}(t_{m}+(m-i)\tau)^{1/2})$$

$$\theta_{i} = \exp((nF/RT)(E_{i}-E^{0})) \qquad (6-2)$$

This equation yields charge-potential profiles for a potential step or staircase ramp thus providing calculated results which can be compared to experimentally determined values. These calculated results thus serve as a model to predict what experiments should be conducted and what the results should yield. The calculations are complex and time consuming to calculate by hand because the current (or charge) for a given step in the staircase waveform is dependent upon the current from all previous steps and so a summations of terms must be completed for each step. These equations were therefore programmed into a computer for rapid analysis. The programming was organized to accomplish four tasks:

 show current-potential voltammograms to compare with existing staircase theory;

- 2. generate charge-potential voltammograms to predict the interrelationships of experimental parameters;
- 3. provide current-time profiles for any step along the potential waveform;
- 4. provide charge-time profiles for any step along the potential waveform;
- 5. calculate a charging current error associated with the current measurement in staircase voltammetry.

All programs were written in FORTRAN and the data files were output in a MULPLT format for plotting. The staircase voltammetry equations contain no charging current contributions and assume an ideal potential step.

C.O Faradaic and Charging Current

Linear scan stationary voltammetry calculations show that charging current errors are large for dilute solutions. For example, a lx10⁻⁶ M solution of a univalent ion, shows a 30 percent charging current error at a sweep rate of 500 mV/sec. This error increases very rapidly with sweep rate. At a sweep rate of 10 v/sec the error has increased to 130 percent. Because sweep rates in excess 1000 v/sec are needed to study fast electrochemical reactions, the charging current error presents the researcher with an unworkable environment unless special charging amplifiers and cell designs are employed.

Staircase voltammetry, when taken from a quantitative point of view, is preferred to linear scan voltammetry because of the ability to separate the Faradaic current from the charging current. Equation 1-21 and 1-22 predict

charging and Faradaic current for staircase voltammetry respectively. The error created by the charging current depends on the relative magnitude of the capacitive and Faradaic currents at the time the current is measured. The purpose of the programming at the first level was to get a quantitative measure of the charging current errors encountered in staircase voltammetry under various experimental conditions.

After a potential step is taken, the capacitive current decays exponentially with time. At a potential where the electrochemical reaction is occurring, the Faradaic current decays as a function of the reciprocal square root of time. The error of the charging current is complex because of the many factors which effect the decay of the curves and also because the charging current delays the attainment of the step potential. Neglecting the non-ideal potential rise, equations 1-21 and 1-22 were programmed into the computer to show what factors influence current measurements and what the optimal point in time would be to make current measurements.

Figure 6-1 shows the decay of the capacitive and the Faradaic current as calculated by program STEPI.FTN.

Figure 6-2 shows the flow chart for the program. The Faradaic current decay is calculated for lx10⁻⁶ M CdCl₂ in 1 M KCl at the step potential -.5 V vs. SCE (EO=-.637 V vs. SCE) and with a step size of 10 mV. The sample time on the x-axis shows the time measured 5 msec after the potential

FAR.(A) and CAP.(B) CURRENT = 500 ms; t = 5 ms; step = 10 mv; E = -.5; E = -.637

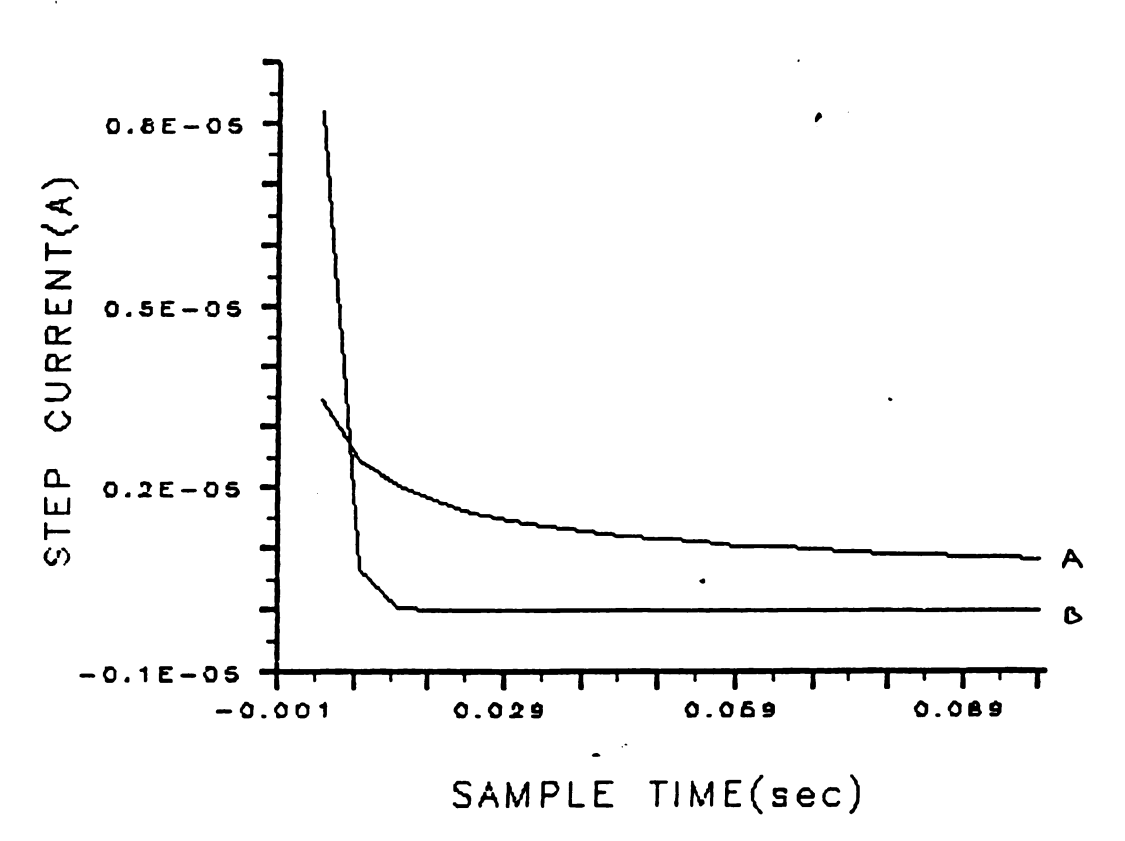
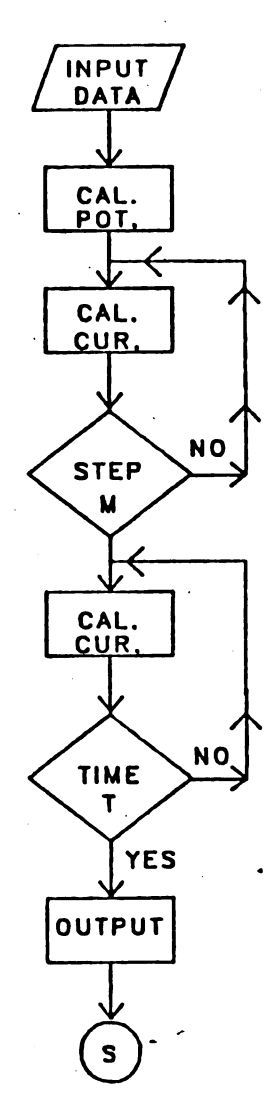


Figure 6-1. The Faradaic and capacitive current decay curve. Step size=10 mv, step potential= 0.5 V, reduction potential=-0.637 V, step time τ =500 ms, and t_m =5 ms.



FLOW CHART

FOR STEP

CURRENT

Figure 6-2. Flow chart for STEPI.FTN.

step rise. At time zero the charging current and the Faradaic current are highest. The two currents then begin to decay according to their time function dependence. The charging and the Faradaic current decay curves intersect at a time when the charging current crosses the Faradaic current level. Experimental conditions which extend this crossing point can result in increasing the charging current error.

Figure 6-3 shows an increase in uncompensated solution resistance from 100 to 1000 Ω . The decay curve with the higher solution resistance decays at a slower rate and thus results in a greater charging current error. Thus solution resistance is expected to cause wave distortions when staircase voltammetry is employed in studies where the resistance changes from one solution to the next. Such problems are expected to occur with the use of flow through thin layer cells commonly used in electrochemical detectors for liquid chromatography. Additional problems occur in thin layer cells because of difficulties encountered in placing the reference electrode close to the working electrode to reduce uncompensated resistance and also because of solubility problems encountered with nonaqueous solutions.

An increase in electrode capacitance from 5 to 40 μF is shown in Figure 6-4. The increase in electrode capacitance also delays the charging current decay curve. The electrochemical parameters of the cell used in these studies are: an electrode area of approximately 0.032 cm2, a KCl

CAPACITANCE CURRENT VS SOLUTION RESISTANCE T=500ms; t=5ms; step=10mv; RES.= (A)100,(B)1000 ohms

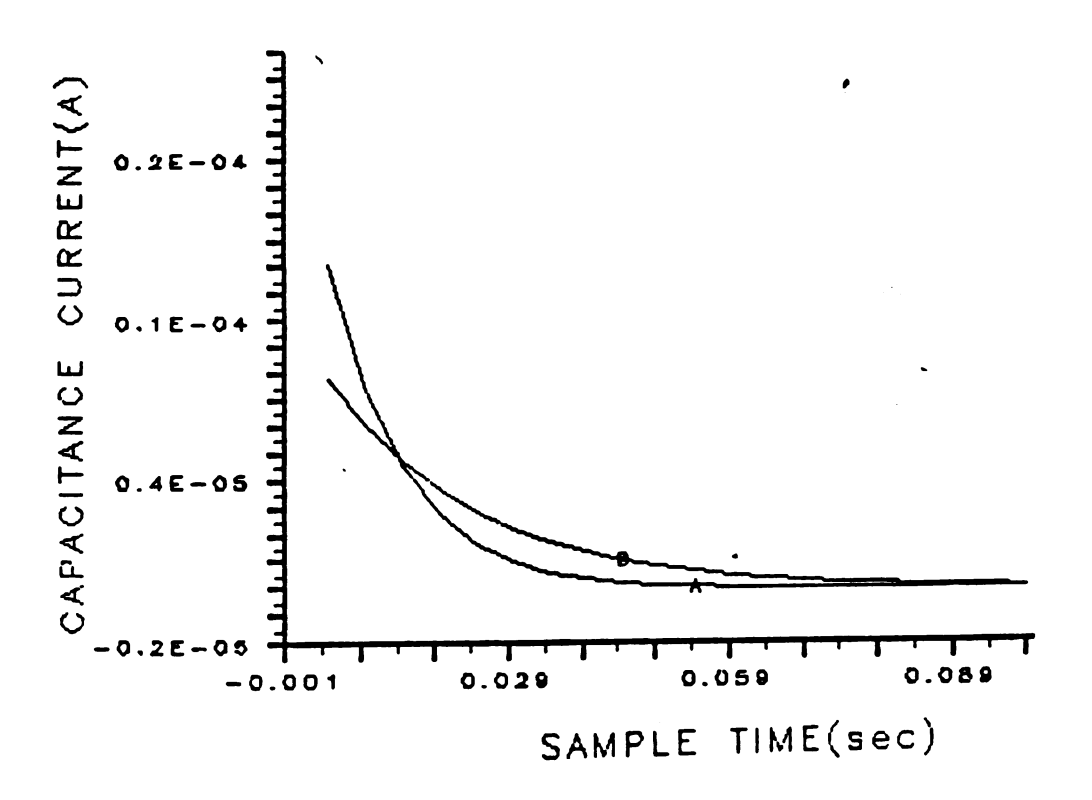


Figure 6-3. Effect of solution resistance on the capacitive current decay curve. Resistance A=100 Ω , B=1000 Ω ; step size=10 mV and t_m=5 ms.

STEP CURRENT VS SAMPLE TIME

7=500ms, t=5ms, step=10mv, cap.= (A)40, (B)5µF

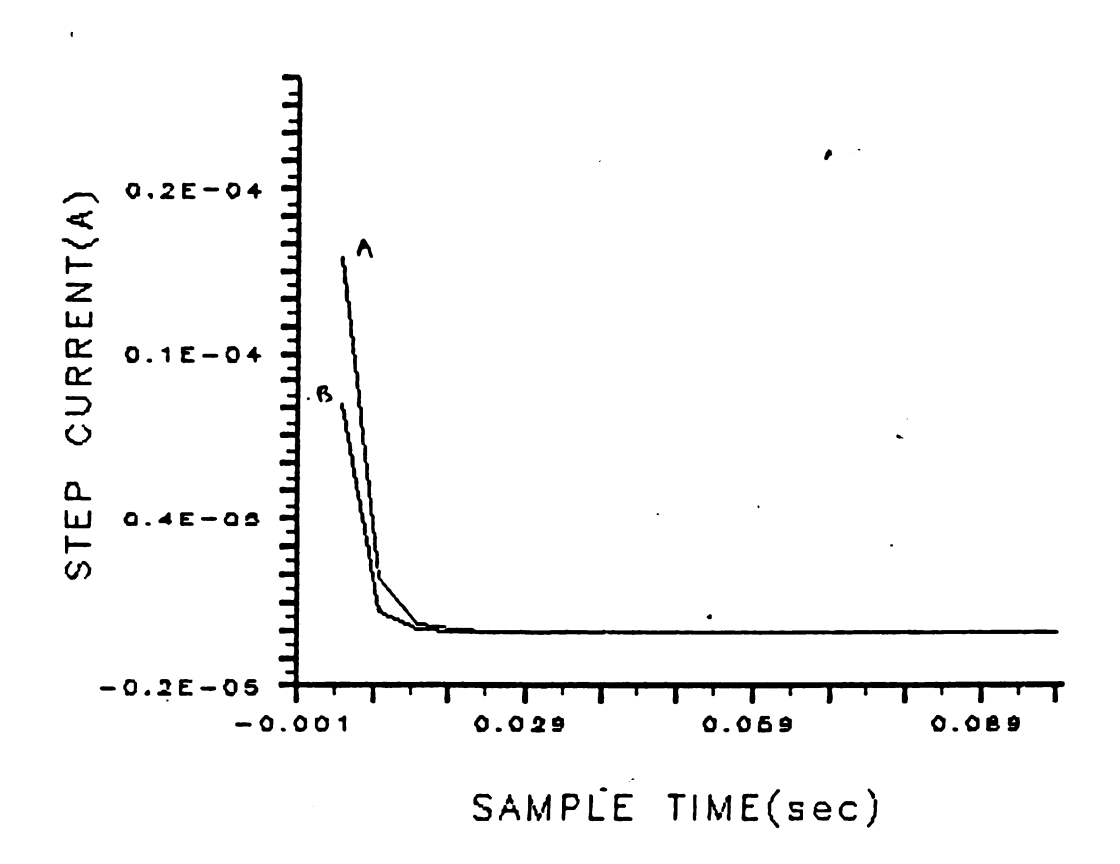


Figure 6-4. The effect of electrode capacitance on the charging current decay curve. Electrode capacitance A=40 μF , B=5 μF , step time $\tau = 500$ ms, and $t_m = 5$ ms.

electrolyte concentration of 0.01 M, an electrode capacitance of about 40 μF and a cell resistance of 1000 Ω . Increasing the electrode surface area will decrease the cell resistance but will increase the electrode capacitance. Decreasing the electrode area will decrease the cell current and can decrease the signal to noise ratio. The electrochemical cell has electrical properties which can be changed in a complex manner by changing the electrode areas and the cell geometry. It was therefore important to fix the electrodes in a stationary geometry and to be consistent in reproducing the electrode areas. The counter electrode was constructed from a coil of platinum wire which had a surface area several times that of the working electrode and encircled the working electrode.

Step size is another experimental factor which is important when considering the effects of charging current on staircase voltammetry. Figures 6-5 and 6-6 show how the charging and the Faradaic current decay curves change with increasing step size. The step time τ and the step size both changed in this example to keep the sweep rate ($\Delta E/\tau$) constant at 3.8 V/sec. For the 6 mV step, the step time τ is 2080 msec but for the 10 mV step the step time τ has increased to a value of 2600 msec. After the potential step, a 5 msec delay is given for the charging current to decay before the cell current is measured. The plots show that the crossing point of the charging and the Faradaic current graphs occur at longer times when the step size is increased

FAR.(A) and CAP.(B) CURRENT
t=5ma; r=2080ma; 3.5 v/sec; step=6mv

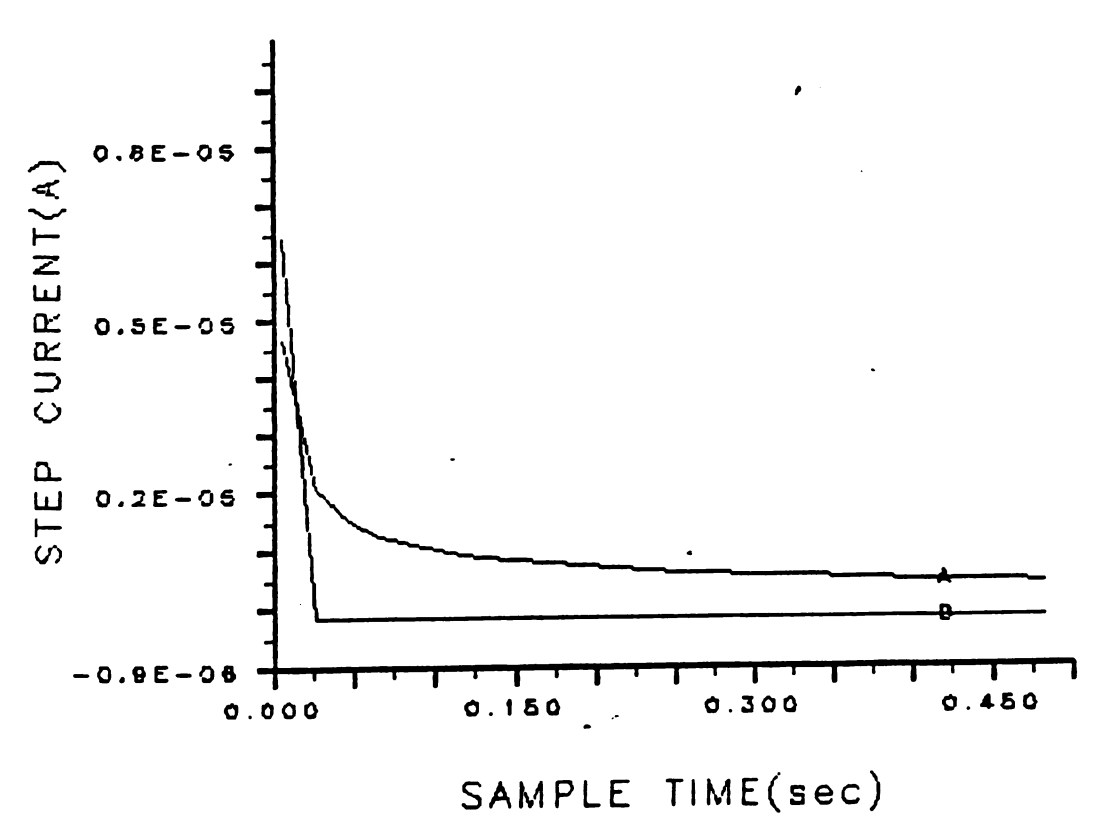


Figure 6-5. The effect of step size on the Faradaic and charging current decay curve at a constant sweep rate. Step size=6 mV, t_m =5 ms step time τ =2080 ms and sweep rate=3.8 v/s.

FAR.(A) and CAP.(B) CURRENT t=5ms; r=2600ms; 3.8 v/sec; step=10mv

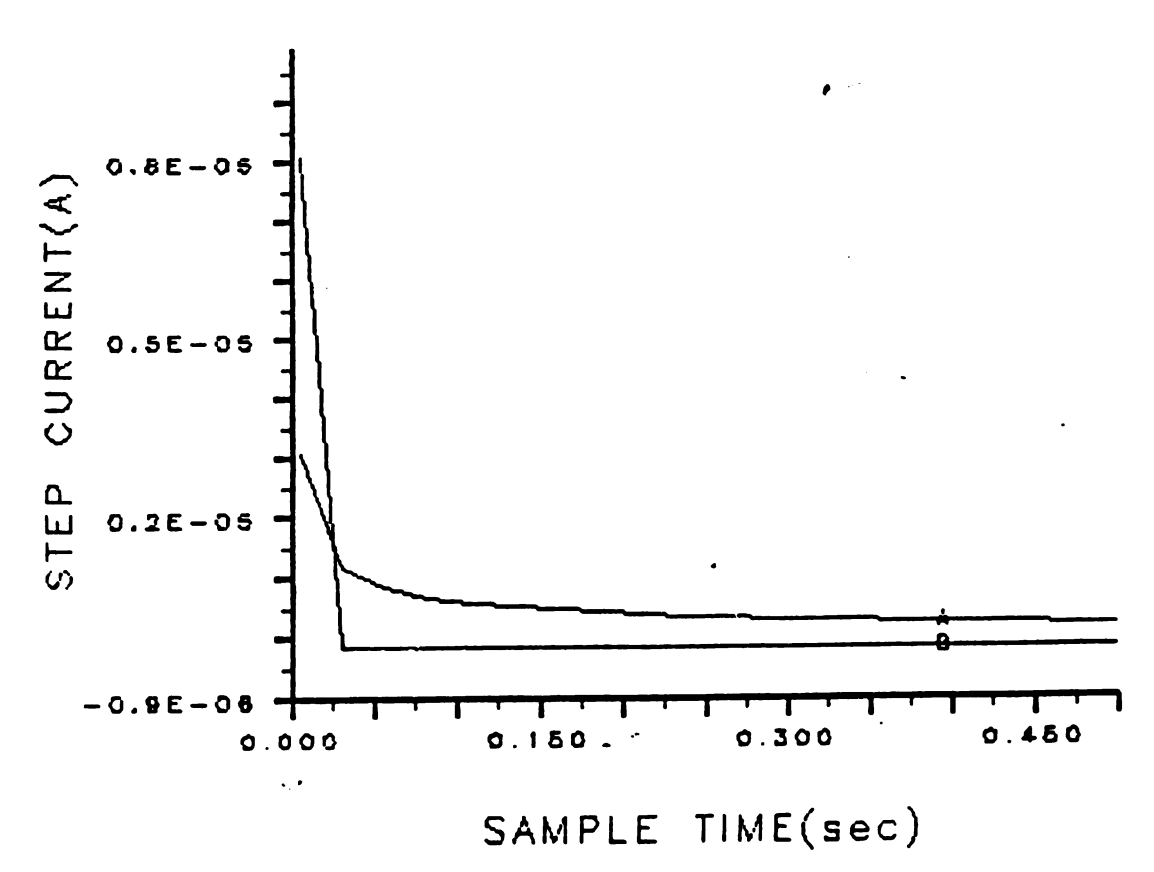


Figure 6-6. The effect of step size on the Faradaic and charging current decay curve at a constant sweep rate. Step size=10 mV, t_m =5 ms step time τ =2080 ms and sweep rate=3.8 v/s.

to larger steps. Plots were made for step sizes of 2, 4, and 5 millivolts. Figure 6-7 shows that the ratio of charging current to the Faradaic current increases sharply as the step size increases from 5 to 10 mV and thus the relative error also increases. This indicates that it would be advantageous to delay more time for the larger step size so that the capacitive current will fall below the Faradaic current before the current sample is taken.

One of the disadvantages of conventional staircase voltammetry is that it is difficult when running an experiment to choose the proper sweep rate, step size, and sampling time to optimize the measurement and maximize the sensitivity. This is because of the many interrelated factors which influence the capacitive and Faradaic current decays. Usually, a simple solution to this problem is to experiment with test runs to decide which conditions appears to be best for the test solution at hand. In non-aqueous solutions with high resistance it is often not possible to obtain undistorted voltammograms under any set of condi-These distortions are similar to those shown in Figure 1-6. Because these distortions resemble a quasireversible system it can't be determined with certainty if a reversible reaction is occurring at the electrode. problems of the potentiostat were explained in chapter 1. The coulostatic method offers solutions to some of these problems.

CAPACITIVE ERROR VS STEP SIZE t=5ms; 3.8mv/sec; step=2, 4, 5, 6, 10mv

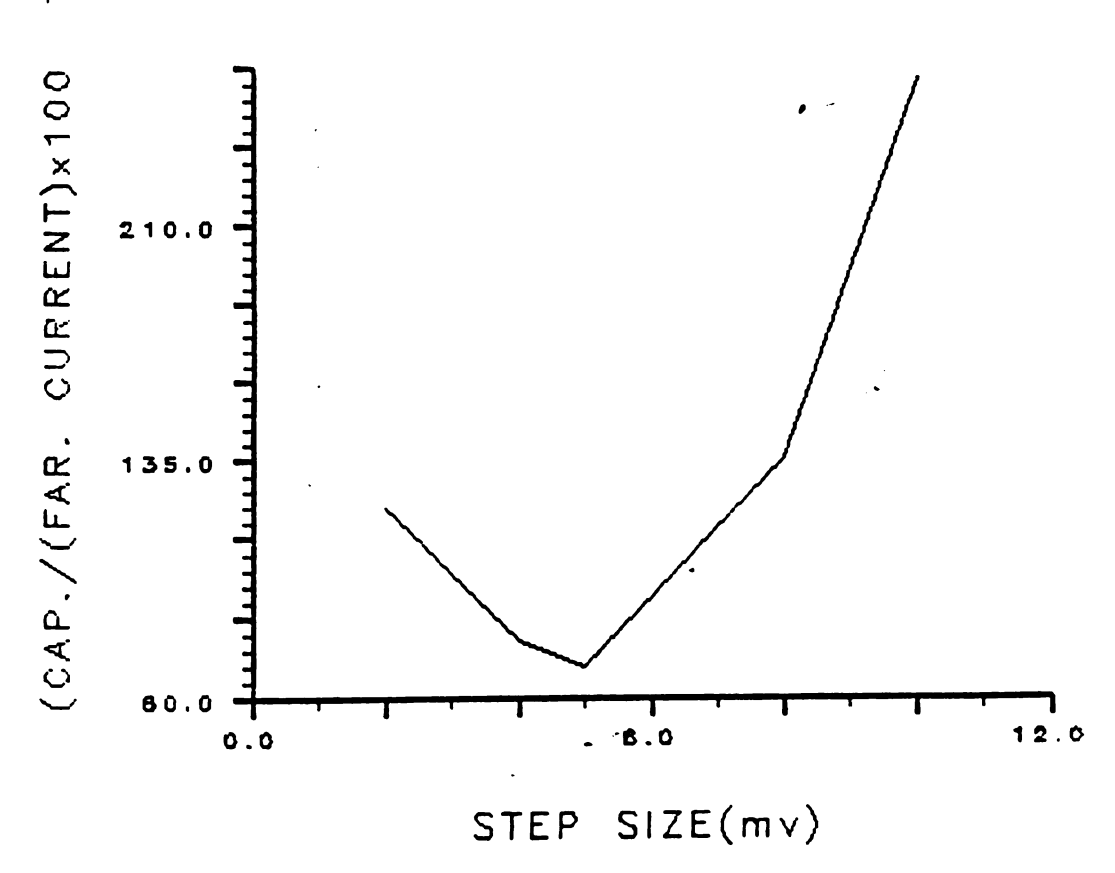


Figure 6-7. The effect of step size on the ratio of capacitive current to Faradaic current at constant sweep rate. Sweep rate=3.8 mV/s and $t_m\!=\!5$ ms.

D.0 Step Charge

It may be stated that a potentiostat varies the current to control the potential. With a scanning coulostatic method, on the other hand, the charge is the forced or controlled variable and the potential is left to vary. charging current error must therefore be considered differently in experiments where coulostats are employed. There is no longer an exponential decay of charging current as with the potentiostat. The double layer charge is put onto the electrode with an injection pulse which lasts, even in the presence of a large solution resistance, only the length of the injection pulse. The cell is placed at open circuit after the charge injection so no further charging can occur from the external circuit. The charging current problem is therefore avoided but the method will encounter other problems such as the ability to achieve the desired step potential when the double layer capacitance is changing over the potential range of interest and the ability to maintain a constant step potential. These errors and non-ideal effects will be covered in a later section.

The charge predicted for an ideal potential step can be calculated by integrating the current equations over the proper limits. The sooner the integration period begins after the potential step has settled, the greater the total charge acquired for the step. Figure 6-8 shows how the step charge changes with the time at which the integration begins for the determination of 1×10^{-6} M CdCl₂. The step size is

set to 10 mV and the cell potential jumps from the previous staircase step to -0.6 V vs. SCE. The plot assumes that it is possible for the cell potential to jump 10 mV and settle instantaneously at the desired step potential. After a delay period of 1 µsec, the cell current is integrated to the end of the step. Beginning the integration period shortly after the potential step, catches the Faradaic current high in its decay curve. But if 50 to 100 msec are required to pass before the integration process starts, lower step charge profile results, as indicated in Figure 6-8. It is therefore advantageous to begin the integration period as soon as the potential has settled to the desired step potential value. When charging a real electrode, if the integration period begins before the potential step has settled to the desired value, the double layer charge will be included with the Faradaic charge. This then sets the limit to how fast the electrode potential may be changed. If the charge injector can not bring the electrode potential to the desired step potential within the designated time limit imposed by the sweep rate, a charging current error results.

E.O The Step Time Parameters

It is important to be able to predict the effect of changes in the step parameters on the shapes of current voltammograms and to note any differences in shapes of corresponding charge voltammograms which are generated by integrating the step current.

STEP CHARGE VS STEP TIME 1x10-6 cdc12, STEP--.6 v

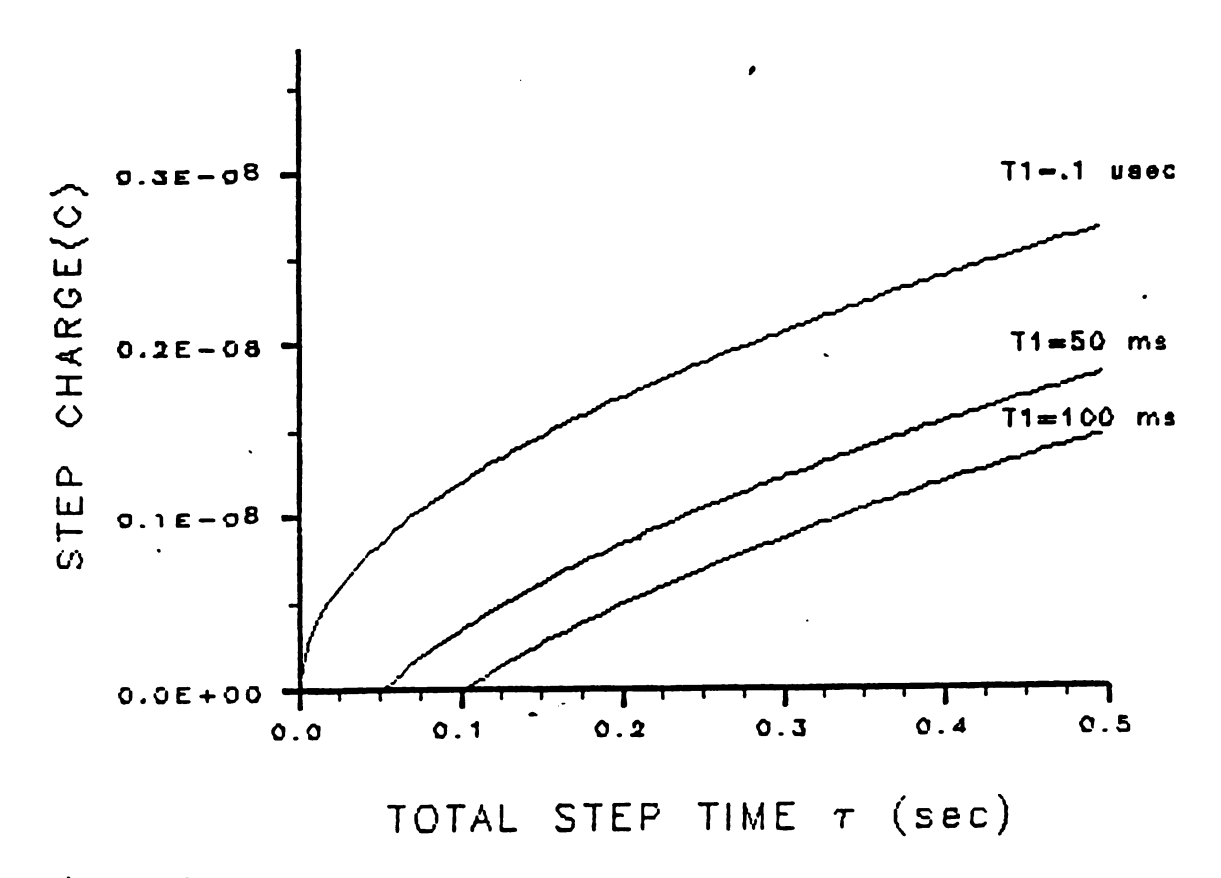


Figure 6-8. The calculated change in step charge with time for 1×10^{-6} M CdCl₂ at a step potential of -.6 v vs. SCE.

The first parameters tested were the influence of the ratio of τ/t on a conventional staircase voltammogram.

Table 6-I A-D shows the calculated current function values and plots are shown in Figures 6-9 A-D. To make the plots as general as possible, a current function term is plotted on the y-axis and a potential function on the x-axis. The current function is:

$$i_n = i/nFAC(D_0^{\tau \pi})^{1/2}$$
 (6-3)

and the potential function is:

$$E_{i} = -n(E_{i} - E_{0}) \qquad (6-4)$$

where \mathbf{i}_n is a normalized current, \mathbf{E}_i is the step potential at step number i, and the other symbols have their usual meaning.

Table 6-I A. Calculated Current Function Values for Various Potentials $\tau/t_m=1$

-n (E-E ₀)	i Function	-n(E-E ₀)	i Function	
-0.240	0.472E-04	0.200	0.315	
-0.220	0.136E-03	0.220	0.300	
-0.200	0.324E-03	0.240	0.287	
-0.180	0.729E-03	0.260	0.276	
-0.160	0.161E-02	0.280	0.265	
-0.140	0.352E-02	0.300	0.256	
-0.120	0.763E-02	0.320	0.248	
-0.100	0.164E-01	0.340	0.241	
-0.800E-01	0.349E-01	0.360	0.234	
-0.600E-01	0.720E-01	0.380	0.228	
-0.400E-01	0.140	0.400	0.222	
-0.200E-01	0.247	0.420	0.217	
-0.119E-06	0.375	0.440	0.212	
0.200E-01	0.477	0.460	0.207	
0.400E-01	0.521	0.480	0.203	
0.600E-01	0.515	0.500	0.199	
0.800E-01	0.483	0.520	0.195	
0.100	0.445	0.540	0.191	
0.120	0.410	0.560	0.188	
0.140	0.379	0.580	0.185	
0.160	0.354	0.600	0.181	
0.180	0.333			

Table 6-I B. Calculated Current Function Values for Various Potentials $\tau/t_{m}\,=\,10$

-n (E-E ₀)	i Function	-n (E-E ₀)	i Function
-0.240	0.149E-03	0.200	0.333
-0.220	0.370E-03	0.220	0.314
-0.200	0.839E-03	0.240	0.299
-0.180	0.185E-02	0.260	0.286
-0.160	0.406E-02	0.280	0.275
-0.140	0.884E-02	0.300	0.265
-0.120	0.192E-01	0.320	0.256
-0.100	0.412E-01	0.340	0.247
-0.800E-01	0.871E-01	0.360	0.240
-0.600E-01	0.178	0.380	0.233
-0.400E-01	0.341	0.400	0.227
-0.200E-01	0.580	0.420	0.221
-0.119E-06	0.825	0.440	0.216
0.200E-01	0.949	0.460	0.211
0.400E-01	0.908	0.480	0.207
0.600E-01	0.780	0.500	0.202
0.800E-01	0.649	0.520	0.198
0.100	0.546	0.540	0.194
0.120	0.473	0.560	0.191
0.140	0.421	0.580	0.187
0.160	0.384	0.600	0.184
0.180	0.355	-	

Table 6-I C. Calculated Current Function Value for Various Potentials τ/t_{m} = 100

-n (E-E ₀)	i Function	-n (E-E ₀)	i Function
-0.240	0.472E-03	0.200	0.338
-0.220	0.108E-02	0.220	0.317
-0.200	0.238E-02	0.240	0.301
-0.180	0.520E-02	0.260	0.287
-0.160	0.113E-01	0.280	0.276
-0.140	0.247E-01	0.300	0.265
-0.120	0.534E-01	0.320	0.256
-0.100	0.115	0.340	0.248
-0.800E-01	0.242	0.360	0.241
-0.600E-01	0.491	0.380	0.234
-0.400E-01	0.930	0.400	0.228
-0.200E-01	1.55	0.420	0.222
0.119E-06	2.10	0.440	0.217
0.200E-01	2.23	0.460	0.212
0.400E-01	1.88	0.480	0.207
0.600E-01	1.38	0.500	0.203
0.800E-01	0.970	0.520	0.199
0.100	0.707	0.540	0.195
0.120	0.551	0.560	0.191
0.140	0.459	0.580	0.188
0.160	0.402	0.600	0.185
0.180	0.365		

Table 6-I D. Calculated Current Function Values for Various Potentials τ/t_{m} = 10,000

-n (E-E ₀)	i Function	-n (E-E ₀)	i Function
-0.240	0.472E-02	0.200	0.382
-0.220	0.103E-01	0.220	0.338
-0.200	0.225E-01	0.240	0.310
-0.180	0.491E-01	0.260	0.292
-0.160	0.107	0.280	0.278
-0.140	0.232	0.300	0.266
-0.120	0.502	0.320	0.257
-0.100	1.08	0.340	0.248
-0.800E-01	2.27	0.360	0.241
-0.600E-01	4.60	0.380	0.234
-0.400E-01	8.66	0.400	0.228
-0.200E-01	14.2	0.420	0.222
-0.119E-06	18.8	0.440	0.217
0.200E-01	18.9	0.460	0.212
0.400E-01	14.5	0.480	0.207
0.600E-01	9.10	0.500	0.203
0.800E-01	5.08	0.520	0.199
0.100	2.74	0.540	0.195
0.120	1.51	0.560	0.191
0.140	0.908	0.580	0.188
0.160	0.610	0.600	0.185
0.180	0.460		

REVERSIBLE CASE $\tau/t=1$

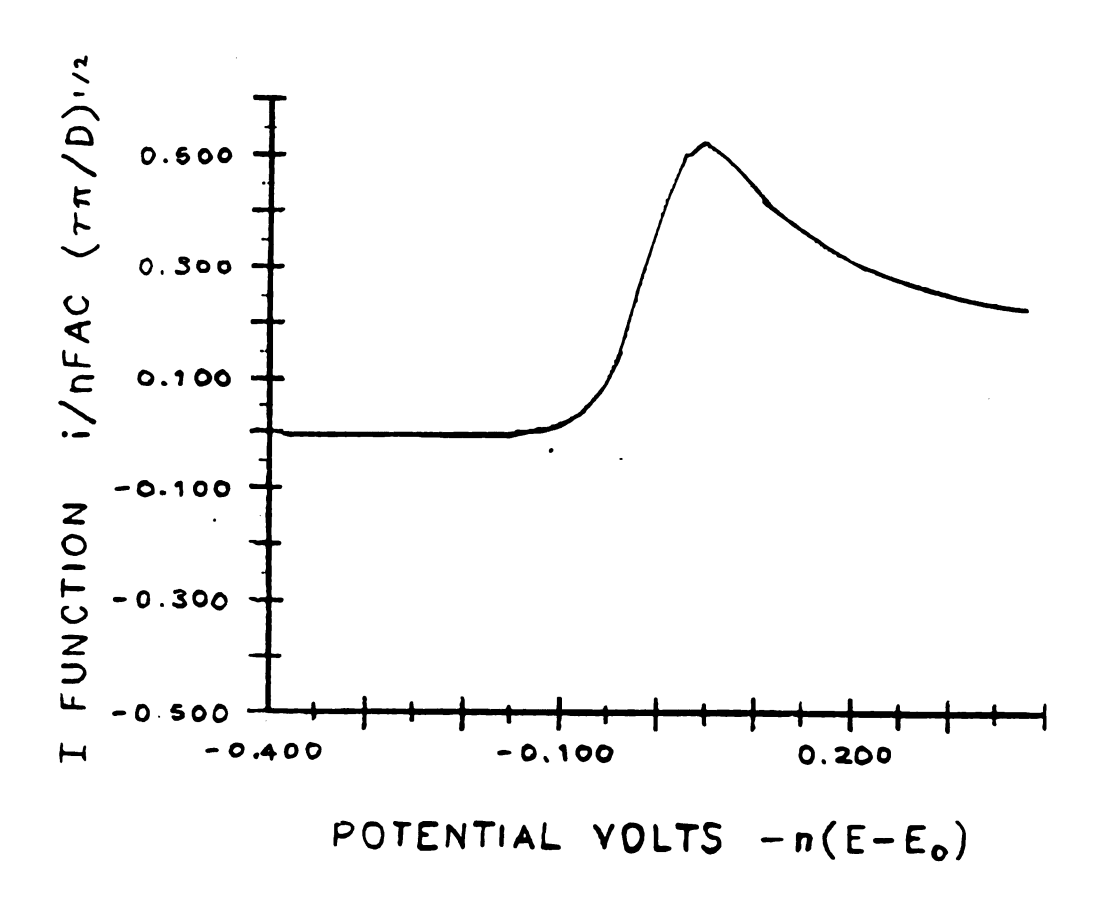


Figure 6-9 A. Influence of the ratio of */tl on reversible current voltammograms. Step size 10 mV.

REVERSIBLE CASE T/t=10

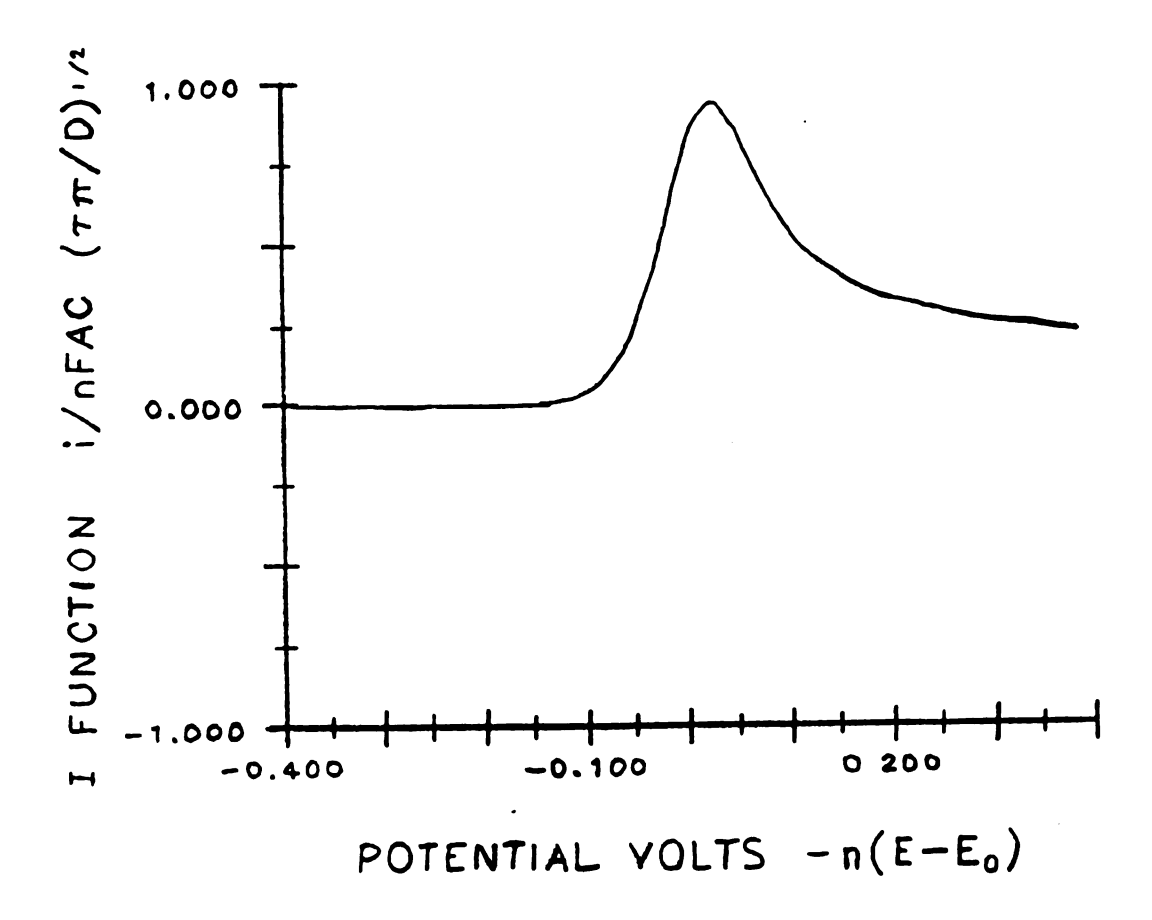


Figure 6-9 B. Influence of the ratio of τ/tl on reversible current voltammograms. Step size 10 mV.

REVERSIBLE CASE $\tau/t=100$

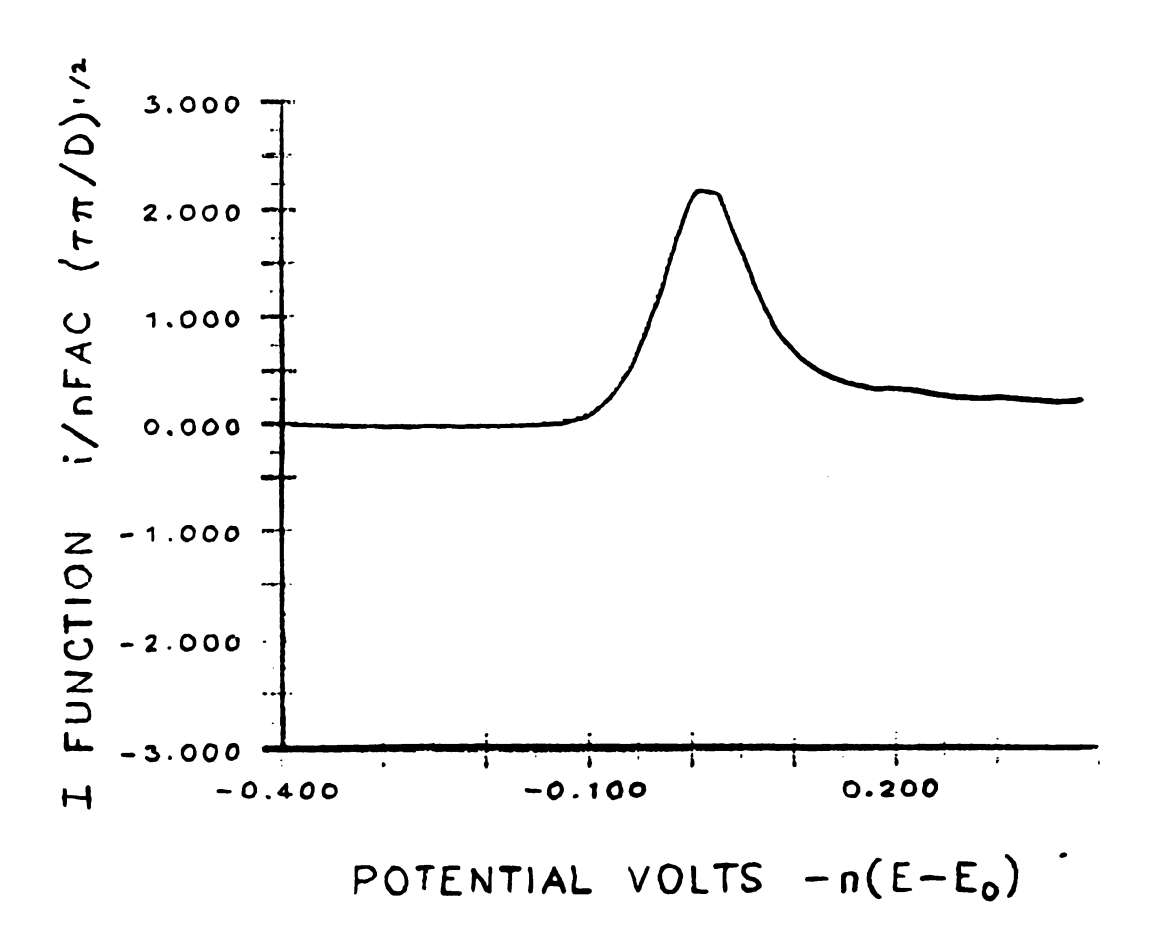


Figure 6-9 C. Influence of the ratio of τ/tl on reversible current voltammograms. Step size 10 mV.

REVERSIBLE CASE $\tau/t=10,000$

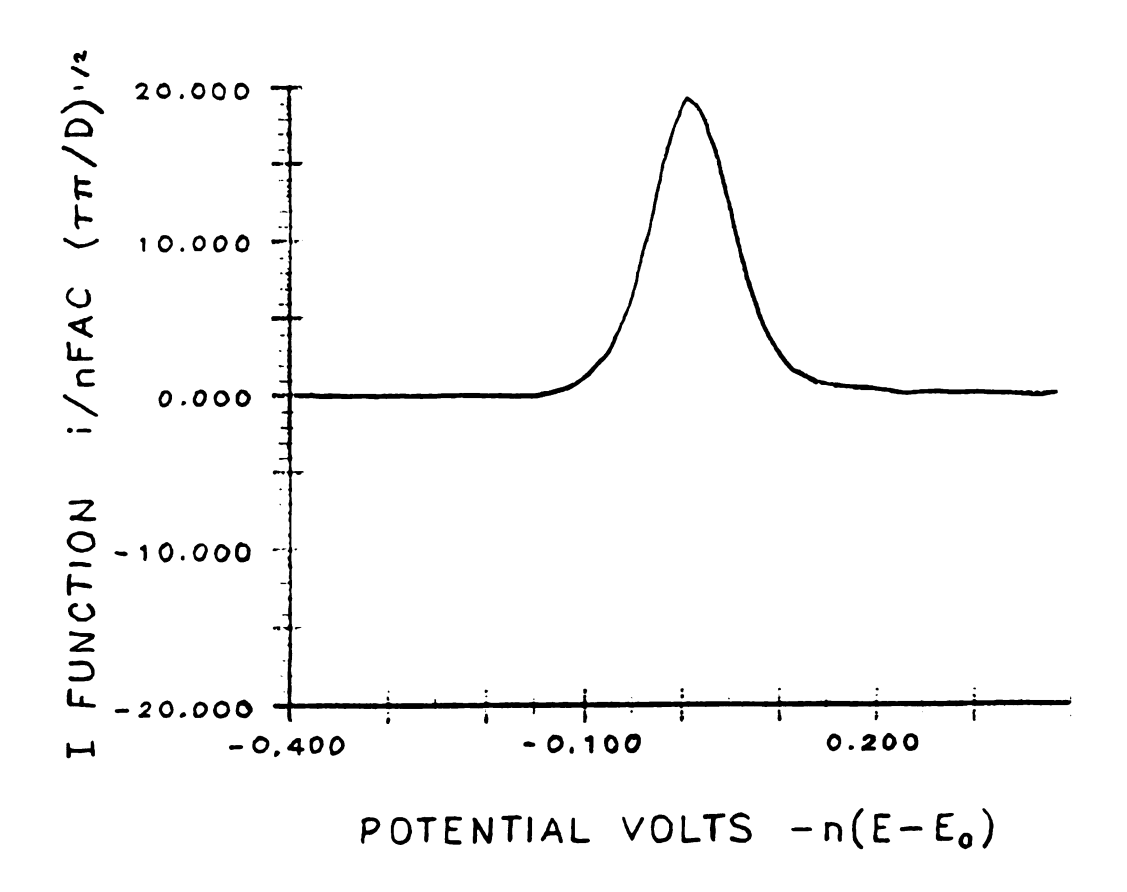


Figure 6-9 D. Influence of the ratio of τ/tl on reversible current voltammograms. Step size 10 mV.

F.O Sampling Time

A τ/t ratio of 1, as shown in plot 6-9A indicates that the current sample is taken at the end of the potential step. As the ratio of τ/t becomes greater the voltommagrams have a greater peak current and the waves becomes more graussian shaped. These changes in wave shape can be understood by considering the current to be conceptually and mathematically made up of currents from two sources. The

first current source is from all previous steps and the second source is from the last new step. The last term in Equation 1-22 is equal to the current from the last new step. The last term of the summation is:

$$i_{m} = (1-(1+\gamma\theta_{m})/(1+\gamma\theta_{m-1})D_{0}^{1/2}$$
 (6-5)

where i_{m} stands for the current from the last potential step and the other symbols have their usual meaning.

The current due to the last step m, when in a potential region near the peak where the numerator of Equation 6-3 is not zero, can vary over several orders of magnitude. This is because t_m is always less than or equal to τ . When t_m is small, the current is high.

The current from all steps but the last can be expressed by Equation 6-3 when the summation interval is changed to cover all but the last step (from i=1 to i=m-1). The current from all previous steps is limited when t_m is small because $(t_m + (m-i)\tau)$ can never be less than τ . In the potential region past the peak, the concentration of the reducible species at the electrode is zero and no new current can be produced by subsequent new steps; only current from previous steps can contribute to the measured current.

To summarize, the effects of τ/t are shown in Figures 6-9 A-D. It becomes apparent that the voltammogram peak current is enhanced with increasing τ/t ratio, the peak current is greatly increased with the τ/t ratio but the current beyond the peak is not greatly effected. Also note

that the peak potential moves closer to E0 as the ratio of τ/t increases.

Charge voltammograms were generated by integrating Equation 6-3. The flow chart for the program is shown in Figure 6-10. The potential step is divided into two regions and the integrated current from each region is separately plotted (see Figure 6-11). The first region is given the symbol Tl and the current integrated over T_1 is called the "presample charge". Assuming that an ideal potential step is taken and the double layer charge is neglected, the first time period Tl will contain the calculated Faradaic charge lost before the second integration period. The experimental potential step taken by the charge injector on a real cell is not reached instantaneously but slowly rounds up to the desired value. The experimental potential step will therefore differ from the ideal step since it requires more time to reach the desired potential and also because it contains the double layer charge. The second region is given the symbol T2 and the integrated current from this region is called the "sample charge". Since the electrode will be charged by this time, it will be free of double layer charge.

With a constant step time, as the T1 time increases the presample charge accumulated in this time period increases and the charge acquired during time period T2 decreases. When T1= τ , time period T2 is equal to zero and the total step charge is contained in period T1. Tables 6-II A-H

show the calculated charge function values obtained. Figure
6-12 A-D shows the plotted voltammograms.

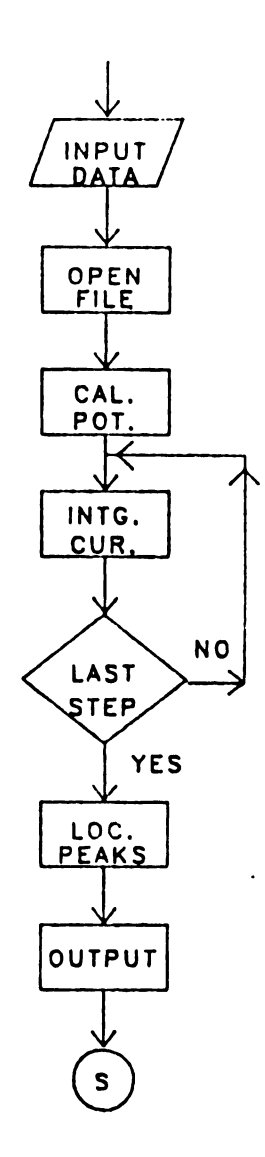


Figure 6-10. Flow chart for charge voltammograms.

STEP TIME

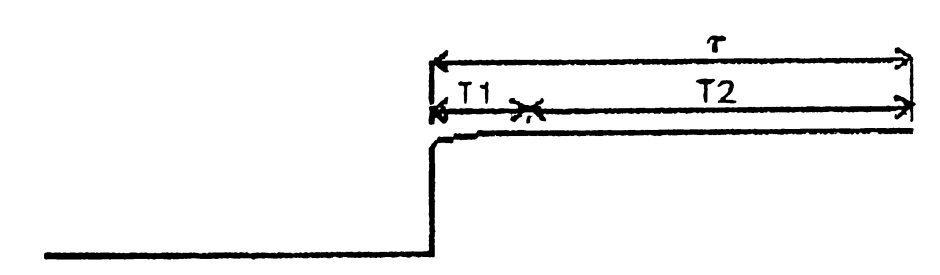


Figure 6-11. Step time periods T1 and T2 for a potential step.

Table 6-II A. Calculated Charge Function Values for Various Potentials τ/Tl = 1, Pre-Sample Charge

-n (E-E ₀)	Rel. Charge	-n (E-E ₀)	Rel. Charge
-0.240	0.944E-04	0.200	0.325
-0.220	0.245E-03	0.220	0.308
-0.200	0.563E-03	0.240	0.294
-0.180	0.125E-02	0.260	0.281
-0.160	0.275E-02	0.280	0.270
-0.140	0.599E-02	0.300	0.261
-0.120	0.130E-01	0.320	0.252
-0.100	0.279E-01	0.340	0.244
-0.800E-01	0.592E-01	0.360	0.237
-0.600E-01	0.121	0.380	0.231
-0.400E-01	0.234	0.400	0.225
-0.200E-01	0.402	0.420	0.219
-0.119E-06	0.585	0.440	0.214
0.200E-01	0.698	0.460	0.209
0.400E-01	0.704	0.480	0.205
0.600E-01	0.641	0.500	0.201
0.800E-01	0.563	0.520	0.197
0.100	0.495	0.540	0.193
0.120	0.442	0.560	0.189
0.140	0.401	0.580	0.186
0.160	0.370	0.600	0.183
0.180	0.345		

Table 6-II B. Calculated Charge Function Values for Various Potentials $\tau/T1$ = 10, Pre-Sample Charge

-n (E-E ₀)	Rel. Charge	-n (E-E ₀)	Rel. Charge
-0.240	0.299E-04	0.200	0.335E-01
-0.220	0.697E-04	0.220	0.316E-01
-0.200	0.155E-03	0.240	0.300E-01
-0.180	0.340E-03	0.260	0.287E-01
-0.160	0.743E-03	0.280	0.275E-01
-0.140	0.162E-02	0.300	0.265E-01
-0.120	0.350E-02	0.320	0.256E-01
-0.100	0.751E-02	0.340	0.248E-01
-0.800E-01	0.159E-01	0.360	0.240E-01
-0.600E-01	0.323E-01	0.380	0.234E-01
-0.400E-01	0.614E-01	0.400	0.227E-01
-0.200E-01	0.103	0.420	0.222E-01
-0.119E-06	0.142	0.440	0.216E-01
0.200E-01	0.154	0.460	0.211E-01
0.400E-01	0.136	0.480	0.207E-01
0.600E-01	0.106	0.500	0.203E-01
0.800E-01	0.798E-01	0.520	0.198E-01
0.100	0.621E-01	0.540	0.195E-01
0.120	0.510E-01	0.560	0.191E-01
0.140	0.439E-01	0.580	0.188E-01
0.160	0.392E-01	0.600	0.184E-01
0.180	0.360E-01		

133
Table 6-II C. Calculated Charge Function Values for
Various Potentials \(\tau/T1 = 100\), Pre-Sample Charge

-n (E-E ₀)	Rel. Charge	-n (E-E ₀)	Rel. Charge
-0.240	0.944E-05	0.200	0.343E-02
-0.220	0.210E-04	0.220	0.320E-02
-0.200	0.462E-04	0.240	0.302E-02
-0.180	0.101E-03	0.260	0.288E-02
-0.160	0.220E-03	0.280	0.276E-02
-0.140	0.477E-03	0.300	0.266E-02
-0.120	0.103E-02	0.320	0.256E-02
-0.100	0.222E-02	0.340	0.248E-02
-0.800E-01	0.467E-02	0.360	0.241E-02
-0.600E-01	0.948E-02	0.380	0.234E-02
-0.400E-01	0.179E-01	0.400	0.228E-02
-0.200E-01	0.295E-01	0.420	0.222E-02
-0.119E-06	0.396E-01	0.440	0.217E-02
0.200E-01	0.408E-01	0.460	0.212E-02
0.400E-01	0.329E-01	0.480	0.207E-02
0.600E-01	0.224E-01	0.500	0.203E-02
0.800E-01	0.143E-01	0.520	0.199E-02
0.100	0.933E-02	0.540	0.195E-02
0.120	0.659E-02	0.560	0.191E-02
0.140	0.509E-02	0.580	0.188E-02
0.160	0.425E-02	0.600	0.185E-02
0.180	0.375E-02		

Table 6-II D. Calculated Charge Function Values for Various Potentials $\tau/T1$ = 10,000, Pre-Sample Charge

-n (E-E ₀)	Rel. Charge	-n (E-E ₀)	Rel. Charge
-0.240	0.944E-06	0.200	0.431E-04
-0.220	0.206E-05	0.220	0.362E-04
-0.200	0.450E-05	0.240	0.321E-04
-0.180	0.979E-05	0.260	0.296E-04
-0.160	0.213E-04	0.280	0.279E-04
-0.140	0.463E-04	0.300	0.267E-04
-0.120	0.100E-03	0.320	0.257E-04
-0.100	0.215E-03	0.340	0.248E-04
-0.800E-01	0.452E-03	0.360	0.237E-04
-0.600E-01	0.917E-03	0.380	0.232E-04
-0.400E-01	0.172E-02	0.400	0.228E-04
-0.200E-01	0.283E-02	0.420	0.222E-04
-0.119E-06	0.373E-02	0.440	0.216E-04
0.200E-01	0.375E-02	0.460	0.212E-04
0.400E-01	0.286E-02	0.480	0.207E-04
0.600E-01	0.177E-02	0.500	0.203E-04
0.800E-01	0.965E-03	0.520	0.198E-04
0.100	0.499E-03	0.540	0.195E-04
0.120	0.258E-03	0.560	0.193E-04
0.140	0.141E-03	0.580	0.186E-04
0.160	0.839E-04	0.600	0.187E-04
0.180	0.567E-04		

Table 6-II E. Calculated Charge Function Values for Various Potentials $\tau/T1$ = 1, Sample Charge

-n (E-E ₀)	Rel. Charge	-n (E-E ₀)	Rel. Charge
-0.240	0.000	0.200	0.000
-0.220	0.000	0.220	0.000
-0.200	0.000	0.240	0.000
-0.180	0.000	0.260	0.000
-0.160	0.000	0.280	0.000
-0.140	0.000	0.300	0.000
-0.120	0.000	0.320	0.000
-0.100	0.000	0.340	0.000
-0.800E-01	0.000	0.360	0.000
-0.600E-01	0.000	0.380	0.000
-0.400E-01	0.000	0.400	0.000
-0.200E-01	0.000	0.420	0.000
-0.119E-06	0.000	0.440	0.000
0.200E-01	0.000	0.460	0.000
0.400E-01	0.000	0.480	0.000
0.600E-01	0.000	0.500	0.000
0.800E-01	0.000	0.520	0.000
0.100	0.000	0.540	0.000
0.120	0.000	0.560	0.000
0.140	0.000	0.580	0.000
0.160	0.000	0.600	0.000
0.180	0.000		

Table 6-II F. Calculated Charge Function Values for Various Potentials $\tau/T1=10$, Sample Charge

-n (E-E ₀)	Rel. Charge	-n(E-E ₀)	Rel. Charge
-0.240	0.646E-04	0.200	0.291
-0.220	0.175E-03	0.220	0.276
-0.200	0.408E-03	0.240	0.264
-0.180	0.912E-03	0.260	0.253
-0.160	0.200E-02	0.280	0.243
-0.140	0.437E-02	0.300	0.234
-0.120	0.949E-02	0.320	0.227
-0.100	0.204E-01	0.340	0.220
-0.800E-01	0.433E-01	0.360	0.213
-0.600E-01	0.890E-01	0.380	0.207
-0.400E-01	0.172	0.400	0.202
-0.200E-01	0.299	0.420	0.197
-0.119E-06	0.443	0.440	0.193
0.200E-01	0.544	0.460	0.188
0.400E-01	0.568	0.480	0.184
0.600E-01	0.535	0.500	0.180
0.800E-01	0.483	0.520	0.177
0.100	0.433	0.540	0.174
0.120	0.391	0.560	0.170
0.140	0.357	0.580	0.167
0.160	0.330	0.600	0.165
0.180	0.309		

Table 6-II G. Calculated Charge Function Value for Various Potentials $\tau/T1=100$, Sample Charge

-n(E-E ₀)	Rel. Charge	-n (E-E ₀)	Rel. Charge
-0.240	0.850E-04	0.200	0.321
-0.220	0.224E-03	0.220	0.305
-0.200	0.517E-03	0.240	0.291
-0.180	0.115E-02	0.260	0.278
-0.160	0.253E-02	0.280	0.268
-0.140	0.551E-02	0.300	0.258
-0.120	0.120E-01	0.320	0.250
-0.100	0.257E-01	0.340	0.242
-0.800E-01	0.545E-01	0.360	0.235
-0.600E-01	0.112	0.380	0.228
-0.400E-01	0.216	0.400	0.223
-0.200E-01	0.373	0.420	0.217
-0.119E-01	0.545	0.440	0.212
0.200E-01	0.658	0.460	0.207
0.400E-01	0.671	0.480	0.203
0.600E-01	0.619	0.500	0.199
0.800E-01	0.549	0.520	0.195
0.100	0.486	0.540	0.191
0.120	0.435	0.560	0.188
0.140	0.396	0.580	0.184
0.160	0.365	0.600	0.181
0.180	0.341		

Table 6-II H. Calculated Charge Function Value for Various Potentials $\tau/T1=10,000$, Sample Charge

-n (E-E ₀)	Rel. Charge	-n (E-E ₀)	Rel. Charge
-0.240	0.935E-04	0.200	0.325
-0.220	0.243E-04	0.220	0.308
-0.200	0.559E-03	0.240	0.294
-0.180	0.124E-02	0.260	0.281
-0.160	0.273E-02	0.280	0.270
-0.140	0.594E-02	0.300	0.261
-0.120	0.129E-01	0.320	0.252
-0.100	0.277E-01	0.340	0.244
-0.800E-01	0.587E-01	0.360	0.237
-0.600E-01	0.120	0.380	0.231
-0.400E-01	0.232	0.400	0.225
-0.200E-01	0.399	0.420	0.219
-0.119E-06	0.581	0.440	0.214
0.200E-01	0.695	0.460	0.209
0.400E-01	0.701	0.480	0.205
0.600E-01	0.639	0.500	0.201
0.800E-01	0.562	0.520	0.197
0.100	0.494	0.540	0.193
0.120	0.441	0.560	0.189
0.140	0.401	0.580	0.186
0.160	0.370	0.600	0.183
0.180	0.345		

REVERSIBLE CHARGE $\tau/t=1$ STEP SIZE-10my: A-SMP. CHARGE B-PRE SMP

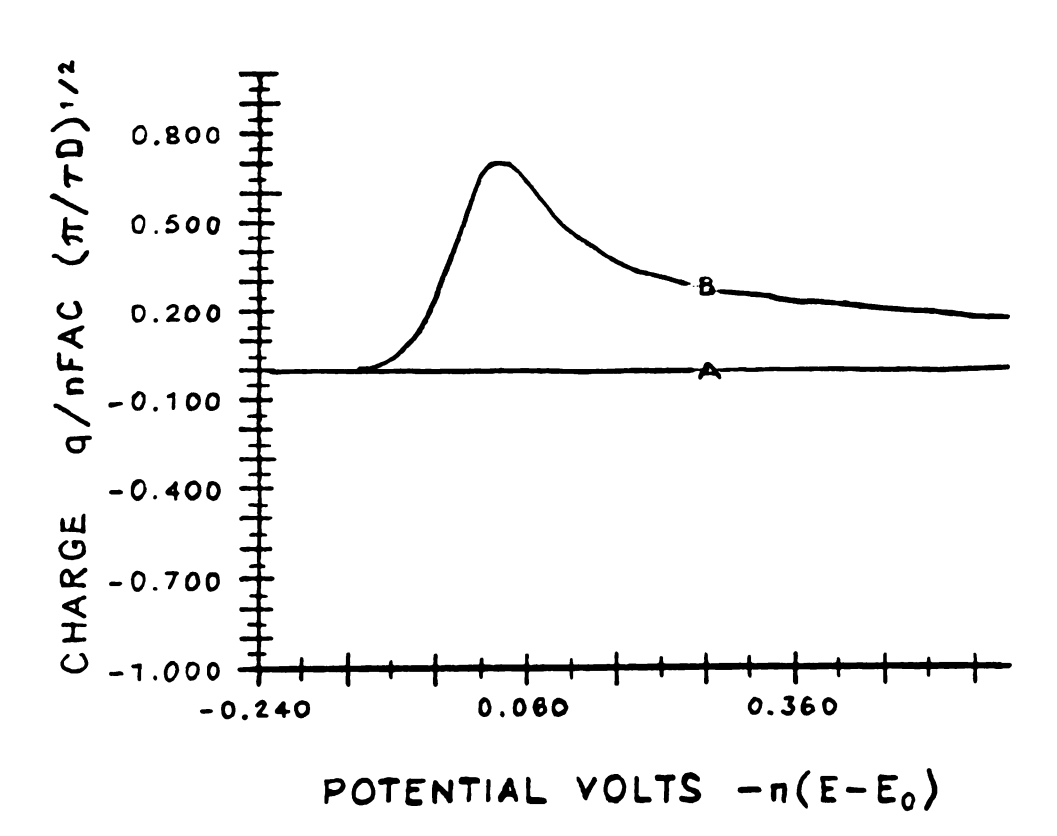


Figure 6-12 A. Influence of the ratio of τ/tl on reversible charge voltammograms. Step size = 10 mV, A = sample charge, B = pre-sample charge.

Fig

REVERSIBLE CHARGE $\tau/t=10$ STEP SIZE-10 mv; A-SMP. CHARGE B-PRE SMP

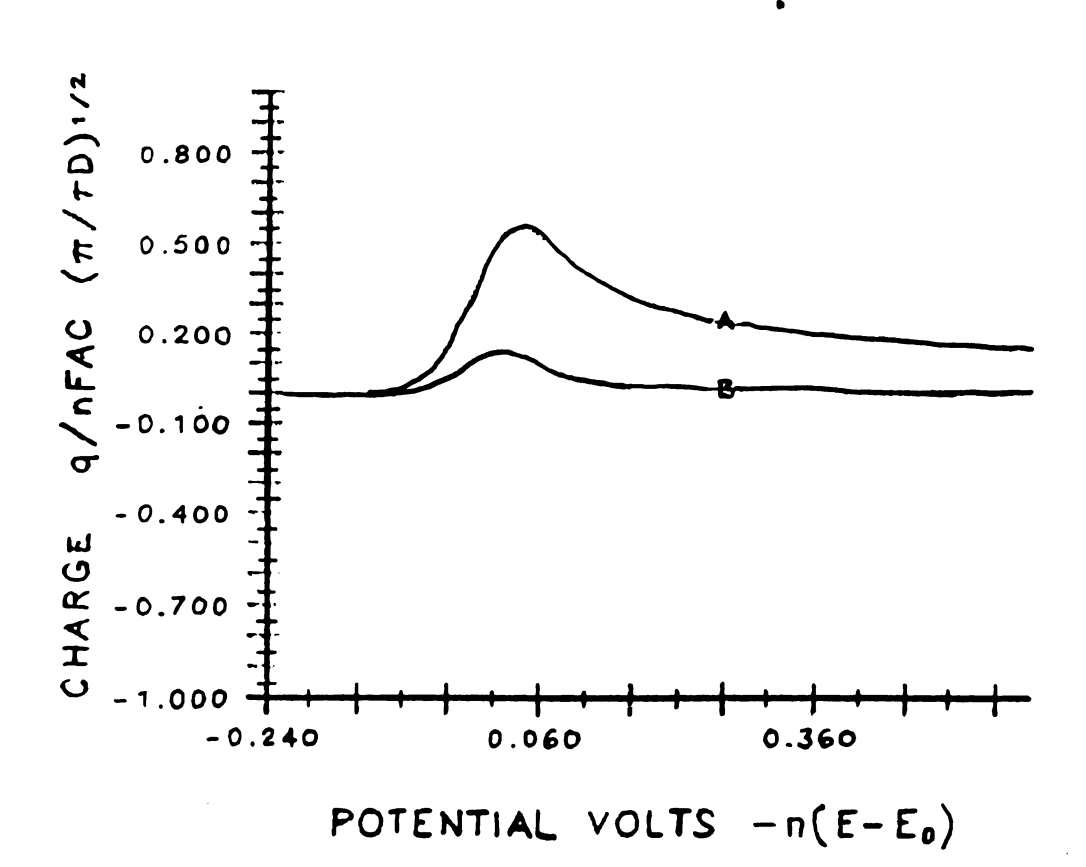


Figure 6-12 B. Influence of the ratio of τ/tl on reversible charge voltammograms. Step size = 10 mV, A = sample charge, B = pre-sample charge.

REVERSIBLE CHARGE $\tau/t=100$ STEP SIZE-10mv: A-SMP. CHARGE: B-PRE SMP.

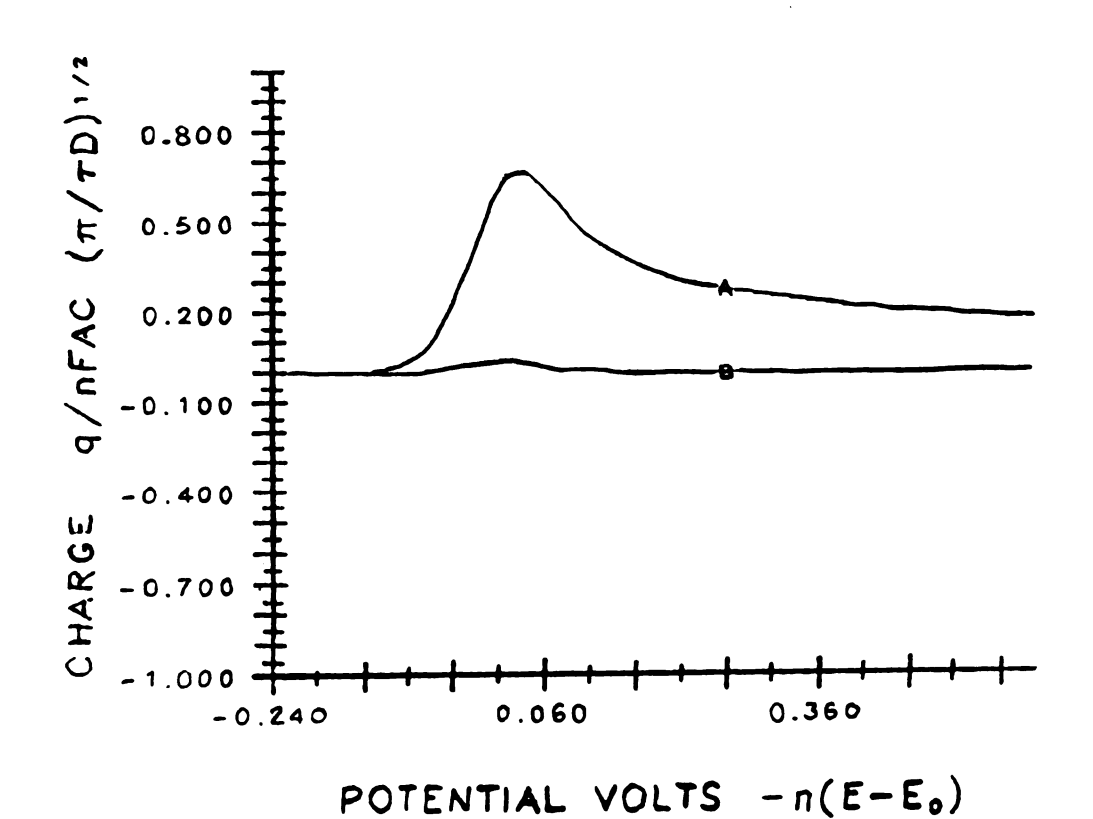


Figure 6-12 C. Influence of the ratio of τ/tl on reversible charge voltammograms. Step size = 10 mV, A = sample charge, B = pre sample charge.

REVERSIBLE CHARGE $\tau/t=10.000$ STEP SIZE-10 mV; A-SMP. CHARGE, B-PRE SMP

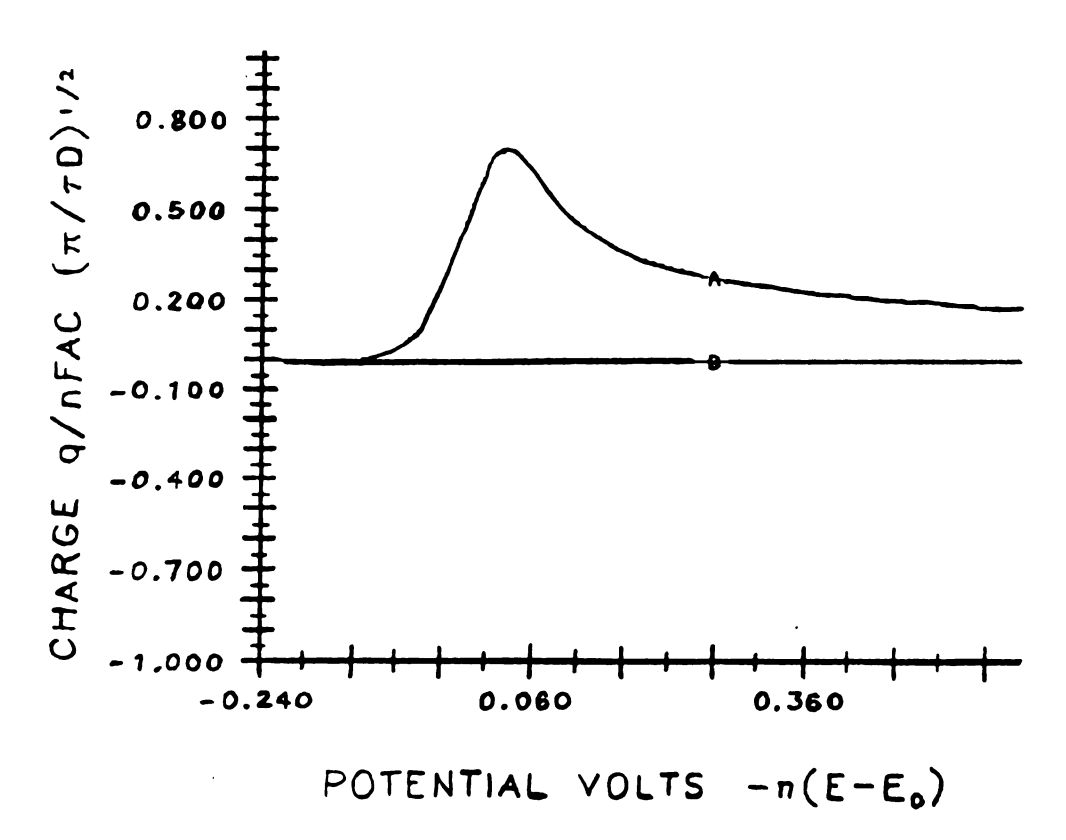


Figure 6-12 D. Influence of the ratio of τ/tl on reversible charge voltammograms. Step size = 10 mV, A = sample charge, B = pre-sample charge.

G.O Experimental Determinations

Experiments were performed on a real cell to measure the amount of Faradaic charge which would be included with the double layer charge in the time period Tl. Faradaic charge in Tl is excluded from the T2 charge because it is included with the double layer charge. The number of charge injections needed to attain and maintain the desired step potential for time period Tl are counted and stored in a

rat ехр qua dai this decr to 6 larg

seg

plq

ti

SIL

na!

ado

cha

jo.

cho

COI

bed

tio

kee

the

the

Pot

100

separate memory register M2. It is therefore possible to plot these charges separately. A further programming distinction is made between the large charge injections and the small charge injections delivered in time period T1. This makes it possible to compare the relative amounts of charge added to attain the potential with large injections with the charge added in small injections to trim and maintain the potential at the desired value.

A test solution of 1×10^{-4} M CdCl₂ in 0.1 M KCl was chosen for analysis because it was found that solution more concentrated than this were not possible to test. This is because for more concentrated solutions the maximum injection rate of the instrument (5 KHz) was not fast enough to keep up with the depletion of charge from the electrode by the Faradaic reaction. Thus large potential deviations from the desired step potential are encountered at electrode potentials where the Faradaic reaction current was too high.

In the experiment the step time τ was maintained at 100 msec and the time period Tl varied in length. The sweep rate was 100 mV/sec which is a typical value used in CV experiments. An important analytical consideration for quantitative experiments is the minimum ratio of the Faradaic Tl charge to the T2 charge. It is desired to minimize this ratio by decreasing the Tl period. As Tl period was decreased to 2 msec, the ratio of Tl and T2 charge decreased to 6 percent. When the Tl period was decreased below 2 msec, large potential step deviations were encountered because not

enough time was given for the charge injector to bring the step potential to the desired value. For solutions which are more dilute it is possible to decrease the Tl time and the ratio of Tl to T2 Faradaic charge further without substantial deviations in the desired potentials. For concentrated solutions run at fast sweep rates the ratio of the Faradaic charge in Tl and T2 will increase and introduce measurement problems because of difficulties encountered in reaching the desired step potential and acquiring enough charge injections during T2 to yield sufficient precision for analysis.

Figure 6-13 shows an experimental plot of the charge acquired in time period Tl over the potential scan range. The Tl period is 10 msec and the sweep rate is 89 mV/sec. The step size is 10 mV and the injecting capacitor size was The amount of charge delivered by large charge injections remains constant over the entire potential range and this charge is indicated by plot A. The amount of charge delivered by the small charge injections is shown in plot B. This charge changes over the potential range of the staircase ramp. A low number of small charge injections are required in the potential region where little Faradaic reaction is taking place. But as the reduction potential is approached, more small charge injections are required to maintain the desired step potential. A small charge peak is noted when this charge is plotted over the potential range of the staircase ramp. The peak is due to the consumed

Faradaic charge in this period. The baseline of this peak is curved indicating changes in the charge required to bring the double layer to the desired step potential. Figure 6-14 shows the deviation between the desired and the actual cell potential. Every step potential value was reached within one least significant bit of the DAC. The Tl period could be decreased to as low as 2 msec without substantial deviations in the desired step potential.

CAP. BIG & SMALL CHARGE 1X10**-5 CdCl2 .01KCl

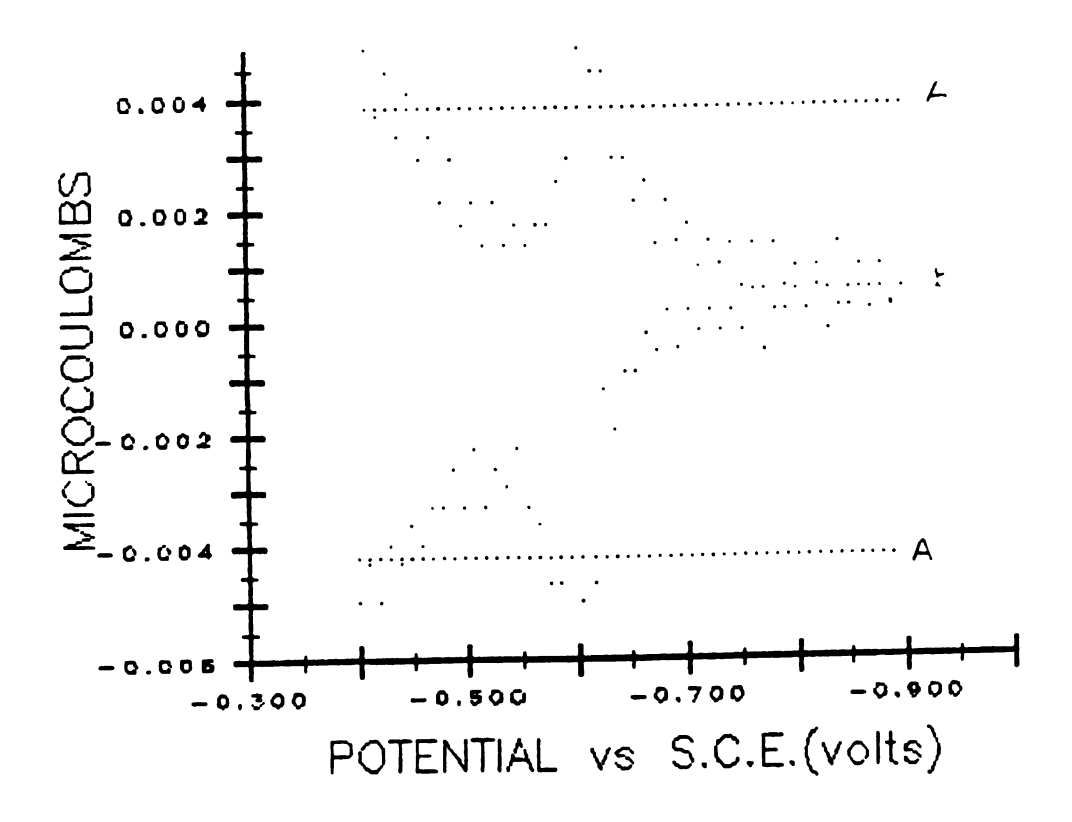
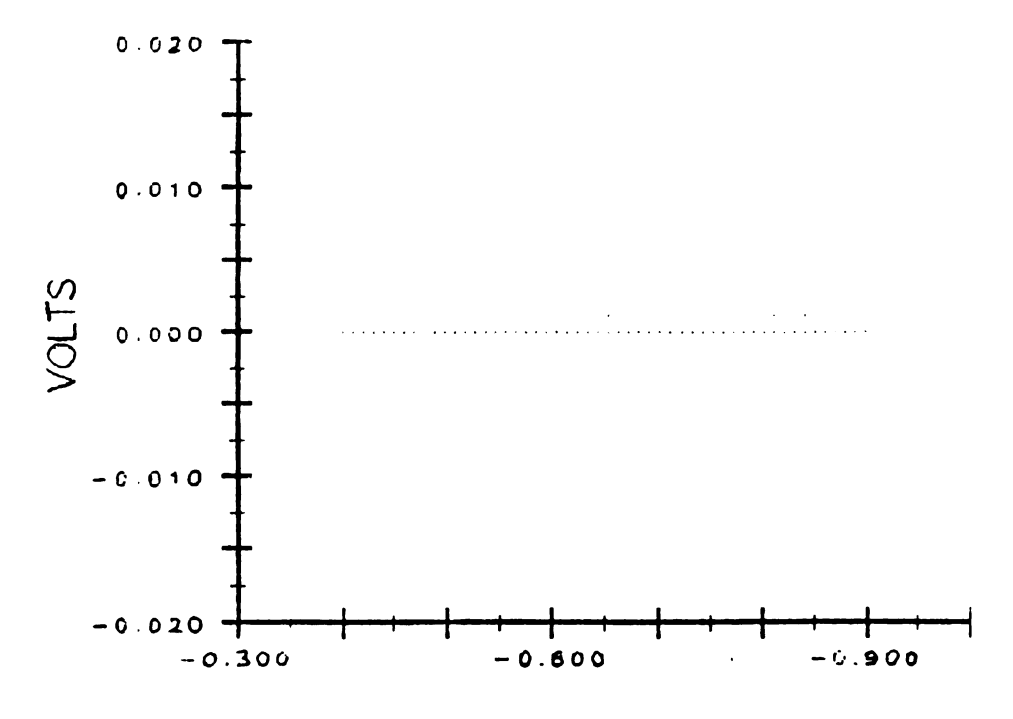


Figure 6-13. Charge injected during time T1. A = large injections, B = small injections. 1×10^{-5} M CdCl₂ in 0.01 M KCl.

POTENTIAL DEVIATIONS



POTENTIAL V.S. S.C.E.

Figure 6-14. Deviations of the cell potential from the desired cell potential. 1 x 10⁻⁵ M CdCl₂ in 0.01 M KCl.

The program for controlling the staircase voltammogram was modified to maintain the cell potential which was reached after the large injections. No trim injections were made to ensure a linear scan. The Tl period could then be reduced to the programming limit of 0.1 msec. The potential scan was found to be non-linear as expected and to change with electrode area (see Figure 6-15). The increase in the integration charge period did not result in a noticeable improvement in sensitivity when tested over a wide concentration range. This is because the additional charge

acquired in T2 by decreasing T1 was not large in comparison to the total step charge acquired in T2. It was therefore shown that the small trim injections do not extend the T1 time sufficiently to result in a large decrease to sensitivity.

STAIRCASE VOLTAMMETRY FILE=CV5002.DAT, EXP=(0), THY=(-)

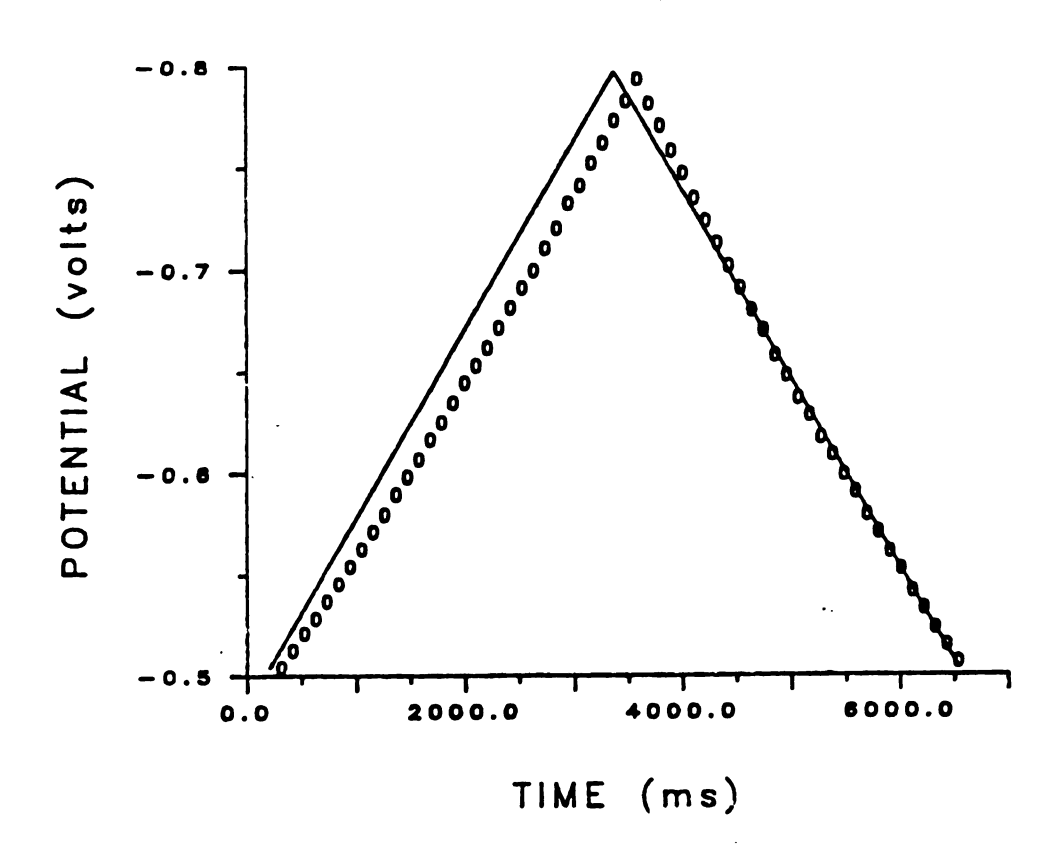


Figure 6-15. Non-linear potential scan resulting when no trim injections are applied. The solid line is the ideal scan from theory and circles are experimental points.

H.0 Reduction Potential Location Using Computer Modelling The location of E^0 or the reduction potential is often an important determination in electrochemical experiments. Therefore plots were made from calculated results to locate the percent up the wave the reduction potential occurs for charge voltammograms and current voltammograms. For charge voltammograms the reduction potential for a two electron transfer is 83.1 percent up the wave for $\tau/t=1$ and a step size of 10 mV. The reduction potential for current voltammograms run under these same conditions is located 72.1 percent up the wave. As the τ/t ratio increases for current voltammograms the peak potential moves closer to the reduc-

tion potential.

For charge voltammograms as the ratio of τ/t increases the location of the peak potential also moves closer to the E0 point. Table 6-III shows the percentage up the wave that E0 is indicated for both the T1 and T2 charge files. Note that for a given τ/t ratio the location of the peak potential is closer to E0 for the presample charge T1 file than for the sample charge T2 file. For example, with a τ/t ratio of 10,000, E0 is located 99.5 percent up the wave for the T1 data and 82.9 percent up the wave for the T2 data file. These results may be compared with the location of the peak potential for current voltammograms and either of the two extremes of the reduction potential location may be approached in charge voltammograms by changing the T1 period from the beginning to the end of the step. This is because

including charge from early in the step life into the integration period will move the peak potential closer to the E^0 point but including charge from late in the step life will put E^0 closer to the 72.1 percent limit of current voltammograms with $\tau/t=1$.

Table 6-III. Location of the Reduction Potential on the Voltammogram

Presample Peak		Sample Peak	
τ/t	Percent Up Peak	τ/t	Percent Up Peak
1	83.1		
10	92.2	10	78.0
100	97.1	100	81.2
10,000	99.5	10,000	82.9

I.0 Step Size

The step size can affect the shape of a voltammogram greatly. The step size may be varied at a constant sweep rate by changing τ appropriately. Figure 6-16 shows the effect of changing the step size at a constant sweep rate of 3.3 v/sec. The step size takes values of 2, 10, and 50 mV. The smallest step size is shown to yield the greatest current function value. When the step size and the step time approach zero at a constant scan rate, the current function approaches the stationary linear voltammetry limit.

For charge voltammograms the current is integrated over the step time so the longer the step time, the larger the

peak charge. Figure 6-17 shows how the peak changes with step size at a constant sweep rate. To keep the sweep rate the same with increasing step size, the step time τ increases from 0.6, 3.0, to 15 msec. Larger changes in the step potential and thus longer integration periods yield the largest peak charge values. The relative peak heights indicate peak charge results which are opposite to those obtained in Figure 6-15 for the sampled current staircase voltammograms.

REVERSIBLE STEP SIZE EFFECT $\tau/t=1$ (3.33 \sqrt{eec}), (-)=n(2mv), (x)=n(10mv); (*)=n(50mv)

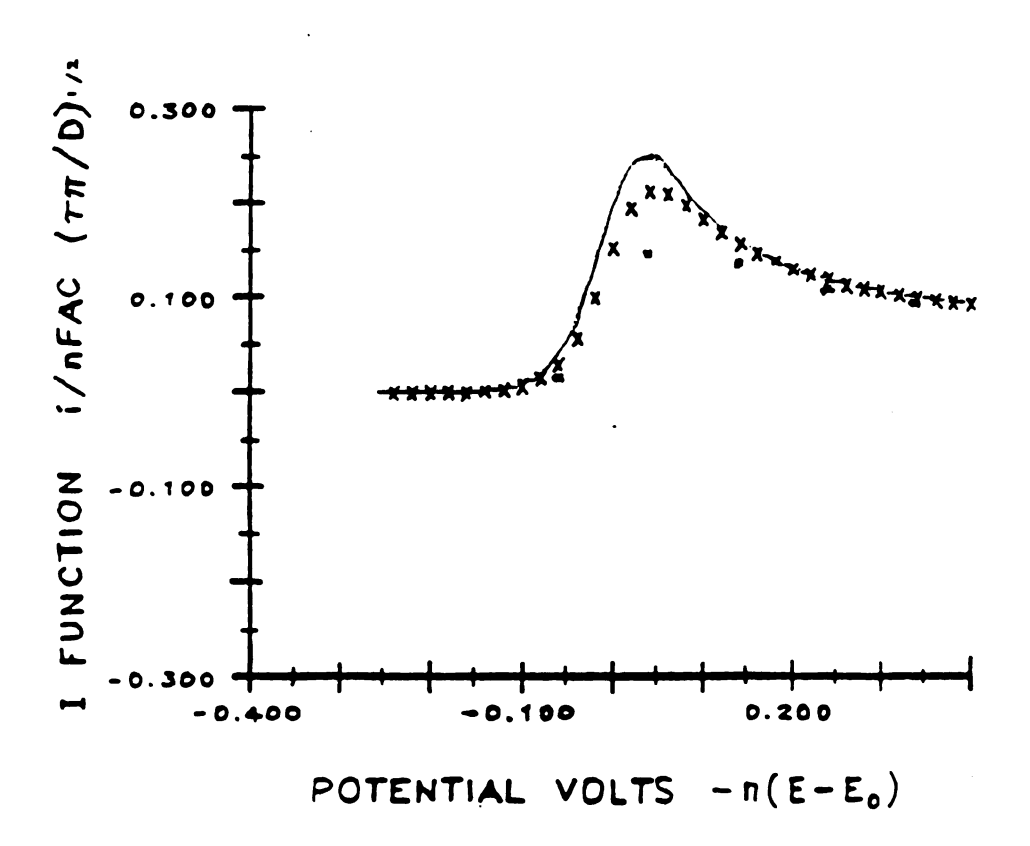


Figure 6-16. Current voltammogram increase in the step size at a constant sweep rate.

REVERSIBLE STEP SIZE EFFECT $\tau/t=1$ (3.33v/sec): (-)=n(2mv): (x)=n(10mv): (*)=n(50mv)

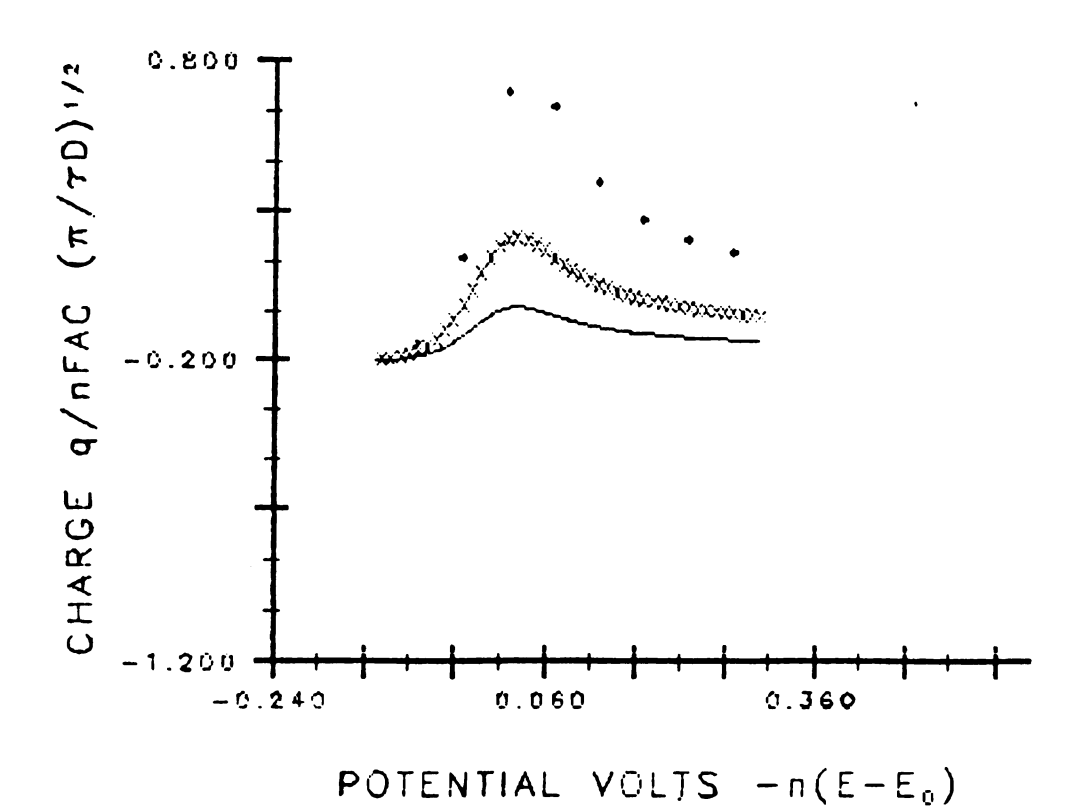


Figure 6-17. The effect of an increase in step size on charge voltammograms at a constant sweep rate. Sweep rate 3.33 v/s, $\tau/t_m=1$, (-) = n(2)mv, (x)=n(10)mv, (*)=n(50)mv, where n is the number of electrons.

The sweep rate may be varied by changing the potential step size and keeping τ constant. Decreasing the step size decreases the sweep rate. This is analogous to decreasing the sweep rate in linear scan voltammetry. Larger peak current functions are observed with larger steps. Large step sizes take on the behavior observed with the potential step technique and show the greatest change in the peak current function with the sampling time. To show this

e: l w v

1 -

st st

V(

t/ da

be.

effect, voltammograms were plotted at four ratios, $\tau/t=1$, 10, 100, 10,000. For each ratio the peak current function was determined for step sizes of 2, 10 and 50 mV. The peak values of the current function for t_m less than τ were then divided by the peak current functions for t_m equal to τ for corresponding step sizes. This is shown in Table 6-IV. For a τ/t_m ratio of 10 the influence of the sampling time is the greatest for the largest step. When the τ/t ratio increases, the current function ratio also increases showing the greater influence of the sampling time at shorter times.

Table 6-IV. Influence of the Step Size on the Current Function

	n (2mV)	n(10mV)	n(50mV)
10	1.3	1.8	2.2
100	2.2	4.3	6.0
10,000	15.0	36.3	56.4

Charge voltammograms may also be plotted for decreasing sweep rate. When changing the step size and holding the step time τ constant, larger peaks are obtained for larger steps just as in the sampled current experiment. Charge voltammograms do not, however, show the same great change with step size at various τ/t ratios (see Table 6-V). For $\tau/t=1$ the entire step charge is contained in the presample data file. For $\tau/t=10,000$ all but a small portion of the beginning of the step is contained in the sample charge

g

C.

r

to

T

CC

to

iŋ

Table 6-V. Influence of the Step Size on the Charge Function

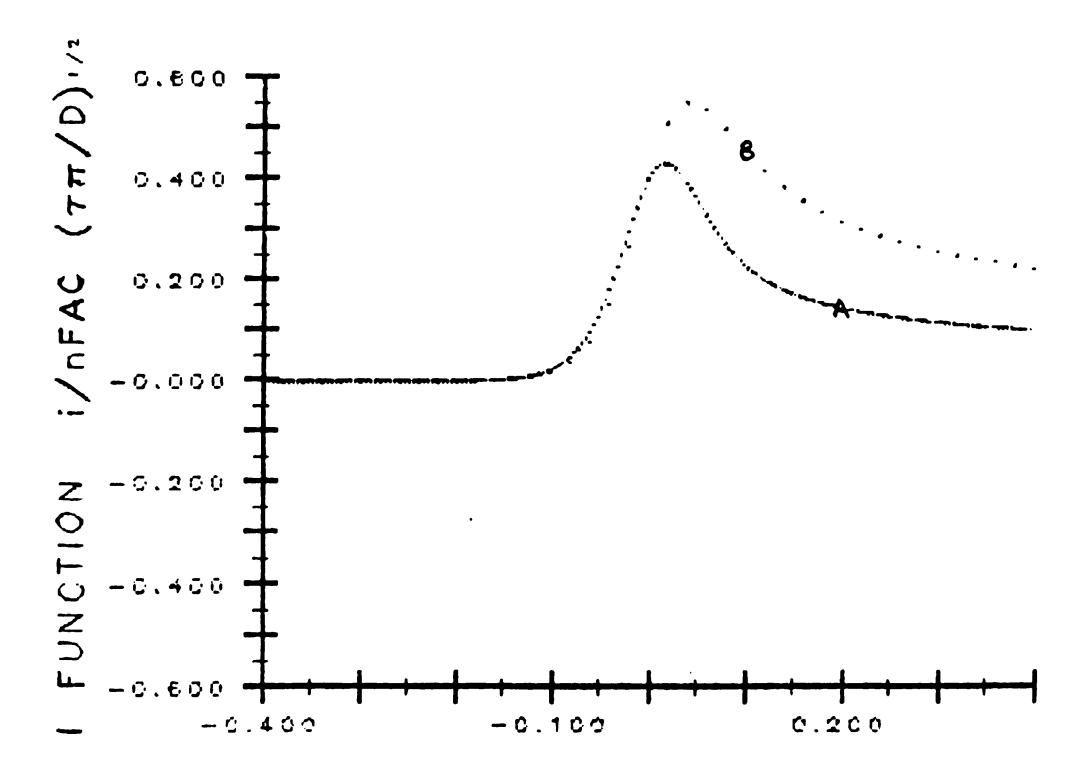
Sample Charge Ratio T2							
τ/t	n (2mV)	n(10mV)	n (20mV)				
100	.86	.81	. 7.6				
10,000	1.00	1.00	.99				
	Presample Ch	narge Ratio Tl					
τ/t	n(2mV)	n(10mV)	n(20mV)				
100	.15	.22	.27				
10,000	.001	.01	.01				

data file. Therefore, the ratio of these two charges are nearly equal to one as shown in Table 6-V. The same charge is shown not to change greatly with the step size as in the case of the instantaneously sampled current staircase exper-This is because the integration period covers a wide range of instantaneous current decay curves. The instantaneous current function at the beginning of a step shows a greater change with step size than the instantaneous current function at the end of the step. For $\tau/t=1$ the entire step charge is contained in the integration period, so that the ratio of step charge for shorter integration periods to this total step charge must be less than one. The values in Table 6-V thus indicate what fraction of the total charge is Contained in the integration interval. This fraction of the total step charge decreases slightly as the step size in Creases for the T2 data file. This is because less of the total charge will be determined in the same T2 integration period for larger steps. On the other hand, when the T1 data is noted in Table 6-V, a slight increase in the ratio is noted with increasing step size. This is because the greatest change in the total step charge occurs at the beginning of the potential step.

When increasing the step size and maintaining a constant sweep rate the peak potential shifts. This is shown in Figure 6-18. Both plots are made at the same sweep rate of 260 mV/sec. The instantaneous currents are shown for 20 and 500 msec. A peak potential shift of over 25 mV is noted in the cathodic direction. The shift in the peak potential occurs for two reasons:

- 1. The ratio of τ/t changes.
- 2. The step size increases.

The two effects can be separated by noting the shift in the peak potential with the step size at a constant τ/t ratio. There is a potential shift with changing step size but it is not readily predictable. The potential shift increases with increasing τ/t ratio but the increase is not linear with the increase in τ/t ratio.



POTENTIAL VOLTS -n(E-E0)

Figure 6-18. Shift in peak potential with increasing step size. "A" step size 2 mV, t_{m} = 20 ms, τ = 520 ms, "B" step size 10 mV, t_{m} = 500 ms, τ = 2600 ms.

J.O Comparisons of Computer Modelling and Experiments

There are three ways that the sweep rate in staircase voltammetry may be changed while keeping the step size constant. They are:

- 1. Change τ while keeping t constant.
- 2. Change τ and t while keeping their ratio constant.
- 3. Change t while keeping τ constant.

The third method involves changing the "effective sweep rate" since $\Delta E/\tau$ remains constant. As the sample time is increased, the decay curve is sampled at lower points and the measured current values obtained are lower. Thus this results in effectively lowering the sweep rate.

The second method of changing τ and t while keeping their ratio constant is a convenient method of changing the sweep rate. The peak current is linear with the square root of the sweep rate and the line has an intercept of zero because at long step times or low sweep rates the sampled current goes to zero.

The first method of changing the step time while holding the sample time constant is also a valid method of changing the sweep rate. Since τ can never be less than t the sweep rate can only be increased to a maximum value of $\Delta E/\tau$. The peak potential will also shift as the τ/t ratio changes.

The sweep rate is changed in the same manner for charge voltammograms. The peak height however is inversely related to the sweep rate (see Figure 6-18). This is because although current decreases with time, the total charge passed through the cell for any given step increases with time. Figure 6-19 shows experimental charge voltammograms determined at sweep rates of 15, 80, 190 and 814 mV/sec. The largest peak charge is obtained at the slower sweep rate because the longer the T2 period, the longer the step current is integrated and the more charge acquired.

Experimental charge voltammograms were obtained at sweep rates from 15 mV/sec to 4 V/sec. The step size was 10 mV and τ was varied at a constant Tl time of 2 msec. The peak charges were then compared with the values determined from theory under the same conditions. The peak charges were then plotted against the square root of the sweep rate. The result is shown in Figure 6-20.

FARADAIC CHARGE VS STEP TIME

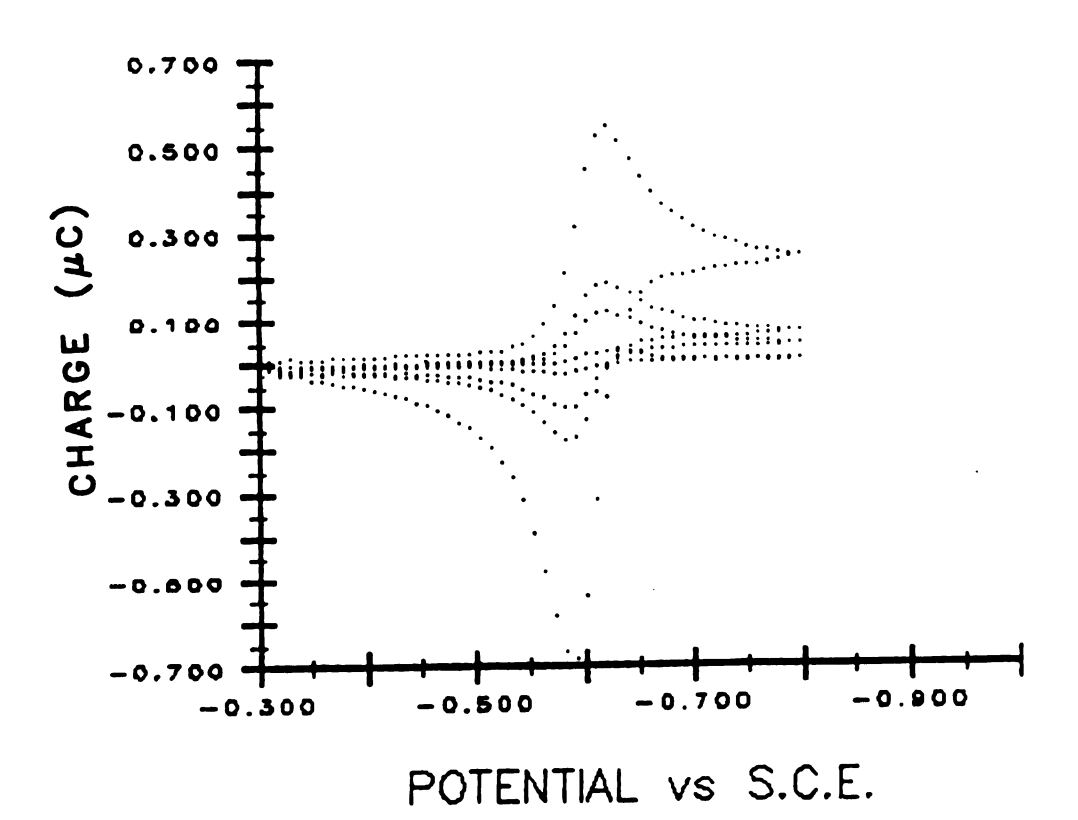


Figure 6-19. Experimental charge voltammograms at increasing sweep rate. From largest voltammogram to smallest, the sweep rate is: 15, 80, 190, 814 mV/sec.

THEORY(-) VS EXPERIMENT(x) STEP SIZE= 10 mv: 7=varies; t=2 ma

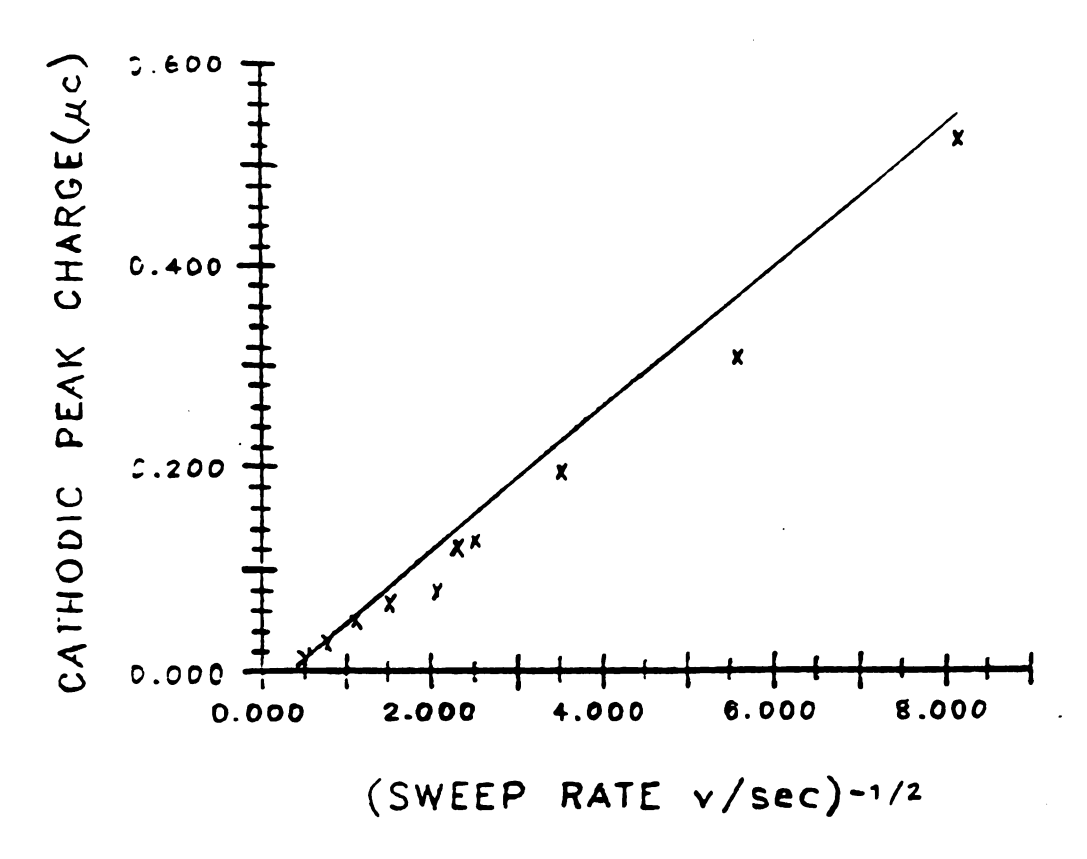


Figure 6-20. Theory and experiment peak charge vs. sweep rate. Step size = 10 mV and T1-2 ms.

One of the best tests to characterize a new electrochemical instrument to determine the concentration range over which the instrument responds in a linear manner. The instrumental response to both high and low concentrations can be tested and limitations of the measurement noted. Solutions of CdCl_2 in 0.1 KCl were chosen for this analysis because the chemical system is a well characterized reversible system with little adsorption. Solutions ranging in concentration from 1.0 x 10^{-3} to 1.0 x 10^{-8} M in CdCl_2 were

prepared. The water used for dilution was purified by filtering distilled water through a millipore filter. To reduce weighing and dilution errors, large volumetric flasks (1 and 2 liter) were used in solution preparation. To avoid loss due to adsorption of Cadmium on the walls of the dilution flask, the solutions were immediately run after preparation. To remove all traces of oxygen from the test solution, purified nitrogen gas was bubbled through the the test solution for twenty minutes. A hanging mercury drop of 0.032 cm^2 was used for the working electrode. A step size of 10 mV, T1 time of 5 msec, and a T2 time of 100 msec was chosen to yield a sweep rate of 93 mV/sec. The injection capacitors were chosen to be 1.0 nF because this allowed the addition of 0.1 to 2.5 nC of charge by conveniently changing the DAC value.

Program CKCV.OBJ was downloaded into the microcomputer and pertinent experimental parameters were entered into the PARM subprogram. The experimental parameters for each solution are always passed along with the raw data so that this information is not lost. After running each solution, the raw data was uploaded from the microcomputer to the minicomputer (DEC 11/40) and stored on magnetic tape. The raw data file was then processed with the aid of the program CV.FTN. This program allows the raw data to be processed into files of real numbers containing one of the following output choices:

- 1. Charve vs. Potential
- 2. Current vs. Potential
- 3. Potential vs. Time
- 4. Experimental Parameter Output

The raw data file may be processed in any or all of the above choices. Any of the first three choices above produces three output files from a single raw data file. The selection of number one, charge vs. potential, produces the following three files:

- 1. Tl Charge vs. Potential
- 2. T2 Charge vs. Potential
- 3. Total Step Charge vs. Potential

The selection of current vs. potential produces the following three files:

- 1. Tl Current vs. Potential
- 2. T2 Current vs. Potential
- 3. Total Step Current vs. Potential

And the selection of potential vs. time produces the following three files:

- 1. Calculated desired step potential
- 2. Experimental step potential
- 3. Deviation of the experimental value from the calculated desired value.

All these data files are generated in MULPT format to allow latter plotting.

The charge voltammograms were then calculated from theory by computer methods for comparison with experiment. Each solution concentration was determined by running the program REAL.FTN and entering all pertinent experimental information. The program REAL.FTN places the charge-potential data for periods T1 and T2 into separate data files. These data files can then be analyzed by program CVANALY.FTN to correct for baseline and locate the peak values. The following constants were entered into the program: a reduction potential of -0.61 V vs. SCE, diffusion consant of $8.1 \times 10^{-6} \text{ cm}^2/\text{sec}$ for oxidized cadmium in an aqueous solution and a diffusion constant of $1.6 \times 10^{-5} \text{ cm}^2/\text{sec}$ for reduced cadmium metal in liquid mercury. Figure 6-21 shows the results of the theory and experimental results plotted together.

It is interesting to process the raw data and compare the total charge (file 3) with the T2 charge file (file 2) and the T1 charge file (file 1). These plots are shown in Figures 6-22, 6-23 and 6-24. Figure 6-22 shows the total charge (T1+T2) file. Note that the base line is curved making the peak height difficult to measure. Note also the large separation of the cathodic and the anodic base lines. This is due to the large double layer capacitance which changes with the cell potential. When the concentration of the electroactive species is low, the double layer charge is large in comparison to the Faradaic charge. This makes it difficult to measure an accurate peak height. This same

problem is also encountered with linear scan voltammetry because the total cell current is always the sum of the double layer current and the Faradaic current.

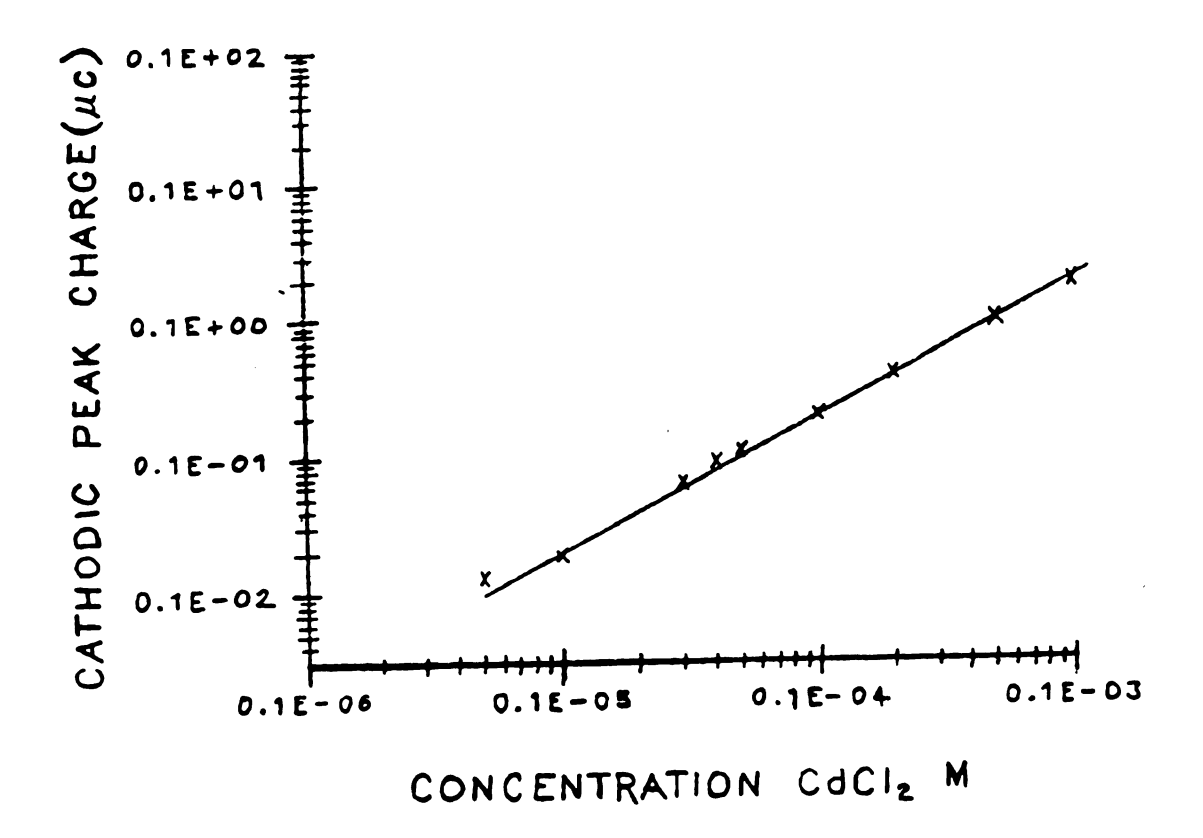


Figure 6-21. Theory and experiment peak charge vs. concentration. Step size 10 mV, τ = 105 ms, and Tl = 5 ms.

TOTAL CHARGE 1X10-6 CdCl2 IN .02 KCl

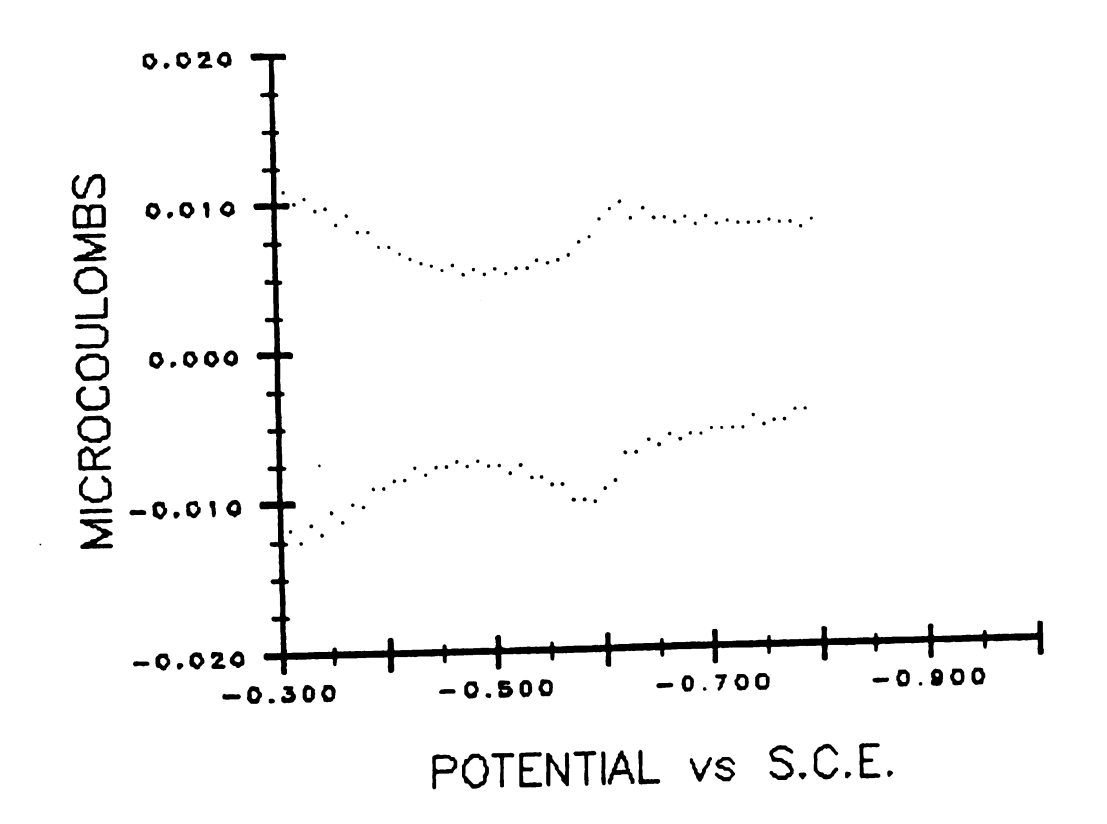


Figure 6-22. Total step charge voltammogram CdCl_2 in 0.02 KCl.

CAPACITIVE CHARGE 1X10-6 CdCl2 .02KCl

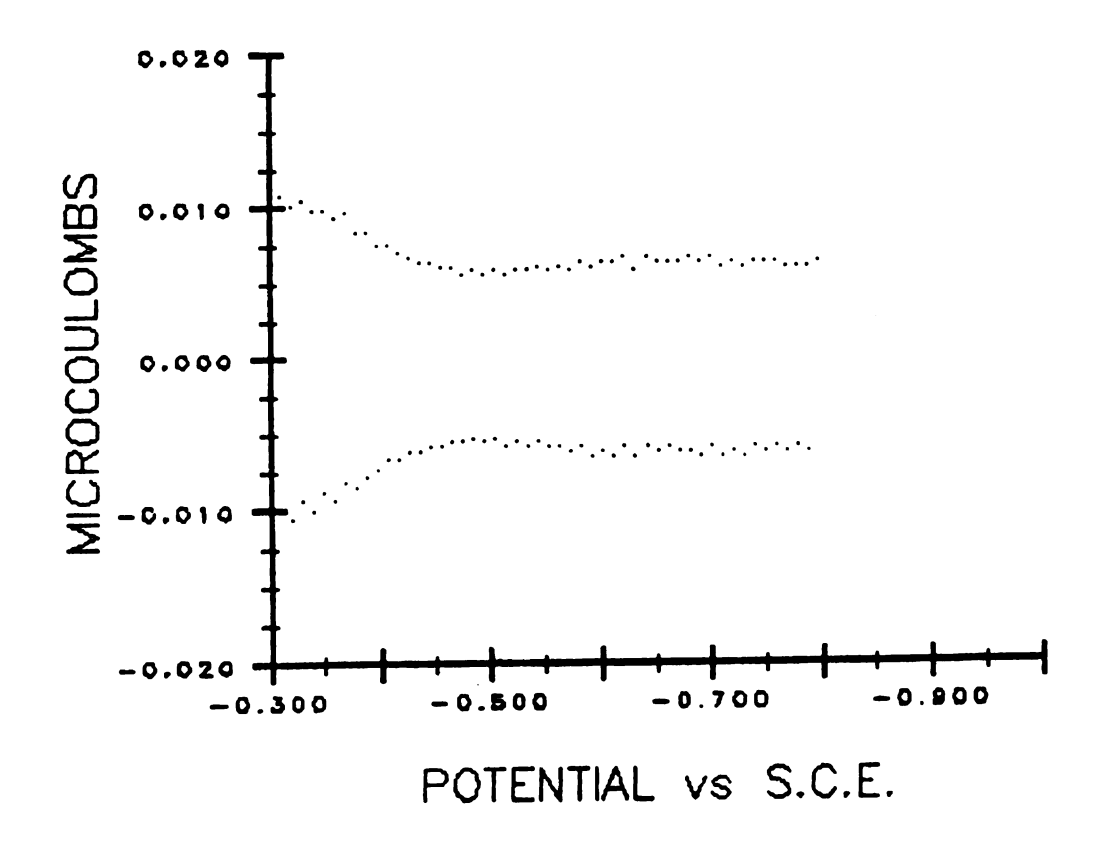


Figure 6-23. Tl charge voltammogram $CdCl_2$ in 0.02 KCl.

FARADAIC CHARGE 1X10-6 CdCl2 .02KCl

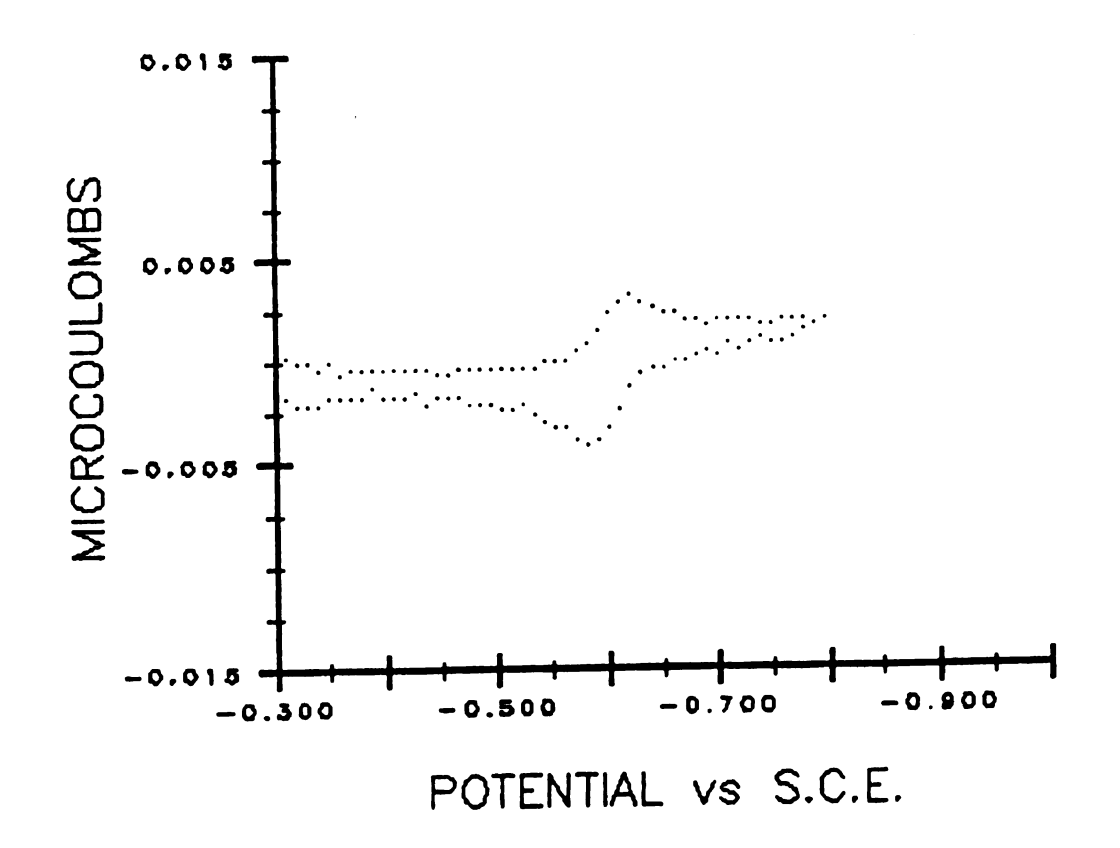


Figure 6-24. T2 charge voltammogram CdCl₂ in 0.02 KCl.

Figure 6-23 shows the Tl charge. This charge contains the double layer charge and the Faradaic charge consumed in this time period. The amount of Faradaic charge consumed in this time period is small as noted by the absence of a peak at the reduction potential for Cadmium.

Figure 6-23 shows the T2 charge. The baseline is flat making the peak height easy to determine. The flat baseline indicates that the double layer charge has been excluded from this file and therefore demonstrates the ability of the

method to reject the double layer charge interference. The T2 peak charges for all solutions tested were determined and compared with the values predicted from theory.

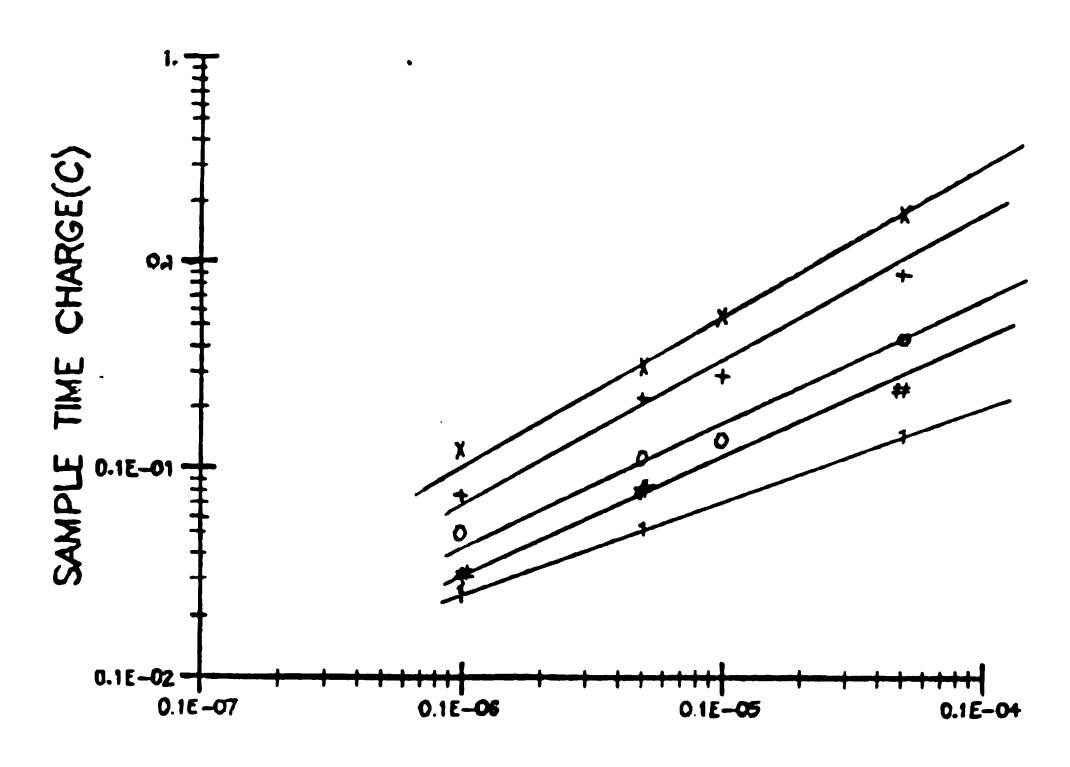
The integration of the step current over the step time acts as a noise filter and increases the signal-to-noise ratio. If the Faradaic current were constant for the entire step, the signal-to-noise ratio would improve with the square root of the number of injections. Because the Faradaic current is not described by a simple function of time, it is not possible to state a general improvement of the signal-to-noise ratio.

The signal-to-noise ratio may be improved by ensemble averaging. For a reversible system multiple scans may be applied to the same drop in rapid succession provided the surface of the drop does not change. Each succeeding voltammogram will be larger than the previous one until a steady state condition is reached. At this point the amount of new electroactive material gained is equal to the amount lost from the bulk solution. The current voltammograms have characteristically flat baselines as noted by Sevcik (3). The number of scans may be increased until the scan time becomes too large and the noise level increases due to convection. Charge voltammograms were determined for concentration of $CdCl_2$ ranging in concentration from 1 x 10^{-7} M to 5×10^{-5} M. The number of scans took on values of 25, 16, 9, 4 and 1. The charge for each scan was added to the previous scan for each step in the voltammogram.

it was desired to show the increase in sensitivity gained by summing multiple scans, the charge values were not divided by the number of scans. The increase in sensitivity gained by summing multiple scans is difficult to determine because the increase in peak charge is not a simple function of the scan number. Therefore a calibration curve was prepared. The calibration graph of peak charge vs. concentration was plotted and found to be linear over the entire concentration range tested (see Figure 25). Because the computer enables multiple scans to be quickly summed together, an increase in sensitivity can be conveniently obtained with this method with an aid of a calibration curve.

The peak charge is a convenient point to obtain from graphs. But when using a computer for data analysis, it is just as easy to use other criterion for data evaluation. The computer was programmed to determine the baseline for a charge voltammogram by fitting the initial points to a linear least square line. The charge above this base line was then summed for each step. Charge voltammograms of 1×10^{-5} M PbCl₂ were analyzed in this manner for various ratios of τ/t . The peak charge was found to be linear with the summed step charge for all τ/t ratios. This is shown in Figure 6-26. It is therefore possible to increase sensitivity by including in addition to the peak value, charge from all steps in the cathodic scan.

SCAN INTEGRATIONS (X)=25; (+)=16; (0)=9; (#)=4; (1)=1 9cors



CONCENTRATION OF CdCI2 .1 M KCI

Figure 6-25. Peak charge vs. concentration obtained for summed multiple scans. Number of scans = (x) = 25, (+) = 16, (0) = 9, (#) = 4, (1) = 1.

TOTAL CHARGE VS PEAK CHARGE FOR 1.0×10-5 M PbCI2

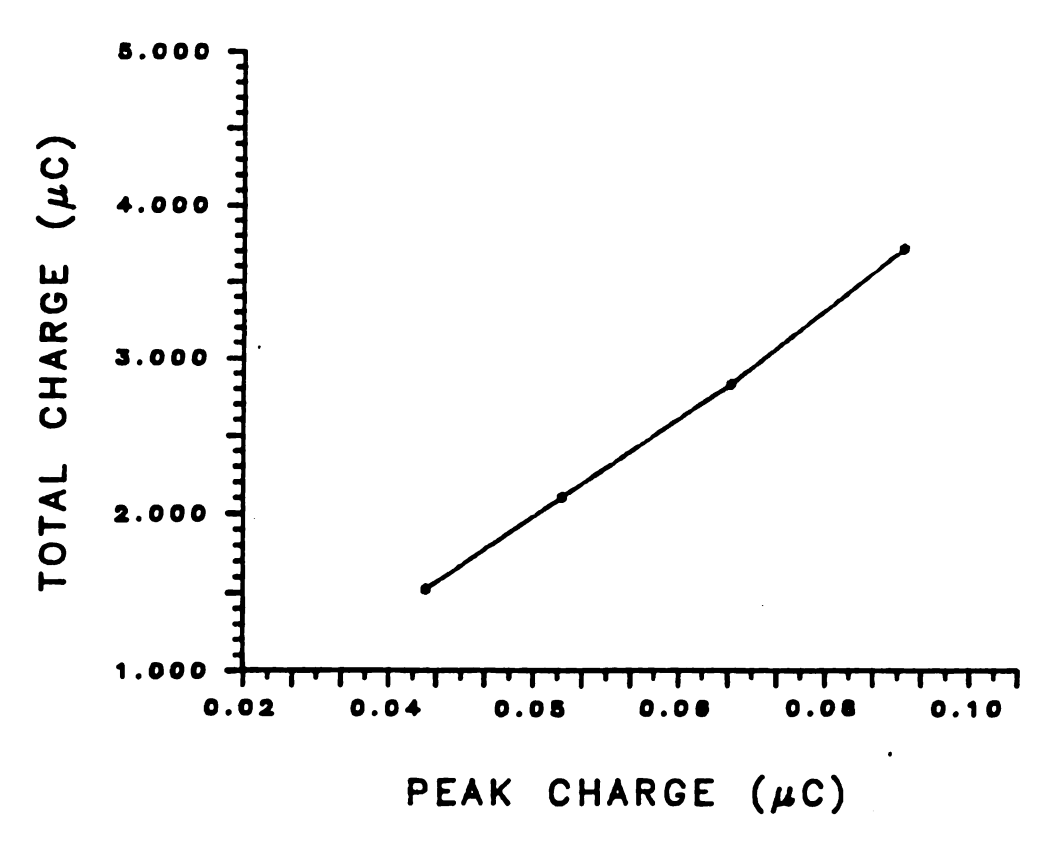


Figure 6-26. Total charge under voltammogram vs. peak charge. 1 x 10^{-5} M PbCl₂.

VII ADSORPTION STUDIES

A.0 Introduction

The Gouy-Chapman-Stern model showed that the differential capacitance of the electrode is made up of two components that can be separated as capacitors in series. first is termed the Helmholtz capacitance and is generated by ions held at the outer Helmholtz plane. The second component is the capacitance generated by ions in the diffuse layer. Because capacitors in series add as reciprocals the total capacitance is governed by the smaller of the two components. In solutions with low electrolyte concentration, it is found that near the potential of zero charge the total capacitance is governed by the diffuse layer capacitance. At higher electrolyte concentrations or at potentials removed from the potential of zero charge, the diffuse layer capacitance becomes so large that it no longer contributes to the total capacitance.

The Gouy-Chapman-Stern model can account for the behavior of many real chemical systems, but there are some systems which do not follow this model. Deviations from this model occur when the solution becomes involved in chemical interactions with the electrode surface. This chemical interaction of ions with the electrode is termed specific adsorption and can be thought of as short-range,

bonding with the electrode surface. Adsorption changes the electrode capacitance and other characteristics of the electrode.

In the study of voltammetry, nonideal waveforms are often encountered due to adsorption of compounds on the surface of the electrode. The adsorbing compound may form a layer which partially or completely covers the electrode. Adsorption affects the electrochemical response because it affects the concentration as well as the potential distribution around the electrode. Adsorbed material may block the electrode surface or act as a catalyst for the redox reaction.

In the presence of weak adsorption, the difference in energetics between the adsorbed and dissolved species is small and voltammograms exhibit enhancement of peak currents since the electron transfer of the adsorbed species is at nearly the same potential as the diffusing species. Both the adsorbed species and the diffusing species contribute to the total current. In a solution initially containing only the oxidized species [0], if [0] is adsorbed, the height of the cathodic peak is enhanced compared to that in the absence of adsorption. The anodic peak height is not increased as greatly as the cathodic peak because [R], which is generated at the electrode surface, will diffuse to the bulk solution where its concentration is zero. Thus, a portion of [R] is lost to the bulk of the solution as it continues to diffuse away from the electrode on the reverse

potential sweep. The ratio of anodic to cathodic peak current is a function of the sweep rate and is less than one, found in the absence of adsorption. In the case of weak adsorption of [R] the anodic peak is enhanced greater than the cathodic peak and the ratio of the peak currents is greater than one.

As the free energy of adsorption increases, an adsorbed reactant becomes more difficult to reduce and the reduction occurs at more cathodic potentials. In the presence of what is termed strong adsorption, the adsorbed material is sufficiently difficult to reduce that a separate peak will occur. The adsorption peak will occur prior or after the normal peak of the diffusing material depending on the relative strength of adsorption of [0] and [R]. If [0] is adsorbed more strongly, the voltammogram is displaced toward the negative potentials beyond the position of the normal reversible wave of a diffusing species. This peak is termed a postwave. If [R] is adsorbed more strongly, the wave occurs at more positive potentials than the normal reversible wave of a diffusing species and a prewave appears.

In the case of either strong or weak adsorption, the relative contribution of adsorbed material increases at increasing sweep rates and increases with decreasing concentration of the bulk solution. At very high sweep rates in the presence of weak adsorption the peak current is proportional with the sweep rate, while at low sweep rates

is proportional to the square root of the sweep rate. If not taken into account, even weak adsorption can lead to spurious results by distorting the proportionality of current and concentration. Non-ideal waveforms in voltammetry may be due to the oxidation or reduction of an adsorbed compound, increased migation current resulting from the disruption of diffusion by ionic interactions with the adsorbed compound, catalytic reactions or other possible mechanisms. To obtain meaningful results, it is often necessary to add a "surfactant" to reduce the non-ideal effects. The mechanism by which the surfactant works is not always known but the general plan of attack is to replace a non-ideal electrode surface with a well behaved one.

B.O A Chemical System for the Study of Adsorption

In addition to making data interpretation difficult, adsorption puts an added burden on the instrumentation by making added demands of charge and potential control. To test the charge injector and the applicability of staircase cyclic voltammetry on the study of adsorption, a chemical system was sought in which the degree of adsorption could be varied from weak to strong. With such a chemical system, the effects of adsorption could be easily studied by noting changes in the shape of voltammograms, determining the amount of adsorbed charge, and by noting deviations in the voltage levels of the staircase waveform at increasing sweep rates.

The ability to produce a reproducible electrode surface presented a further requirement of study. Adsorption on platinum is complicated by the difficulty of reproducing a consistant electrode surface from one experiment to the next. Computer averaging and multiple scan techniques can be used to reduce these problems on platinum. However, the hanging mercury electrode is the electrode of choice because the electrode surface can be easily renewed. The desired electrochemical system for adsorption study would have the following characteristics:

- adsorption on mercury;
- 2. variable adsorption strength.

Anion induced adsorption of metals on mercury meet the above requirements. The degree of adsorption can be changed from weak to strong by changing the concentration of anion (supporting electrolyte). Metal ions of group IIB, IIIB, IVB and VB of the periodic table often show this type of adsorption on mercury in the presence of halid anions. Ions of metallic elements which have been studied include cadmium(II), lead(II), zinc(II), thallium(I), and indium(III). Anions studied include chloride, bromide, and iodide. Fluoride doesn't adsorb to any great extent.

Studies have also been carried out with thiocyanate. For induced adsorption to occur it is necessary that the inducing anion be specifically adsorbed on the electrode and form complexes with the metal cation. Anion induced adsorption

can be reduced or eliminated at negative potentials where adsorption of the anion is unfavorable. At negative potentials anion desorption may not be complete before the onset of metal reduction. If the anion does not form a complex with the metal then anion induced adsorption does not occur at any potential.

Two different mechanisms have been proposed to explain the dependence of adsorption on the charge of the electrode and the concentration of the anion. The first mechanism assumes a complex is formed between the metal ion and the anion in solution, then after this formation it is adsorbed on the mercury surface.

$$ML + Hg ----> LM-L-Hg$$

Ml is the adsorbing metal-anion complex. The charge on ML has been omitted. Hg is the adsorption site on the mercury. The adsorbed species is a complex to which a ligand anion is bound to both the mercury surface and the metal cation. The second mechanism assumes the anion is initially adsorbed on the surface on mercury:

$$ML + L - HG ----> LM-L-HG$$

Data supporting this second mechanism has been obtained for a number of metal cations. It might be reasoned that a chloride ion bound to a cation would be polarized making it less able to interact with the positive charge of the electrode. The preferred metal complex to coordinate with

the electrode is thought to be the neutral complex since it is the more insoluble of the complexes and would not have a coordinate sphere of water molecules. However, data indicate a negatively charged complex of the adsorbing complex for lead (II) chloride. The formation constant (K3) is small for the reaction:

$$PbCl_2 + Cl^- ----> PbCl_{3-}$$

A repulsion interaction of the lone pair of electrons on the lead atom and the chloride ion may account for the small size of K3 (10 times less than K4) and may help account for the fact that PbCl2 does not strongly coordinate with adsorbed chloride ions (). The amount of chloride induced absorbtion of lead(II) greatly exceeds the amount of cadmium(II) adsorption despite the fact that chloride complexes of cadmium(II) are more stable than lead. chloride bond, however, is stronger than the cadmium chloride bond and would provide a greater driving force for Under conditions where the coverage of the electrode is not complete, the current due to the reduction of the adsorbed lead follows the anion concentration. high concentrations of anion, where the coverage is complete and the anion is packed very tightly, no adsorption current is observed. It is believed that steric limitations prevent the metal complex from bonding with the adsorbed anions.

C.O A Method for the Study of Adsorption

In the presence of adsorption it is necessary to modify the theoretical analysis in the calculation of the shape of voltammograms. Assumptions must be made as to the choice of an adsorption isotherm, the rate of adsorption-desorption for the attainment of equilibrium, the extent of coverage which may be greater or less than a monolayer and the strength of adsorption which may be weak or strong or something in between. Rather than obtaining information from the shape and position of the peak current it is possible to utilize the integral of the voltammetric curve. Although this method is also dependent on some simplifying assumptions, it can also be used to obtain information about adsorption. This method can be used to advantage in the cases wehre adsorption and diffusion peaks are close together on the potential axis because it is often difficult to determine small changes in the peak height when adsorption is weak. The total charge obtained by integrating a voltammetric curve may be expressed as:

$$Q_t = KC/V^{1/2} + Q_{d1} + Q_{ad}$$

where C is the bulk concentration of the electroactive material, v the sweep rate, $Q_{\rm dl}$ the charge needed to charge the double layer, and $Q_{\rm ad}$ the charge due to the adsorbed species. K is a constant which depends on the integration interval, temperature, and the electrode surface area. The above equation predicts that $Q_{\rm t}$ plotted against $v^{1/2}$ will

be a straight line with an intercept determined by the sum of Q_{dl} and Q_{ad} . This relationship assumes that Q_{dl} and Q_{ad} do not change with sweep rate, which is often the case. order to determine Q_{ad} from the intercept using the above equation, it is necessary to determine Qd1. In the presence of adsorption it is not possible to obtain Q_{d1} from a blank because the electrode capacitance can change greatly when adsorption occurs. Also, it cannot be assumed that C_{dl} will remain constant over the potential scan range. must therefore be determined in some other way. A graphical method may be used to determine Q_{d1} in the presence of adsorption and diffusion. The method involves plotting several linear graphs and determining the intercepts. first set of graphs consists of plotting peak charge against the reciprocal of the square root of sweep rate for several concentrations of the electroactive material. square line is drawn through the points and extrapolated to the zero intercept. At the zero intercept, the sweeprate is infinite and the charge due to diffusion is zero since the electroactive species has no time to reach the electrode The charge at this point must be due to through diffusion. the double layer charge plus any charge due to adsorption. A second graph is then made by plotting the intercepts of the first graphs against concentration. This graph yields a linear plot through which a least square line is drawn to the intercept of zero concentration. The charge at the zero concentration intercept is mainly the double layer

charg speci

each

trac

firs

it i

D.0

the

inje Pure

thro

nigh

1.0 elec

mer

give

This time

tain

the size

mv/se

Slim

gud I

charge since adsorption cannot occur when the electroactive species is not present. The charge due to adsorption at each concentration tested can then be determined by subtracting the double layer charge from intercepts of the first graphs. Because this method requires extrapolation, it is subject to errors due to noise in the data.

D.0 Experimental

D. Bair performed in a senior research project studied the adsorption of lead chloride using the coulostatic charge injector and the technique of staircase cyclic voltammetry. Pure lead chloride was prepared from ACS grade lead nitrate through precipitation with hydrochloric acid. The lead chloride was washed and dried in an oven at 110° C overnight. Three solutions of lead chloride were prepared 1.0×10^{-5} , 1.5×10^{-5} , and 2.0×10^{-5} M. The supporting electrolyte was recrystallized KCl. After preparing a mercury drop of known area, a delay time of 3.0 minutes was given to assure the attainment of adsorption equilibrium. This equilibrium time was ascertained by increasing the time before each scan until consistant results were obtained. The initial potential was -.076 V vs. S.C.E. and the switching potential was -.775 V vs. S.C.E., the step size was 10 mv and the sweep rate was held constant at 89 mv/sec. The step times Tl and T2 were varied while their sum was held constant. T1 and T2 took on values of T1=1 and T2=99, T1=50 and T2=50, T1=90 and T2=10, and T1=95 and

T2=5 msec. The total step time always remained constant at The data was uploaded to the DEC 11/40 computer and converted into two charge files. The first, contained the charge obtained in time period Tl and the second T2. FORTRAN program was written to analyze the charge files. The program scanned the data and located maximum and minimum values. It determined a least square line for a selected number of points on the baseline of the cathodic scan. estimate of the double layer charge was calculated at the initial potential by calculating $\Omega_{\mbox{\scriptsize dl}}$ from the intercept of the base line with the charge axis (y axis). The results indicated that the charge acquired during T2 was diffusion charge and that when the T2 period was made small the charge decreased rapidly to zero. The charge contained during time period Tl contained, in addition to the charge due to diffusion, double layer charge and charge from any adsorbed species. Decreasing time period Tl resulted in a decrease in acquired charge from diffusion. However, the charge required for the double layer and the adsorbed species remained fixed as Tl was decreased. The desired step potential would not be reached by the end of time period Tl, if this surface charge was not supplied to the electrode. Tl charge, therefore, did not decrease to zero with decreasing T1 period as did the T2 charge. Because the charge due to adsorption was small in comparison to the double layer charge and background noise, it was not possible to separate double layer charge from adsorbed charge in time period T1

IJ.

t

F

0

using this method of constant sweep rate. G. Inman in three terms of senior research worked with staircase cyclic voltammetry, linear scan voltammetry, conductance measurements, FORTRAN programming, and MULPLT. He studied the adsorption of PbCl, and CdCl, on mercury and compared the performance of the charge injector and the PAR 170 instrument in the cyclic voltammetry mode. An investigation was made of solution resistance and electrolyte concentration. The voltammograms of lead chloride were studied to note the effects of: initial potential, time during which the initial potential was held before the scan, and sweep rate. A precision study was made to note how charge injection size effects The maximum injection rate was determined by decreasing the injection size until potential step deviations occurred. The resistance of several concentrations of chloride were determined in the electrochemical cell using an A.C. conductance bridge. To avoid contamination of the solution with KCl from the filling solution of the S.C.E. electrode, an AgCl reference electrode was prepared for use by anodizing a pure silver wire. A chart recorder was used to monitor the cell potential of each solution to test the electrode stability and to note the cell potential dependence on electrolyte concentration. The cell potentials were found to be stable for several hours and showed a Nernstian concentration dependence. The concentration of all solutions were prepared 100 times more concentrated in chloride than lead. The solutions were tested on the PAR

170 and on the charge injection instrument using staircase cyclic voltammetry. At low concentrations of KCl the ad $sorption of PbCl_{2}$ was very strong and consistent data were not obtained. At concentrations of KCl above, 0.3 M the voltammograms of the two instruments gave comparable results. The graphical method was used to analyze solutions of lead chloride containing the following concentrations: $1.0 \times 10^{-5} \text{ M}$, $1.5 \times 10^{-5} \text{ M}$ and $2.0 \times 10^{-5} \text{ M PbCl}_2$. Charge voltammograms were analyzed at constant lead concentration and various KCl concentrations to determine a suitable KCl concentration in which weak adsorption prevailed. staircase cyclic voltammograms were analyzed at step times of 45, 95, 165, and 350 msec. Tl was held constant a 5 It was found that a concentration of 0.3 M KCl was suitable to avoid strong adsorption. At concentrations of KCl lower than this value, the cathodic peak widened and eventually became a separate peak. It was found that three minutes was a sufficient time after the mercury drop was formed for adsorption equilibrium to be established. Voltammograms run after this time all had the same shape. data were processed at each sweep rate by computer and the graphical method applied to the data. The first plot constructed consists of total charge plotted vs. the square root of time (see Figures 7-1 A-C). This plot was extrapolated back to zero time, or infinite sweep rate. tercepts of these plots were then plotted vs. concentration to obtain Figure 7-2. The data were not of sufficient

accuracy to permit consistant determination of the amount of adsorption present because scatter in the data resulted in large errors after extrapolation. The precision studies confirmed that the maximum rate of charge injection was 5 kHz. The total charge for the step remained constant to within one charge injection up to the maximum injection rate. The precision study results will be presented further in the next chapter on experimental error.

TOTAL CHARGE Vs. SQRT CHARGE T

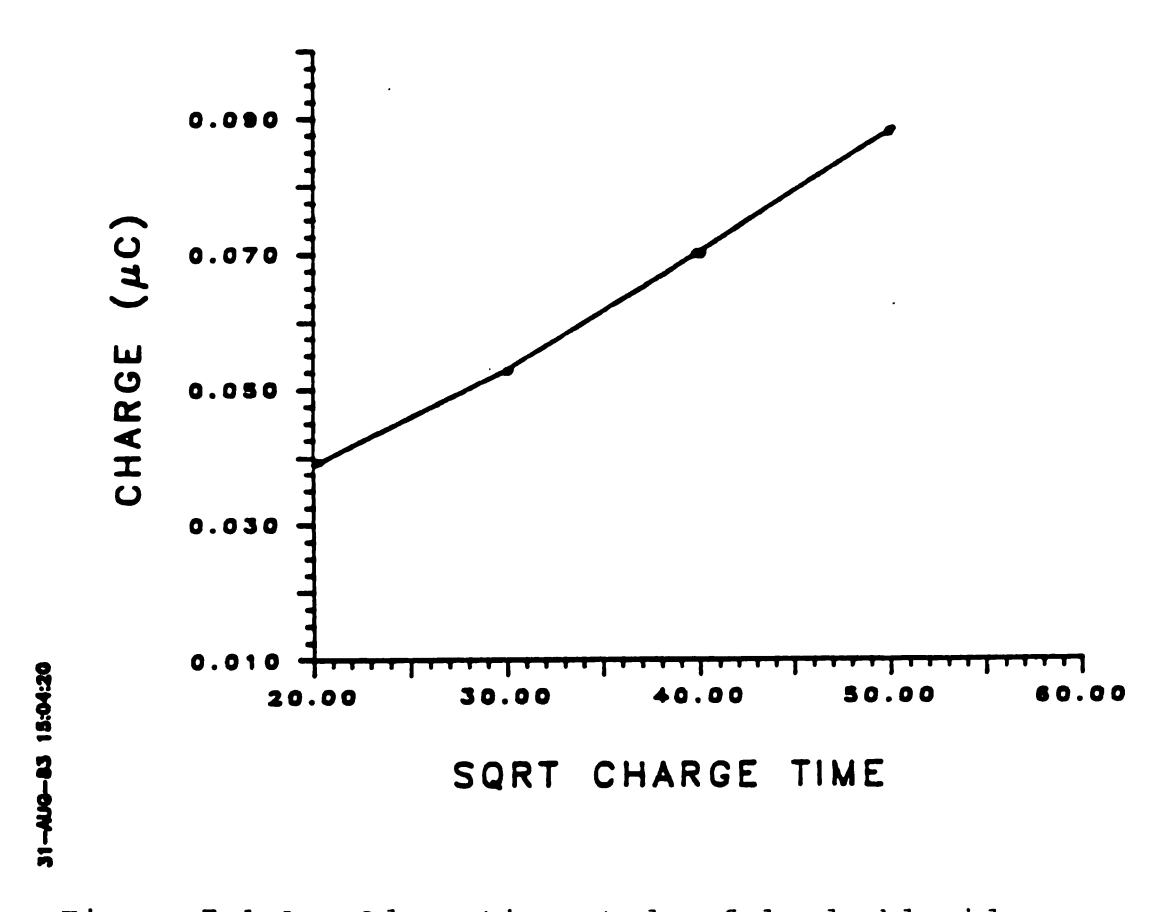


Figure 7-1 A. Adsorption study of lead chloride.

TOTAL CHARGE VS. SQRT CHARGE T

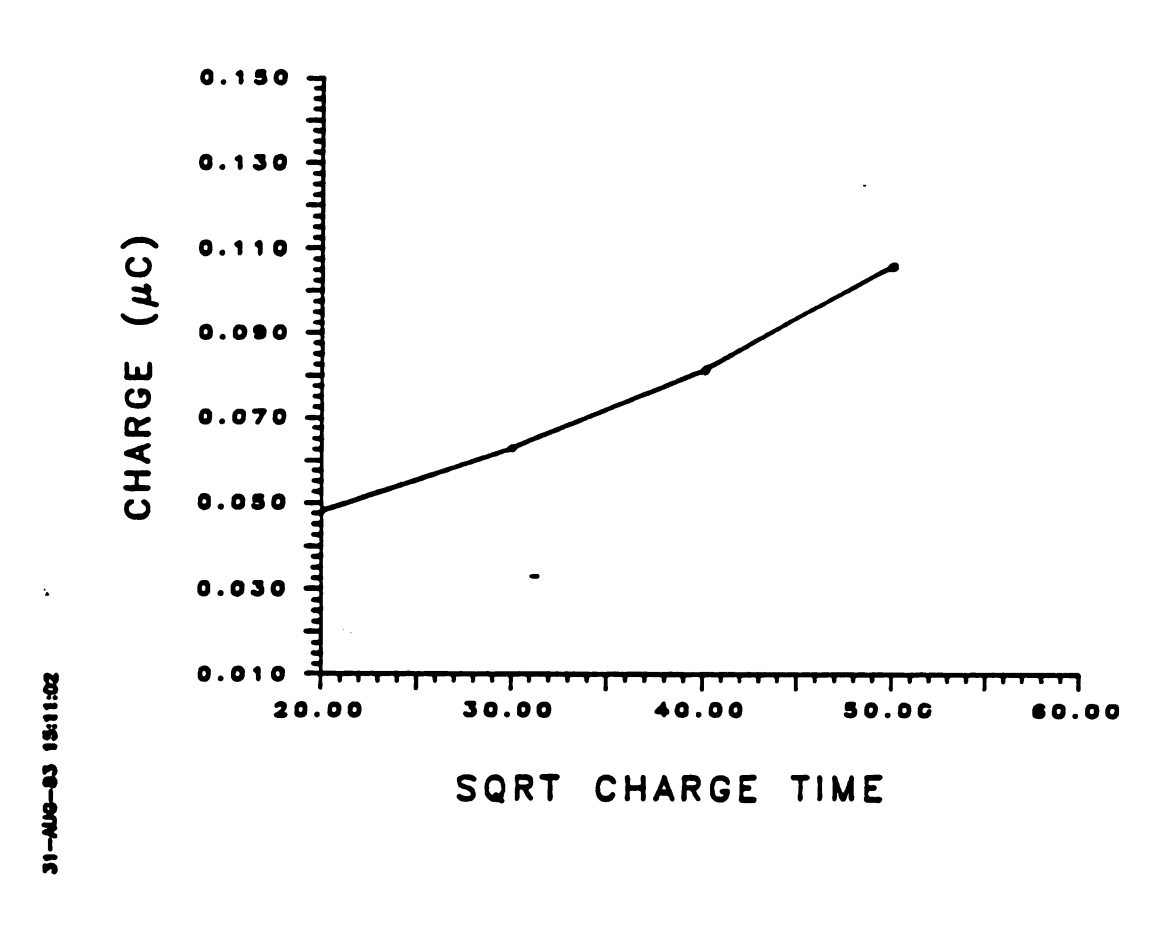


Figure 7-1 B. Adsorption study of lead chloride.

TOTAL CHARGE VS. SQRT CHARGE T

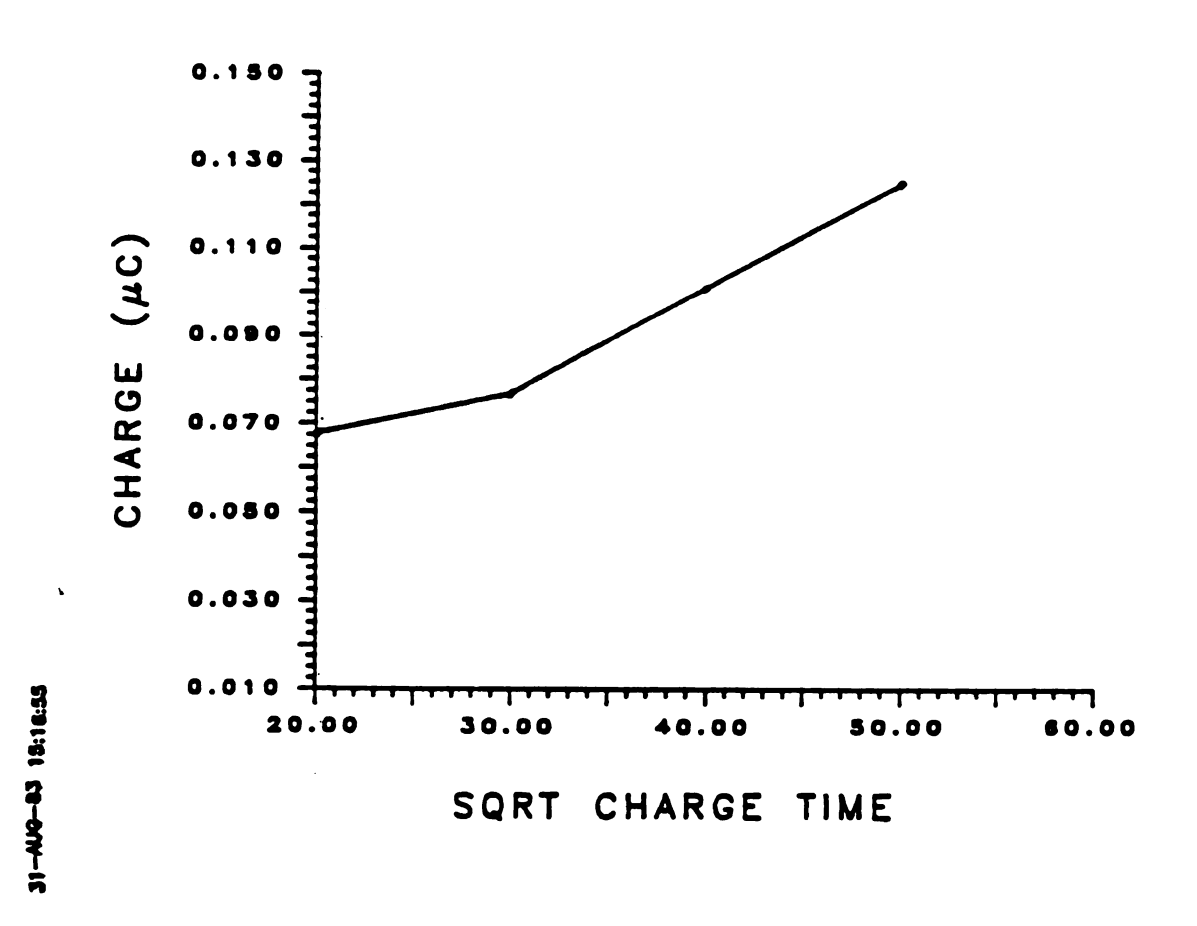


Figure 7-1 C. Adsorption study of lead chloride.

INTERCEPT CHARGE VS CONCENTRATION Q INTER FROM Q VD (SQRT V) PLOT

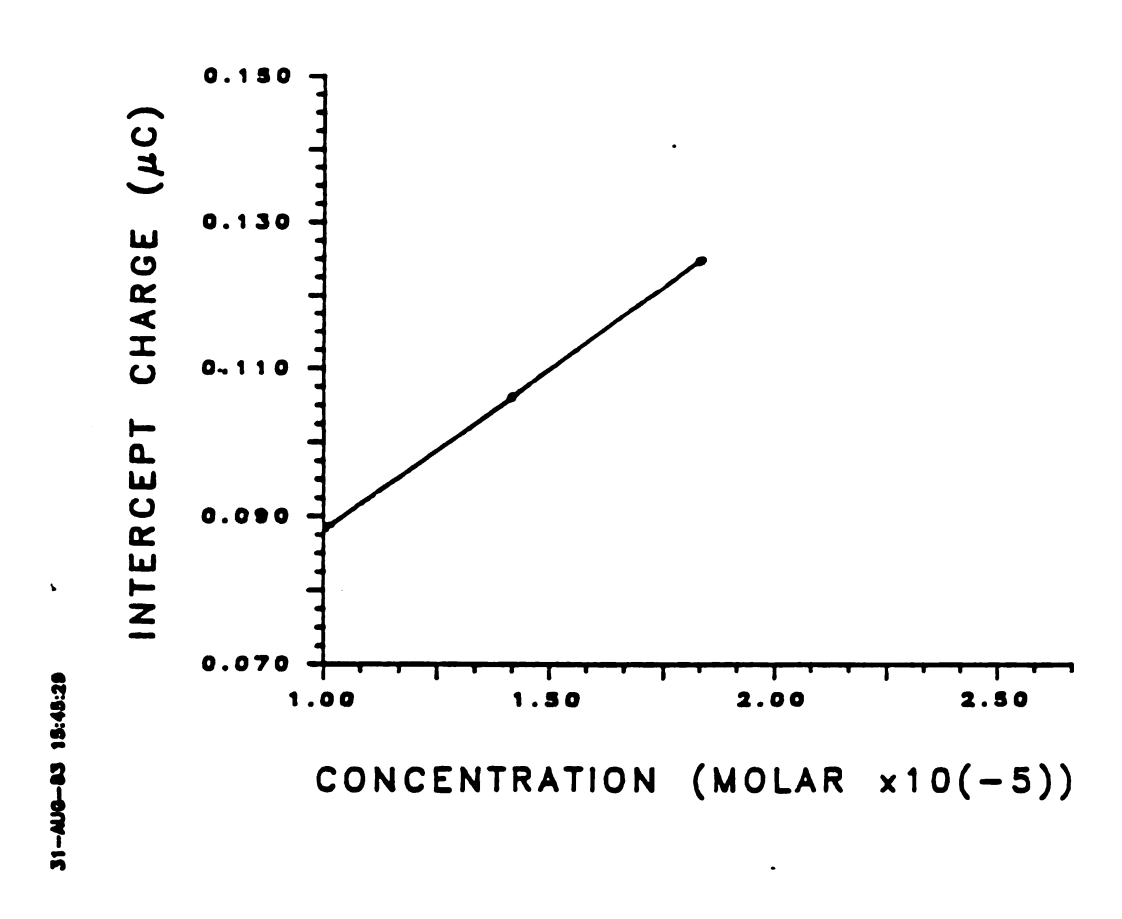


Figure 7-2. Determination of the adsorption of lead chloride.

VIII LIMITATIONS AND IMPROVEMENTS

Staircase voltammetry as performed in this research is a hybrid of charge injection and staircase voltammetry. This hybrid method will therefore contain characteristics of both techniques. It is the purpose of this chapter to point out the advantages and disadvantages of this technique. The sources of error will be identified and the future outlook of this method and other variations of the method will be discussed.

Staircase voltammetry is also a hybrid of two electrochemical methods. It combines the potential jump technique and linear scan voltammetry. The potential jump method was applied to linear scan voltammetry to gain the advantage of charging current reduction and yet retain the advantages of a scanning voltage sweep. When the potential steps are large, staircase voltammograms show most strongly the characteristics of the potential step method but when the potential steps are small, the voltammograms approach the results of the linear scan experiment. When interpreting experimental results, it is important, therefore, to learn to expect changes in the shape of voltammograms due to the influence of the potential step. Experimental data interpretation is more complicated than linear scan voltammetry because of this hybrid nature. It was found that it was

advantageous to generate voltammograms from theory that could be compared with experimental results. For example, the shift in the peak potential with sampling time is a characteristic which changes with step size. As long as theory is consulted for the location of the reduction potential values on the voltammogram, the experimental data may be correctly interpreted. Because data interpretation is more complicated than in the linear scan experiment, the user must beware of the expected influence of instrumental parameters on the shapes of voltammograms.

Experiments will deviate from results predicted by theory when the potential step is non-ideal. The potential step will be non-ideal because the jump in potential is not instantaneous and is not held fixed to a constant potential value for the duration of the step. Other sources of deviation and error also occur because the applied voltage waveform is staircase and non-linear. The non-ideal effects and sources of errors can thus be grouped into the following catagories:

- 1. Effects of the staircase waveform;
- Instrumental limitations;
- Charge injection effects.

A.O Effects of the Staircase Waveform

The discrete nature of the potential step and the choice of the initial potential creates an uncertainty in the location of the peak potential which is not present in

the linear scan experiment. In an electrochemical cell which is under diffusion control, when the electrode potential is changed, the cell current will fall if mass transport is unable to supply electroactive material to the electrode at a rate fast enough to prevent concentration polarization. The location of the peak potential will deviate from the linear scan result and create an uncertainty, if a step is made which jumps past the potential value where concentration polarization sets in. variation in the location of the peak potential can be tested by changing the initial potential value while keeping the step size the same. The exact determination of the initial potential is also a contributing factor in the error of the peak potential. To maintain the initial potential within a few millivolts of the desired value, the charging voltage (VAPDA) of the injecting capacitors is made small to maintain the initial potential within a narrow voltage range. It was found that the peak potential changed from one experiment to the next by the size of one potential step. The uncertainty in the location of the peak potential can be reduced by decreasing the step size. Decreasing the step size also provides more data points to better represent the shape of the voltammogram. However, a smaller step size can produce a decrease in sensitivity and result in difficulties in generating an accurate and steady potential step.

B.O Charge Injection Effects

When the entire staircase waveform is viewed on an oscilloscope screen, the individual steps may be seen but the many charge injection pulses which generate the steps are too quick and narrow to be easily viewed on the same time scale as the entire waveform. To view the charge injection pulses the time base of the oscilloscope is expanded and the triggering level set to catch the brief voltage spikes. It must be remembered that the staircase waveform is generated by the application of rapid, discrete charge injection pulses. The accuracy and precision of the digital charge injection method as practiced in this research depends on the size and rate of injection of these pulses. The instrumental requirements for generating these pulses will be considered in a later section. To maintain the potential step within a narrow potential range, small charge injections are applied. This voltage range must be small compared to the desired voltage step or an accurate staircase waveform will not be generated. For example, when a ten millivolt potential step is desired, the voltage level is allowed to fall 1.2 mV before the desired step voltage level is restored. The desired step potential will thus change about an average value. The noise level of the instrument is about 1 mV unless special precautions are taken to shield the instrument from room noise. This noise level determines the lower level of control for maintaining the step potential.

The total step charge gained in one step should be large compared to the net change in charge created by the variations in the step voltage otherwise the individual points of the voltammogram will appear noisy and not follow a smooth curve. The larger the potential step, the greater will be the charge acquired for the step. Step sizes from 2 to 50 mV were tested over a wide concentration range. two millivolt step size produced voltammograms that were noisy and required smoothing for analysis. The program NOISE.FTN is used to smooth these data files. The staircase waveform deviated from the ideal wave form by as much as 10 The 50 mV step produced voltammograms which also deviated from the ideal waveform at fast scan rates because the charge injector could not keep up with the demand of charge that the double layer capacitance required and the step potential fell short of the desired step potential at the end of time period Tl. Under these conditions the double layer charge is not separated from the Faradaic charge and thus results in error and distortion of the voltammogram. Two possible solutions exist for solving this problem when it occurs. The sweep rate can be slowed down by increasing the Tl period to allow the charge injector more time to make the necessary charge injections to reach the desired voltage.

The second solution is to increase the large charge injection size. This may be done by increasing the injecting capacitor or increasing the charging voltage of the DAC.

Changing the charging voltage of the DAC or the number of large charge injections does not produce a noticeable change in shape of the voltammogram because the large charge injections are applied rapidly. If the large charging voltage is made too high, the desired step potential may be exceeded and result in a distorted voltammogram. The smaller trim injections require more time to complete because the cell potential is measured between each charge It was found that the shape of a voltammogram does not change greatly with the number of these injections, if time period Tl is short in comparison to the total step The general strategy is thus to add quickly the large charge injections to bring the electrode potential slightly below the desired step potential and then to use small trim injection to reach the desired step potential by the end of time Tl. When it is not possible to add all the small trim injections by the end of time period Tl, these injections will be counted with the small injections in period T2 and double layer charging error and distortion of the voltammogram results. It is, therefore, necessary to check the voltage reached at the end of time period Tl for each step to ensure that the desired step potential has been reached. The program CKDV.OBJ allows these deviations to be checked after each voltage scan on the microcomputer.

C.0 Variation of the Step Charge

There are several possible sources of error which can cause variations in the number of charge injections made during a step.

- 1. DAC quantization error;
- 2. variation in the average step voltage;
- 3. instrumental noise;
- 4. quantized charge size.

D.O DAC Round-Off Error

When the bipolar nature of the DAC is used to change the sign of the charging voltage, the charging voltage is continually set and reset to enable either positive and negative injections during the step. A cumulative round-off error in the decimal-to-binary conversion can result and the least significant bit of the DAC may come up high or low. Errors due to the change in the least significant bit of the DAC result in a 5 mV variation of the charging voltage. With a charging voltage of 1000 mV the round-off error amounts to a 0.5 percent variation in the content of a single injection. It would, therefore, take 200 injections which were each short 0.5 percent to increase the number of injections made during the step by one. The DAC round-off error is just as likely to be high as low, thus the error of a large injection pulse may be canceled by a short one. The DAC round-off error is therefore not expected to cause

1

large variations in the number of injections needed to maintain the voltage step.

When the inverting amplifier is used to change the polarity of the charging voltage, the DAC cannot be changed during time period T2 and so the DAC round-off error will not occur. When comparing separate steps or different voltammograms with another, DAC round-off error does exist.

Instrumental noise present in the measured voltage is a high frequency random noise which may be above or below the desired step voltage. The voltage level which must be exceeded before a charge injection is made is set above the noise level of the instrument so that the charge injector is not responding to noise but a change in the DC voltage level caused by the consumption of charge by the Faradaic The total number of injections for a step is reaction. calculated by subtracting the number of positive charge injection from the number of negative injections made during the step. If the step is a multiple of the frequency of the noise, the net number of injections due to random noise will be zero because the number of positive injections will equal the number of negative injections. Therefore, the instrument averages random noise which should improve the precision of the voltammograms.

The voltage level of a step plateau is maintained to within + one least significant bit of the ADC which is 1.2 mV. The ability of the charge injector to maintain the voltage within these limits is determined by the rate and

size of injections. For example, with a charging voltage of 1000 mV and a 1 nF injecting capacitor, the injected charge will change the voltage of the electrode which has a capacitance of 1 microfarad, by only one millivolt with each injection. Different rates of charge injections can result in the electrode being held at slightly different average potentials for different lengths of time during the step. When the electrode is at a potential where the electrochemical reaction is occurring rapidly, the result of remaining longer at a different average voltage will be the greatest. However, the variation in the average voltage will not change the net charge of the step by a significant amount. Therefore, variations in the average step voltage should not increase the number of charge injections significantly.

The size of the charge injection directly influences the number of injections made during the step and the quantization error of the injection. For example, suppose that the total Faradaic charge to be gained in period T2 is 22 microcoulombs. If the charge injection size is set to 5 microcoulombs, and if 4 charge injections are made, a total of 20 microcoulombs of charge will be injected. This quantization error leaves the total charge injected 2 microcoulombs short of the desired 22 microcoulombs. If 5 charge injections are made, the total charge will be 3 microcoulombs high. The quantization error may occur along any step of the staircase waveform but is not cumulative from

one step to the next. The uncertainty of one count can result in the total count of charge injections.

The quantization error in the step charge can be reduced by decreasing the charge injection size. Reducing the charge injection size also results in a greater precision because there is an increase in the number of charge injections for each step. DAC charging voltages from 2.5 V -249 mV were used with an injection capacitor of 1.0 nF to illustrate how the number of charge injections made during a step changed with the injection size. The solution tested was 5×10^{-5} M CdCl₂ with the total step time set equal to 98 msec and T2 set equal to 90 msec. The number of charge injections made in the peak potential step was obtained from the raw data file. Four voltammograms were run at each charging voltage and the average number of counts per step determined. Figure 8-1 shows the average number of counts plotted vs. the inverse of the charging voltage. A least squares line is drawn through the first nine points. The graph shows that the point corresponding to a charging voltage of 249 mV falls below the least square line. occurs since the number of injections made to the cell is limited by the maximum injection rate of the instrument. As a result of this injection rate limitation, the charge delivered to the cell fell short of that demanded by the Faradaic reactions for the smallest charge injection used.

To check for errors due the quantization of the injection size, the relative standard deviation of the number of

STAIRCASE VOLTAMMETRY LEAST SQ. LINE (-), EXP. (0), T1-8 ms, T2-90 ms

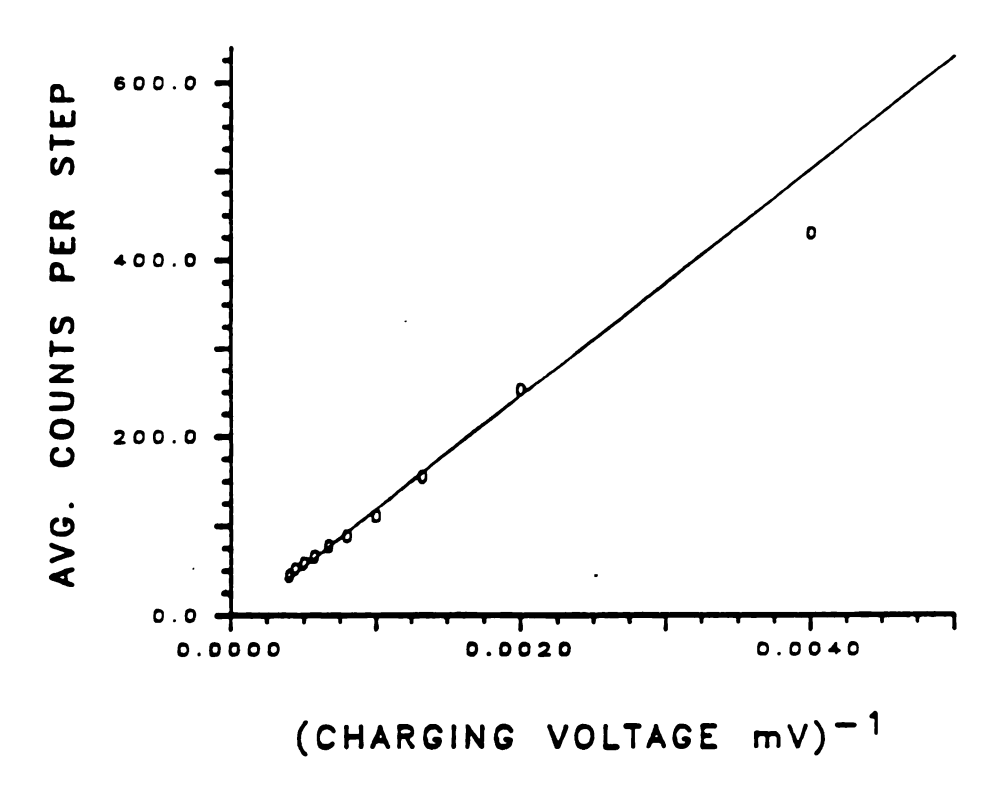


Figure 8-1. Counts vs. charging voltage.

injections made during the peak potential step was determined for charging voltages ranging from 498 to 2500 mV.

Figure 8-2 shows that the relative standard deviation of the number of injections plotted vs. the charging voltage for experiment (A) and a plot of a theoretical error (B). The theoretical error was calculated assuming a gating error of one and expressing this as a ratio to the experimental number of data points obtained (1/ number of injections).

The charging voltage was increased in increments of 250 mV.

Since the maximum injection rate of the instrument is 5

KHz, the maximum number of injections which could be injected in 90 msec would be 450. The average number of total injections with a charging voltage of 2.5 V was 42 for the peak potential step. It increased to 254 when the charging voltage was reduced to 498 mV. As the charging voltage increases, the number of injections decreases and the relative error of the number of injections increases. The relative standard deviation is low when the number of injections is high and the charging voltage low.

RELATIVE STANDARD DEV. vs. CHARGING VOLTAGE

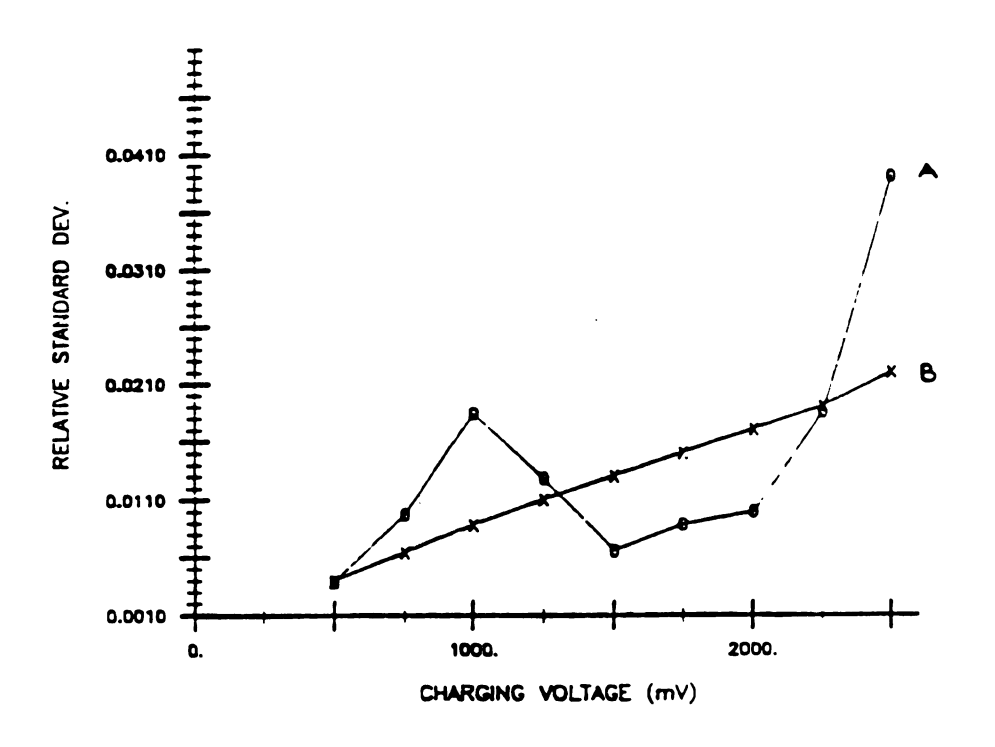


Figure 8-2. Relative standard deviation vs. charging voltage.

In this section the instrumental limitations and errors will be discussed in light of what improvements might be made for the development of an improved charge injection instrument. The new instrument will have improvements and added capabilities in the following areas:

- 1. charge injector;
- 2. DAC precision;
- 3. voltage measurement;
- 4. software control of drop size and rate;
- 5. added numerical calculation power;
- 6. digital filtering capability;
- 7. disk storage;
- 8. hard copy of output;
- 9. added graphic capability.

To maximize the performance of the charge injector it seems best to design an instrument with two charge injectors. One which can inject a large quantity of charge to make large potential steps and another which can inject extremely small charge pulses to maintain the electrode potential very accurately.

The large charge injector will contain special analog switches which can transfer a high power output to the injection amplifier. The large charge injection amplifier should be designed to remain stable when heavily loaded on both its input and theoutput. The maximum output voltage

of this amplifier will be high to enable charge to be quickly forced through a large solution resistance.

The small charge injector will be designed to inject very small pulses of charge at a fast rate. This charge injector will be mounted close to the cell to reduce the length of the wires used to connect the injector to the cell. This will reduce noise and enable smaller charge injections. The injection amplifier will have a very small input and output load and will be able to respond very quickly and yet remain stable.

REFERENCES

- 1. Matheson, Nichols, Trans. Electrochem. Soc., 1938, 73, 193.
- 2. J.E.B. Randles, Analyst, 1947, 72, 301.
- A Sevcik, Collection Czechoslov. Chem. Commun., 1948, 13, 349.
- 4. P.J. Delahay, J. Phys. and Colloid Chem., 1949, <u>54</u>, 1279.
- 5. C.A. Streuli and W.D. Cook, Anal. Chem., 1953, 25, 1691-1696.
- C.A. Streuli and W.D. Cook, Anal. Chem., 1954, 26, 963-979.
- 7. Matsuda, Z. Elektrochem., 1953, 61, 489.
- 8. R. Nicholson, I. Shain, Anal. Chem., 1964, 36, 706.
- 9. P. Kissinger, W. Heineman, J. Chem. Ed., 1983, 60, 702-706.
- 10. A. Fick, Progg. Ann., 1855, 94, 59.
- 11. K. Oldham, Anal. Chem., 1973, 45, 39.
- 12. R. Nicholson, Anal. Chem., 1965, 37, 1351.
- 13. R. Nicholson, Anal. Chem., 1965, 37, 667.
- 14. P. Debye, E. Huckel, J. Phys. Chem., 1966, 70, 2373.
- 15. G. Gouy, J. Phys. Radium, 1910, 9, 457.
- 16. D.L. Chapman, Phil. Mag., 1913, 25, 475.
- 17. O. Stern, Z. Elektrochem., 1924, 30, 508.
- D.C. Grahame, Chem. Rew., 1947, 41, 441.
- 19. R.B. Whitney and D.C. Grahame, J. Chem. Phys., 1941, 9, 827.

- 20. D.C. Grahame, and R.B. Whitney, J. Am. Chem. Soc., 1942, 64, 1548.
- 21. G. Barker and A. Gardner, Fresenius Z. Anal. Chem., 1960, 173, 79.
- 22. C. Mann, Anal. Chem., 1961, 33, 1484.
- 23. C. Mann, Anal. Chem., 1965, 35, 326.
- 24. C. Mann, Anal. Chem., 1966, 36, 2424.
- 25. R. Nigmatullin and M. Vyaselev, Zh. Anal. Khim., 1964, 19, 545.
- 26. J. Christie and P. Lingane, J. Electroanal. Chem., 1965, 10, 176.
- 27. J. Zipper and S. Perone, Anal. Chem., 1973, <u>45</u>, 452-457.
- 28. L. Miaw, P. Boudreau, M. Pichler and S. Perone, Anal. Chem., 1978, 50.
- 29. D. Ferrier and R. Schroeder, J. Electroanal. Chem. Interfacial Electrochem., 1973, 45, 343-359.
- 30. D. Ferrier, D. Chidester, and R. Schroeder, J. Electroanal. Chem. Interfacial Electrochem., 1973, 45, 361-375.
- 31. P. Kissinger and W. Heineman, 'Laboratory Techniques in Electrochemistry', Marcel Dekker, Inc., 1984, New York.
- 32. K. Oldham, J. Electroanal. Chem., 1966, 44, 171-187.
- 33. E. Ahlberg and V. Parker, J. Electroanal. Chem., 1981, 121, 57-71.
- J. Imbeaux and J. Saveant, J. Electroanal. Chem., 1970, 28, 325-338.
- 35. J. Imbeaux and J. Saveant, J. Electroanal Chem., 1971, 31, 183-192.
- 36. W. De Vries and E. Van Dalen, J. Electroanal. Chem., 1965, 10, 183-190.
- 37. S. Roffia, J. Electroanal. Chem., 1969, 22, 117-125.
- 38. Demars and Shain, J. Am. Chem. Soc., 1959, 81, 2654.
- 39. Ross, Demars, and Shain, Anal. Chem., 1959, 28, 1768.

- 40. A. Bard and L. Faulkner, 'Electrochemical Methods. Fundamentals and Applications', John Wiley and Sons, 1980, New York.
- 41. P. He, L.R. Faulkner, Anal. Chem., 1982, 54, 1313A.
- 42. P. Delahay, J. Phys. Chem., 1962, 62, 2204.
- 43. W. Reinmuth, Anal. Chem., 1962, 34, 1272.
- 44. W. Weir, C.G. Enke, J. Phys. Chem., 1967, 71, 275-279.
- 45. W. Weir, C.G. Enke, J. Phys. Chem., 1967, 71, 280-291.
- 46. P. Delahay, Anal. Chim. Acta, 1962, 27, 90-93.
- 47. P. Delahay, Y. IDE, Anal. Chem., 1962, 34, 1580.
- 48. J. Kudirka, R. Abel, and C. Enke, Anal. Chem., 1972, 44, 425-427.
- 49. B. Hahn, Ph.D. Thesis, Michigan State University, East Lansing, Mi., 1974.
- 50. M. Katzenberger, P. Daum, Anal. Chem., 1975, <u>47</u>, 1887-1893.
- 51. C.C. Lee, Michigan State University, East Lansing, Mi., 1982.
- 52. M. Schreiber and T. Last, Anal. Chem., 1981, <u>53</u>, 2095-2100.
- 53. K. Aramata and P. Delahay, Anal. Chem., 1963, <u>35</u>, 1117-1118.
- 54. T. Last, Anal. Chem., 1982, 54, 2327-2332.
- 55. P. Daum, L. McHalsky, Anal. Chem., 1980, 52, 340-344.
- 56. A. Barnes, T. Nieman, Anal. Chem., 1982, 55, 2309-2312.
- 57. J. Reiss, T. Nieman, Anal. Chem., 1983, 55, 1236-1240.
- 58. H.P. van Leeuwen, Electrochimica Acta, 1978, 23, 207-218.
- 59. A.J. Bard, H.P. van Leeuwen, Electroanalytical Chemistry, 1982, vol. 12, Marcel Dekker, Inc., New York, N.Y., 159-238.
- 60. W. Goldsworthy, R. Clem, Anal. Chem., 1972, 44, 1360-1366.

- 61. S. Hourdakis, Dissertation for Ph.D., Michigan State University, East Lansing, Mi., 1978.
- 62. B. Newcome, Dissertation for Ph.D., Michigan State University, East Lansing, Mi., in press.
- 63. R. Thomas, M. Jenkins, Analog Switches and Their Applications, Siliconix, Santa Clara, Ca., 6/1980, 4.
- 64. Malmstadt, S.R. Crouch, C.G. Enke, 'Electronics and Instrumentation for Scientists', 1981, Benjamin/Cummings Publishing Co., 121.
- 65. C. Streuli, W. Cooke, Anal. Chem., 1954, 26, 3000.
- 66. W. French, T. Kunwana, J. Phys. Chem., 1964, 68, 1279.
- 67. Wopschall, I. Shain, Anal. Chem., 1967, 39, 1517.
- 68. Wopschall, I. Shain, Anal. Chem., 1967, 39, 1535.

